

VOL.107 NO.GT6. JUNE 1981

JOURNAL OF THE GEOTECHNICAL ENGINEERING DIVISION

PROCEEDINGS OF
THE AMERICAN SOCIETY
OF CIVIL ENGINEERS





VOL.107 NO.GT6. JUNE 1981

JOURNAL OF THE GEOTECHNICAL ENGINEERING DIVISION

PROCEEDINGS OF
THE AMERICAN SOCIETY
OF CIVIL ENGINEERS



Copyright© 1981 by
American Society
of Civil Engineers
All Rights Reserved
ISSN 0093-6405

William F. Marcuson III, Editor
U.S. Army Engineers

AMERICAN SOCIETY OF CIVIL ENGINEERS

BOARD OF DIRECTION

President

Irvan F. Mendenhall

Past President

Joseph S. Ward

President Elect

James R. Sims

Vice Presidents

Robert D. Bay
Francis J. Connell

Lyman R. Gillis
Albert A. Grant

Directors

Martin G. Abegg	Paul R. Munger
Floyd A. Bishop	William R. Neuman
L. Gary Byrd	Leonard S. Oberman
Larry J. Feeser	John D. Parkhurst
John A. Focht, Jr.	Celestino R. Pennoni
Sergio Gonzalez-Karg	Robert B. Rhode
James E. Humphrey, Jr.	S. Russell Stearns
Richard W. Karn	William H. Taylor
Leon D. Luck	Stafford E. Thornton
Arthur R. McDaniel	Robert E. Whiteside
Richard S. Woodruff	

EXECUTIVE OFFICERS

Eugene Zwayer, *Executive Director*
Julie E. Gibouleau, *Assistant to the Executive Director*
Louis L. Meier, *Washington Counsel/Assistant Secretary*
William H. Wisely, *Executive Director Emeritus*
Michael N. Salgo, *Treasurer*
Elmer B. Isaak, *Assistant Treasurer*

STAFF DIRECTORS

Donald A. Buzzell, *Managing Director for Education and Professional Affairs*
Robert A. Crist, Jr., *Managing Director for Publications and Technical Affairs*
Alexander Korwek, *Managing Director for Finance and Administrative Services*
Alexandra Bellow, *Director, Human Resources*
David Dresia, *Director, Publications Production and Marketing*
Barker D. Herr, *Director, Membership*
Richard A. Jeffers, *Controller*
Carl E. Nelson, *Director, Field Services*
Don P. Reynolds, *Director, Policy, Planning and Public Affairs*
Bruce Rickerson, *Director, Legislative Services*
James M. Shea, *Director, Public Communications*
Albert W. Turchick, *Director, Technical Services*
George K. Wadlin, *Director, Education Services*
R. Lawrence Whipple, *Director, Engineering Management Services*

COMMITTEE ON PUBLICATIONS

Stafford E. Thornton, *Chairman*
Martin G. Abegg
John A. Focht, Jr.
Richard W. Karn
Paul R. Munger
William R. Neuman

GEOTECHNICAL ENGINEERING DIVISION

Executive Committee

Robert Schuster, *Chairman*
Ernest T. Selig, *Vice Chairman*
William F. Swiger
Robert T. Darragh, Jr., *Secretary*
Elio D'Appolonia, *Management Group E Contact Member*

Publications Committee

William F. Marcuson III, *Chairman and Editor*
O. B. Andersland
Warren J. Baker
Dor C. Banks
James M. Bell
Chandra S. Brahama
John T. Christian
G. W. Clough
Tuncer B. Edil
Herbert H. Einstein
Arley G. Franklin
D. H. Gray
Bobby Hardin
Cornelius J. Higgins
William H. Hightner
Robert D. Holtz
Izzat M. Idriss
L. H. Irwin
Jey K. Jayapalan
Reuben H. Karol
H. Y. Ko
William D. Kovacs
Leland M. Kraft
Raymond J. Krizek
E. T. Selig, *Exec. Comm. Contact Member*
Fred H. Kulhawy
C. C. Ladd
Poul V. Lade
Leonard J. Langfelder
Felipe A. Len-Rios
Gholamreza Mesri
Donald J. Murphy
S. V. Nathan
Thom L. Neff
Edward A. Nowatzki
Michael W. O'Neill
Jean H. Prevost
Adel Saada
Surendra K. Saxena
Robert L. Schiffman
Woodland G. Schockley
Marshall L. Silver
Glen S. Tarbox
G. R. Thiers
D. D. Treadwell
Charles R. Ullrich
J. Lawrence Von Thun
R. N. Yong

PUBLICATION SERVICES DEPARTMENT

David Dresia, *Director, Publications Production and Marketing*

Technical and Professional Publications

Richard R. Torrens, *Manager*
Chuck Wahrhaftig, *Chief Copy Editor*
Linda Ellington, *Copy Editor*
Thea C. Feldman, *Copy Editor*
Meryl Mandle, *Copy Editor*
Joshua Spieler, *Copy Editor*
Shiela Menaker, *Production Co-ordinator*
Richard C. Scheblein, *Draftsman*

Information Services

Elan Garonzik, *Editor*

PERMISSION TO PHOTOCOPY JOURNAL PAPERS

Permission to photocopy for personal or internal reference beyond the limits in Sections 107 and 108 of the U.S. Copyright Law is granted by the American Society of Civil Engineers for libraries and other users registered with the Copyright Clearance Center, 21 Congress Street, Salem, Mass. 01970, provided the appropriate fee is paid to the CCC for all articles bearing the CCC code. Requests for special permission or bulk copying should be addressed to the Manager of Technical and Professional Publications, American Society of Civil Engineers.

CONTENTS

Laboratory Study of Hydraulic Fracturing

by Gary W. Jaworski, James M. Duncan, and H. Bolton Seed 713

Hydroconsolidation Potential of Palouse Loess

by Gary T. Lobdell 733

Caissons Socketed in Sound Mica Schist

by Demetrious C. Koutsoftas 743

Prediction of Movements for Braced Cuts in Clay

by Abdulaziz I. Mana and G. Wayne Clough 759

Soil-Steel Structure Response to Live Loads

by Baidar Bakht 779

Cemented Sands under Static Loading

*by G. Wayne Clough, Nicholas Sitar, Robert C. Bachus,
and Nader Shafii Rad* 799

Stability of Loaded Footings on Reinforced Soil

by Joe O. Akinmusuru and Jones A. Akinbolade 819

This Journal is published monthly by the American Society of Civil Engineers. Publications office is at 345 East 47th Street, New York, N.Y. 10017. Address all ASCE correspondence to the Editorial and General Offices at 345 East 47th Street, New York, N.Y. 10017. Allow six weeks for change of address to become effective. Subscription price to members is \$16.00. Nonmember subscriptions available; prices obtainable on request. Second-class postage paid at New York, N.Y. and at additional mailing offices. GT.

The Society is not responsible for any statement made or opinion expressed in its publications.

DISCUSSION

Proc. Paper 16281

In Situ Test by Flat Dilatometer,* by Silvano Marchetti (Mar., 1980).	
<i>by John H. Schmertmann</i>	831
<i>closure</i>	832
In-Situ Volume-Change Properties by Electro-Osmosis—Evaluation,*	
by James K. Mitchell and Sunirmal Banerjee (Apr., 1980).	
<i>by Ian W. Johnston</i>	837
<i>closure</i>	840

INFORMATION RETRIEVAL

The key words, abstract, and reference "cards" for each article in this Journal represent part of the ASCE participation in the EJC information retrieval plan. The retrieval data are placed herein so that each can be cut out, placed on a 3 × 5 card and given an accession number for the user's file. The accession number is then entered on key word cards so that the user can subsequently match key words to choose the articles he wishes. Details of this program were given in an August, 1962 article in CIVIL ENGINEERING, reprints of which are available on request to ASCE headquarters.

*Discussion period closed for this paper. Any other discussion received during this discussion period will be published in subsequent Journals.

16287 LABORATORY STUDY OF HYDRAULIC FRACTURING

KEY WORDS: Cracking (fracturing); Dams; Erosion; Hydraulic fracturing; Laboratory tests; Seepage; Soil density; Soil dynamics; Soil tests (laboratory); Tensile strength (soils); Tensile stress; Water content; Water pressure

ABSTRACT: Laboratory tests on Teton Dam soil were performed by increasing the water pressure in model bore holes and in simulated rock joints. The water pressure required to cause hydraulic fracturing was found to depend on soil density, water content, confining stress and test duration. On the basis of the test results it was hypothesized that: (1) Hydraulic fracturing is a "weak link" phenomenon, in that fracturing will occur in the least resistant soil subjected to increased water pressure; and (2) hydraulic fracturing can probably occur only in the presence of a discontinuity, within which the water pressure can act to create a wedging mechanism, thus creating tensile stresses in the soil.

REFERENCE: Jaworski, Gary W., Duncan, James M., and Seed, H. Bolton, "Laboratory Study of Hydraulic Fracturing," *Journal of the Geotechnical Engineering Division, ASCE*, Vol. 107, No. GT6, **Proc. Paper 16287**, June, 1981, pp. 713-732

16309 HYDROCONSOLIDATION AND PALOUSE LOESS

KEY WORDS: Clay mineralogy; Consolidation (soils); Consolidation tests (soils); Floods; Foundations; Loess; Soil consolidation tests; Soil moisture; Soil stability; Soil tests; Soil tests (laboratory); Subsidence; Washington

ABSTRACT: Many loessial soils are susceptible to structural collapse due to inundation or a rise in ground-water levels near hydraulic structures. These soils are often classified as unstable without adequate testing, as has been the case with a loess formation found in southeastern Washington. A study was conducted to determine if spread footing foundations on Palouse Loess would experience additional settlement due to increases in moisture contents. The physical and mineralogical properties were examined and compared to the corresponding properties of loess found in the midwestern states. Modified consolidation tests were performed on undisturbed specimens to examine the effect of initial water content on the settlement characteristics. Test results indicate that increases in moisture contents do not result in excess settlements. The type of clay cementing loessial soils appears to be the determining factor.

REFERENCE: Lobdell, Gary T., "Hydroconsolidation Potential of Palouse Loess," *Journal of the Geotechnical Engineering Division, ASCE*, Vol. 107, No. GT6, **Proc. Paper 16309**, June, 1981, pp. 733-742

16288 CAISSONS SOCKETED IN SOUND MICA SCHIST

KEY WORDS: Bond stress; Caissons; Deflection; Load distribution; Load tests (foundations); Mica; Rock (material); Skin strength; Stress

ABSTRACT: The behavior of long caissons socketed in sound mica schist is examined with an emphasis on load distribution within the socket. Load tests were conducted on 14 pairs of caissons, 24 in. (61.0 cm) or 30 in. (76.3 cm) in outside diameter and cased to the top of sound rock. Socket lengths varied between 20 ft and 30 ft (6.1 m to 9.1 m). Very high bond stresses were mobilized within the socket at very small deflections. However, the distribution of bond stress within the socket was highly nonuniform, with the maximum stresses occurring near the top of the socket. The shape of the distribution was found to be in good agreement with theoretical solutions which assume linear elastic behavior. The maximum measured bond stress within the socket was 218.3 psi (1,504 kPa), with corresponding vertical deflection of 0.029 in. (0.73 mm). At the maximum mobilized bond stress the socket was still responding in a linear elastic manner which implies that even greater bond stresses could be mobilized had the socket been subjected to greater loads.

REFERENCE: Koutsoftas, Demetrios C., "Caissons Socketed in Sound Mica Schist," *Journal of the Geotechnical Engineering Division, ASCE*, Vol. 107, No. GT6, **Proc. Paper 16288**, June, 1981, pp. 743-757

16312 MOVEMENTS OF BRACED CUTS IN CLAY

KEY WORDS: Base pressure; **Braced excavation;** Clays; **Excavation;** **Field data;** Finite element method; **Heaving;** Movement; Settlement analysis; Shear strength; **Soil stability;** Supports

ABSTRACT: A simplified method is presented for the prediction of wall and soil movements for braced excavations in soft to medium clay deposits. The method is developed by combining the results of field data performance and finite element analyses. A careful review of 130 published and unpublished case histories was carried out to select well-documented projects with similar support systems and free of unusual construction effects. The finite element analyses were directed toward the evaluation of effects of variation of soil shear strength, soil stiffness, support stiffness and system geometry. Both the field data and the finite element results show that a strong correlation exists between system movements and the factor of safety against basal heave. Based on the established behavior trends, nondimensional plots are developed for predicting maximum magnitudes and distributions of wall deflections and ground settlements as a function of the factor of safety against basal heave and the other important parameters of the soil and structural system.

REFERENCE: Mana, Abdulaziz I., and Clough, G. Wayne, "Prediction of Movements for Braced Cuts in Clay," *Journal of the Geotechnical Engineering Division, ASCE*, Vol. 107, No. GT6, **Proc. Paper 16312**, June, 1981, pp. 759-777

16316 SOIL-STEEL STRUCTURE RESPONSE TO LIVE LOADS

KEY WORDS: Backfills; Bending moments; Bridges; Culverts; Empirical equations; **Impact forces;** **Live loads;** **Soil mechanics;** **Steel structures;** Tests; **Thrust**

ABSTRACT: Various existing methods are described for predicting live load effects in conduit walls of soil-steel structures (also referred to as long-span metal culverts). Also described are three live load tests on in-service soil-steel structures. In light of the test results, the current methods are overly conservative. The test results confirm that the metallic shell undergoes little bending, especially if the conduit is circular. The impact factor is not negligible even if the depth of cover is larger than 3 ft. An improved simplified method is presented to calculate the conduit wall thrust due to live loads.

REFERENCE: Bakht, Baidar, "Soil-Steel Structure Response to Live Loads," *Journal of the Geotechnical Engineering Division, ASCE*, Vol. 107, No. GT6, **Proc. Paper 16316**, June, 1981, pp. 779-798

16319 CEMENTED SANDS UNDER STATIC LOADING

KEY WORDS: **Cementation;** Grain shapes; Laboratory tests; **Sands;** Shear strength; Slopes; Soil density; **Soil mechanics;** **Soil stability;** Soil tests; **Static loads;** Tensile strength (soils)

ABSTRACT: Cemented sands are found in many areas of the world; one of their distinguishing characteristics is their ability to stand in steep natural slopes. Large deposits are located along the California coast, and in a number of areas intense urban development has occurred near the crest of high, steep slopes. Because of the hazards posed by slope failures in the cemented sands, a test program was undertaken to define the nature of the cementation and its effect on behavior of the soils. A total of 137 laboratory compression and tension load tests were performed on undisturbed samples of naturally cemented sands and artificially prepared cemented sands. The materials exhibited friction angles similar to uncemented sands, but had a cementation strength intercept and a tensile strength. The primary cementing agents of the sands tested were silicates and iron oxides. The strength of the cemented sands were found to be a function of density, amount of cementing agent, grain shape and grain arrangement.

REFERENCE: Clough, G. Wayne, Sitar, Nicholas, Bachus, Robert C., and Rad, Nader Shafii, "Cemented Sands Under Static Loading," *Journal of the Geotechnical Engineering Division, ASCE*, Vol. 107, No. GT6, **Proc. Paper 16319**, June, 1981, pp. 799-817

16320 STABILITY OF LOADED FOOTINGS ON REINFORCED SOIL

KEY WORDS: Bearing capacity; Fibers; Footings; Laboratory tests; Reinforced earth; Reinforcing materials; Rope; Sand; Soil stability

ABSTRACT: Results are presented of laboratory-scale bearing capacity tests using a 4 in. (100 mm.) square footing on sand reinforced with strips of a rope fiber material. Each layer of reinforcement was arranged in horizontal square grids. The addition of reinforcements increased the bearing capacity of the footing on the unreinforced soil by a factor which depended on the following: the horizontal spacings between strips on each layer, the vertical spacings between layers of reinforcement, the depths above the first layer of the footing, and the number of layers. Depending on the strip arrangement, the ultimate bearing capacity improvement could be up to three times that of the unreinforced earth.

REFERENCE: Akinmusuru, Joe O., and Akinbolade, Jones A., "Stability of Loaded Footings on Reinforced Soil," *Journal of the Geotechnical Engineering Division*, ASCE, Vol. 107, No. GT6, **Proc. Paper 16320**, June, 1981, pp. 819-827

U.S. CUSTOMARY-SI CONVERSION FACTORS

In accordance with the October, 1970 action of the ASCE Board of Direction, which stated that all publications of the Society should list all measurements in both U.S. Customary and SI (International System) units, the following list contains conversion factors to enable readers to compute the SI unit values of measurements. A complete guide to the SI system and its use has been published by the American Society for Testing and Materials. Copies of this publication (ASTM E-380) can be purchased from ASCE at a price of \$3.00 each; orders must be prepaid.

All authors of *Journal* papers are being asked to prepare their papers in this dual-unit format. To provide preliminary assistance to authors, the following list of conversion factors and guides are recommended by the ASCE Committee on Metrication.

To convert	To	Multiply by
inches (in.)	millimeters (mm)	25.4
feet (ft)	meters (m)	0.305
yards (yd)	meters (m)	0.914
miles (miles)	kilometers (km)	1.61
square inches (sq in.)	square millimeters (mm ²)	645
square feet (sq ft)	square meters (m ²)	0.093
square yards (sq yd)	square meters (m ²)	0.836
square miles (sq miles)	square kilometers (km ²)	2.59
acres (acre)	hectares (ha)	0.405
cubic inches (cu in.)	cubic millimeters (mm ³)	16,400
cubic feet (cu ft)	cubic meters (m ³)	0.028
cubic yards (cu yd)	cubic meters (m ³)	0.765
pounds (lb) mass	kilograms (kg)	0.453
tons (ton) mass	kilograms (kg)	907
pound force (lbf)	newtons (N)	4.45
kilogram force (kgf)	newtons (N)	9.81
pounds per square foot (psf)	pascals (Pa)	47.9
pounds per square inch (psi)	kilopascals (kPa)	6.89
U.S. gallons (gal)	liters (L)	3.79
acre-feet (acre-ft)	cubic meters (m ³)	1,233

LABORATORY STUDY OF HYDRAULIC FRACTURING

By Gary W. Jaworski,¹ A. M. ASCE, James M. Duncan,² M. ASCE,
and H. Bolton Seed,³ F. ASCE

INTRODUCTION

The Independent Panel to Review the Cause of the Failure of Teton Dam defined hydraulic fracturing as "the condition leading to the creation and propagation of a thin physical separation in a soil or rock mass due to high fluid pressures." This phenomenon was identified by the panel as one of the possible causes of the failure of Teton Dam, and it is the known or suspected cause of excessive leakage in other dams. Hydraulic fracturing has been responsible for the loss of drilling fluids from boreholes and for the rupturing of soil and rock foundations during grouting.

At the present time, this phenomenon is understood qualitatively to some extent, but there is no established procedure for evaluating the safety of an embankment or any other type of soil mass against hydraulic fracturing. At the present state-of-the-art, the only reliable approach for dam design is to incorporate defensive design features (self-healing filters and wide transition zones) so that if hydraulic fracturing should occur, it would not lead to loss of the dam. There is no quantitative procedure currently available to determine whether an existing dam which lacks the necessary filter and transition zones is safe against hydraulic fracturing, although qualitative and semiquantitative assessments can be extremely helpful in this regard.

The investigations described in the following pages were performed for the purpose of developing an improved understanding of the mechanics of hydraulic fracturing around boreholes, clarifying the influence of some of the factors which affect the water pressure at which hydraulic fracturing will occur, and attempting to relate the results of borehole fracturing tests to conditions which may promote hydraulic fracturing in the cores of embankment dams.

¹Asst. Prof. of Civ. Engrg., Univ. of New Hampshire, Durham, N.H. 03824.

²Prof. of Civ. Engrg., Univ. of California, Berkeley, Calif. 94720.

³Prof. of Civ. Engrg., Univ. of California, 440 Davis Hall, Berkeley, Calif. 94720.

Note.—Discussion open until November 1, 1981. To extend the closing date one month, a written request must be filed with the Manager of Technical and Professional Publications, ASCE. Manuscript was submitted for review for possible publication on September 24, 1980. This paper is part of the Journal of the Geotechnical Engineering Division, Proceedings of the American Society of Civil Engineers, ©ASCE, Vol. 107, No. GT6, June, 1981. ISSN 0093-6405/81/0006-0713/\$01.00.

FIELD EXPERIENCES

Excessive leakage attributable to hydraulic fracturing in embankment dams has been reported at Hyttejuvet Dam in Norway (9), low-level flood control dams in Oklahoma and Mississippi (13), Stockton Creek Dam, Wister Dam, Yard's Creek Upper Reservoir Dam (12), Balderhead Dam (15), and Teton Dam (6). In each of these cases, although it has not been possible to prove by direct observation that hydraulic fracturing has been responsible for excessive leakage or failure, an overwhelming amount of evidence has been accumulated to indicate that this could, in fact, have occurred. Other mechanisms have also been proposed in many of these cases, and it is important to recognize that hydraulic fracturing is by no means the only possible explanation of the leakage which has occurred. Nevertheless, it is a realistic possibility in most of the cases cited.

Field performance records clearly show that sudden increases in leakage through dams, following small increases in the reservoir level, have occurred in a number of instances where high reservoir pressures occur in zones of relatively low earth pressures. Often these occurrences are associated with rapid first filling of the reservoir. In dams where hydraulic fracturing is believed to have been a cause of such leakage, complete failure has been avoided only if the dam had filters capable of preventing erosion of the core during flow through a fracture.

PREVIOUS FIELD AND LABORATORY TESTS

A number of investigators have performed in-situ hydraulic fracturing tests (1,2,6,7,11,14) by increasing the water pressure in either open boreholes or piezometers. A review of all these tests shows clearly that hydraulic fracturing can readily be induced in boreholes. The pressure required to cause hydraulic fracturing is highly variable, however, and it depends on: (1) The in-situ stresses; (2) the rate at which the water pressure is increased; (3) the deformation and strength characteristics of the soil; (4) the shape of the borehole or piezometer; and (5) the method used to create the borehole or place the piezometer in the ground. Unfortunately, the separate effects of each of these factors cannot be effectively evaluated from the results of in-situ tests.

Laboratory investigations into the phenomenon of hydraulic fracturing have been conducted by Haimson (4) and Nobari, et al. (10). Haimson (4) conducted borehole hydraulic fracturing tests on rock and found that in impermeable rock, with the minor principal stress normal to the axis of the borehole, the pressure required to cause hydraulic fracturing was equal to the sum of the tensile strength of the rock and twice the minor principal stress. It was found that, in permeable rock, the pressure required to cause fracturing could not be predicted with certainty; however it was always greater than the minor principal stress but less than that required to cause fracturing in impermeable rock.

Nobari, et al. (10) studied the failure mode, the orientation of the fracture plane, and the manner in which failure progressed during hydraulic fracturing. It was concluded that hydraulic fracturing occurs through tensile fracture on the plane of the minor principal stress. The tensile strength of soil was found to resist fracturing, but typical tensile strength values are so small that tensile strength would have a negligible effect on the possibility of fracturing in a

dam more than 15 m high. It was also found that under conditions of more uniform stress, hydraulic fracturing begins at a point of low effective stress and propagates only as the soil stresses at neighboring points are reduced or the water pressure is increased, indicating that hydraulic fracturing in soil does not involve the rapid propagation of cracks associated with cracking in some materials like glass and rock.

LABORATORY BOREHOLE FRACTURING TESTS

In order to gain an improved understanding of the mechanics of hydraulic fracturing around boreholes, a number of borehole fracturing tests were performed in the laboratory to study the development of fractures under conditions where

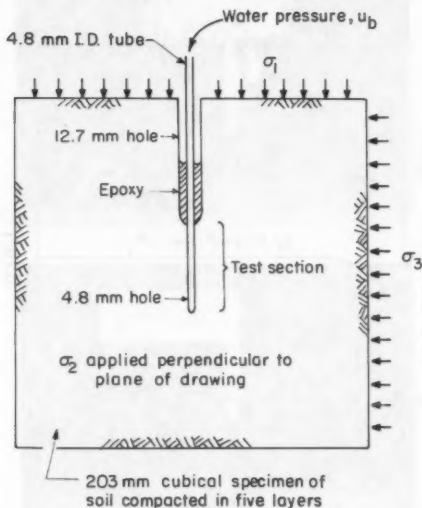


FIG. 1.—Laboratory Test of Hydraulic Fracturing around Model Borehole

the stresses could be controlled accurately, the effects of soil variability could be minimized, and the condition of the soil could be examined after fracture occurred.

For this purpose 20.3-cm (8-in.) cubical soil samples were placed in a cubical stress apparatus where three independent perpendicular stresses could be applied to the faces as shown in Fig. 1. A 0.48-cm (3/16-in.) diam uncased borehole, 5.1 cm (2 in.) long, drilled in the center of the sample, was sealed at the top with an epoxy plug, and water pressure was then applied to the walls of the borehole through a steel tube cemented into the epoxy. The rate at which water flowed into the sample was determined with a timer and a volume change device. Water dyed with rhodamine W.T. was used for the fracturing fluid, so that the resulting stains in the soil could be used to determine the orientation and

extent of the fracture plane following a test. A complete description of this equipment has been given by the first writer (8).

The material used in the experimental study was derived from undisturbed block samples obtained from the core of the remainder of Teton Dam after its failure. This material consisted primarily of ML aeolian silts, with small particles of caliche. The liquid limits of the samples tested varied from 28 to 32, and the plasticity index varied from 3 to 6. Both undisturbed and recompacted block samples were used.

The samples were trimmed or compacted to form 19-cm (7.5-in.) cubes. The samples were then placed in the 20.3-cm (8-in.) cubical stress apparatus, and the remaining gap around the sample was filled with compacted soil of the same origin which passed the No. 8 sieve. This procedure insured a uniform

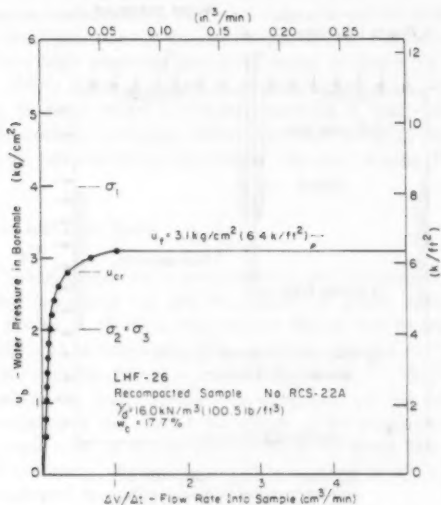


FIG. 2.—Typical Result of Borehole Hydraulic Fracturing Test

fit of the sample in the cubical stress apparatus. The stresses applied to the sample were such that the major principal stress, σ_1 , was equal to twice the minor principal stress, σ_3 . With the exception of one test, the intermediate principal stress, σ_2 , was always equal to σ_3 . The direction of σ_1 was always parallel to the axis of the borehole (vertical) and perpendicular to the compaction planes.

The results of a typical test are shown in Fig. 2. As the water pressure in the borehole was increased, the flow rate from the hole increased. During the early stages of the test the flow rate increased roughly in proportion to borehole water pressure. As the fracturing pressure, u_f , was approached, the flow rate increased very rapidly with little or no increase in pressure. At this stage, water ran from the corners of the cubical cell, indicating that fracture

had resulted in the development of a direct hydraulic connection between the borehole and the margins of the sample. Fractures found in samples after disassembly of the cell are shown in Fig. 3.

Test results of this type are very similar to those obtained in field tests and indicate that the process of hydraulic fracturing around model boreholes in the laboratory is substantially the same as in the field. Thus, it would appear that tests of this type can be useful for studying the factors which control the phenomenon more readily than would be possible in the field.

Tests on Undisturbed Samples of Teton Dam Soil.—The results of three similar tests on undisturbed samples of Teton Dam soil are shown in Fig. 4.



FIG. 3.—Examples of Irregular Fracture Surfaces

Despite the fact that all of the tests were performed on soil from the same controlled fill, using the same values of σ_1 , σ_2 , and σ_3 , the water pressures required to cause fracturing varied considerably—from 2.8 kg/cm² in Test HF-6 to 5.5 kg/cm² in Test HF-2. Extensive study of the possible reasons for these widely differing results indicated that they were not caused by equipment problems or other experimental errors. It was concluded that the variations in results must arise from differences in the compositions, the densities, the water contents of the undisturbed block samples, or any combination of the three. Particles of caliche as large as 4 cm (1.5 in.) were found in some of the undisturbed samples, and it was decided to use recompacted samples in subsequent tests to minimize the effects of sample variability.

These results indicate that the hydraulic fracturing pressure measured in field tests will also be influenced to an important extent by variations in composition, density, and water content, as well as by variations in the magnitudes of the stresses from place to place in the embankment. However, because of what may be termed the "weak link effect," variations of hydraulic fracturing pressure measured in the field would not scatter as widely as those measured in the laboratory, due to the difference in the volume of soil influenced by laboratory and field tests. For example, consider that a borehole in the field (which might be 4 in. in diameter, with a 10-ft long test section) extended through three zones where the conditions of the soil were those of the three block samples tested in Tests HF-2, HF-3, and HF-6. When the water pressure was increased, fracturing would have begun at $u_f = 2.8 \text{ kg/cm}^2$, the value required to cause

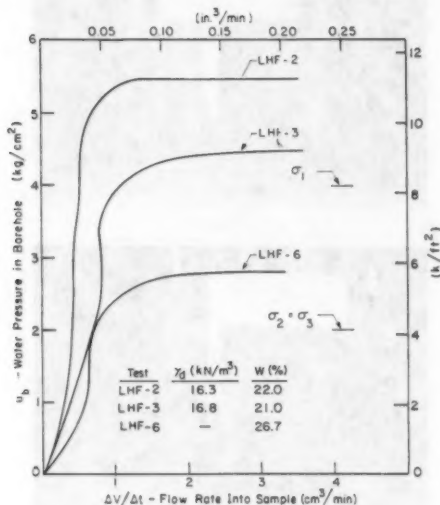


FIG. 4.—Results of Borehole Hydraulic Fracturing Tests on Undisturbed Block Samples

fracturing in Test HF-6. The fracturing pressure measured would thus be 2.8 kg/cm^2 , not the higher values. In either the laboratory or the field, the fracturing pressure measured will be that of the weakest or least resistant soil affected by the test. Because field tests influence larger volumes of soil, it is to be expected that the average fracturing pressure in the field will be lower than in the laboratory. However, the lower bound value of fracturing pressure from field and laboratory tests would be expected to be the same, provided a sufficient number of tests of both types were performed.

Effects of Composition, Water Content, and Density.—In order to eliminate some of the sources of variation involved in using undisturbed block samples in their natural states, a number of samples were remolded and recompacted,

using the same compaction procedure for each sample. The samples were compacted in five layers with a California kneading compactor. Each layer was compacted by 28 blows of a rectangular tamper with a foot pressure of 0.7 kg/cm^2 .

Two groups of tests (I and II) were performed using different batches of Teton Dam soil prepared by remolding and recompacting block samples. As soil was lost or used for water content or Atterberg limit testing, it was replaced

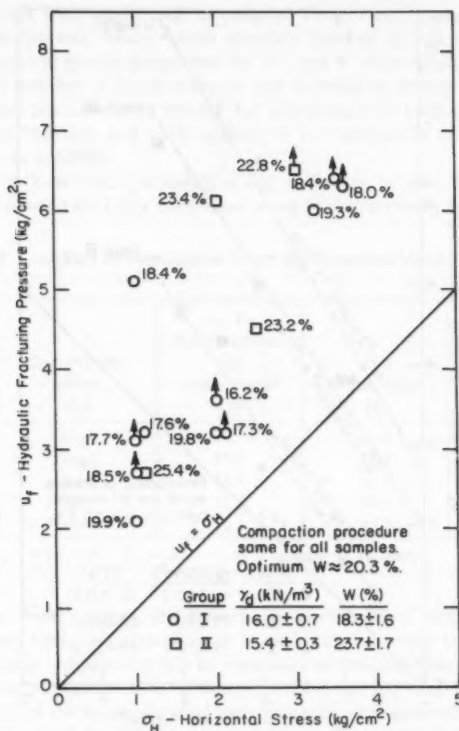


FIG. 5.—Hydraulic Fracturing Tests on Recompacted Samples of Teton Dam Soil (Groups I and II)

with additional soil from other block samples. Thus, there was some variation in composition from test to test in each group. The composition of the Group I samples was distinctly different from that of the Group II samples, being a completely separate batch. Compaction water contents for the Group I samples were about 2% dry of optimum, while those for Group II were about 3% wet of optimum, but all samples were compacted to about the same dry density

as the undisturbed block samples. The actual water contents of all samples are noted in Fig. 5.

The results for the Group I and Group II tests are shown in Fig. 5, where the measured values of hydraulic fracturing pressure, u_f , are plotted against the values of σ_H , the horizontal confining pressure, used in the tests. In all of the tests, the horizontal stresses were the same in both directions, and were equal to half the vertical stress. It may be seen that all the measured values

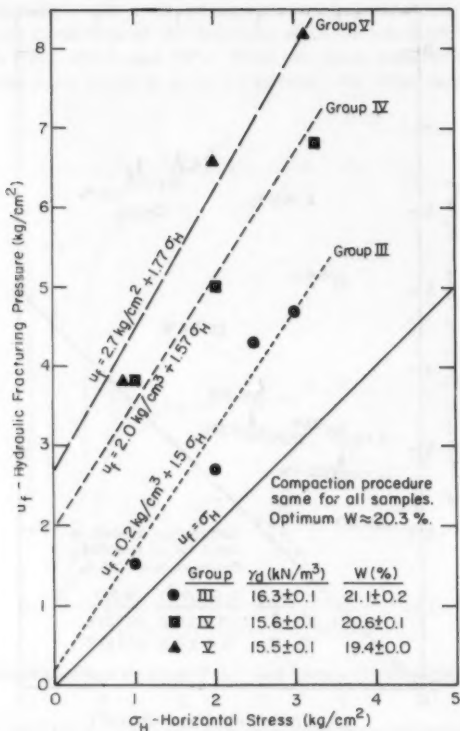


FIG. 6.—Hydraulic Fracturing Tests on Recomacted Samples of Teton Dam Soil (Groups III, IV, V)

of u_f plot above the line for $u_f = \sigma_H$, and that there is considerable scatter in the data. Examination of these results led to the following tentative conclusions:

I. Variations in soil composition have a more important effect on hydraulic fracturing pressure than do variations in density or water content in these tests. This accounts for the fact that the values of u_f measured in the Group II tests are generally higher than those measured in the Group I tests, although

the average water content was considerably lower for the Group I samples.

2. For samples with the same composition and density, measured values of u_f are usually higher for samples having lower water contents.

3. Variations in density did not have a consistent effect on the measured values of u_f . As will be examined later, this was undoubtedly due to the fact that all of the samples were prepared using the same compactive effort, and the variations in density were small.

Additional tests were performed to examine further the dominant effect of composition on the test results. three separate batches of soil were prepared for testing samples in groups designated III, IV, and V. Each batch was prepared by remolding a number of block samples and thoroughly mixing the soil, then separating it into portions large enough for preparation of cube samples. Thus the composition, density, and water content of the samples in each group were as nearly alike as possible.

The results of these tests are shown in Fig. 6. It may be seen that the results for each group of tests are fairly consistent owing to the relatively small variations

TABLE 1.—Effect of Compactive Effort on Measured Values of u_f

Test number (1)	Compactive effort (2)	γ_d , in kilonewtons per cubic meter (3)	w, as a percentage (4)	u_f , in kilograms per square centimeter (5)
LHF-7	High	17.7	14.9	>6.9
LHF-10	High	17.0	17.1	4.5
LHF-12	Low	15.8	17.3	3.1
LHF-19	Low	15.6	16.2	3.3
LHF-22	Low	16.1	19.8	3.4

Note: $\sigma_v = \sigma_1 = 4 \text{ kg/cm}^2$; $\sigma_H = \sigma_2 = \sigma_3 = 2 \text{ kg/cm}^2$ in all tests.

in composition, water content, and density: For each group of tests the measured values of u_f vary fairly consistently with σ_H and increase as the lateral confining pressure increases. Apparently due to variations in composition, water content, and density, the variations of u_f with σ_H are different for each group of tests. Although values of the hydraulic fracturing pressure were generally substantially greater than the total lateral pressure (or total minor principal stress) acting across the surface on which fracturing ultimately developed, the lowest values, which by the weak link theory might control the onset of hydraulic fracturing, exceeded the lateral pressure across the fracturing face by only about 0.6 kg/cm^2 .

The effect of using greater compactive effort was examined by performing two tests on samples compacted using higher tamping pressures and more blows per layer than in previous tests. These results are summarized in Table 1. In spite of the scatter among the results due to variations in composition and water content, it seems clear that higher compactive effort (and higher dry density) leads to higher fracturing pressures.

Effect of Tensile Strength.—Because the mechanism of hydraulic fracturing

is formation of a tensile fracture through the soil, it might be expected that greater resistance to hydraulic fracturing would be due to higher tensile strength of the soil. One simple theory of hydraulic fracturing (see Ref. 8), indicates that

$$u_f \approx \sigma_H + \frac{\sigma_t}{2} \quad (1)$$

in which u_f = fracturing pressure in a borehole; σ_H = horizontal total stress; and σ_t = tensile strength. This theory is based on an elastic analysis of changes in stress around the borehole and the assumption that failure occurs when the tensile stress in the soil becomes equal to the tensile strength. It indicates that the difference between the fracturing pressure and the initial horizontal stress should be one-half the tensile strength of the soil.

Tensile strengths were measured for four samples using the Brazilian tensile test. The measured values of tensile strength are compared to the differences between u_f and σ_H shown in Table 2. It may be seen that the measured values of $u_f - \sigma_H$ are considerably greater than the measured values of σ_t in all four

TABLE 2.—Comparison of Differences between Fracturing Pressure and Horizontal Stress with Measured Values of Tensile Strength

Test number (1)	$(u_f - \sigma_H)$, in kilograms per square centimeter (2)	σ_t , in kilograms per square centimeter (3)
LHF-2	3.5	0.15
LHF-7	5.8	0.17
LHF-12	1.2	0.09
LHF-15	2.9	0.10

tests. Thus, the differences between horizontal stress and fracturing pressure cannot be explained by tensile strength, at least using the simple theory expressed in Eq. 1.

Other theories for computing the water pressure required to cause hydraulic fracturing (see Ref. 14), lead to equations of the form

$$u_f = m\sigma_H + \sigma_t \quad (2)$$

in which m = a factor depending on the manner in which the stresses redistribute themselves around a borehole and on the total stress path for the soil. Depending on the conditions, Vaughan suggested that m might vary between 1 and 2. The results of this study seem to be in general agreement with this approach, with values of m ranging between about 1.5 and 1.8 for the various samples tested. It should be noted, however, that on the basis of the weak link theory, a lower value of m would be more representative of field conditions.

Effect of Test Duration.—Two tests were performed in which the borehole water pressure was raised slowly, so that failure occurred after a period of days rather than hours. The results of these tests are shown in Fig. 7. It may

be seen that the fracturing pressures in these tests, which lasted 9 days and 12 days, are higher than those in tests lasting 3 h-4 h. This effect may be due to differences in the extent of the zone of seepage which developed over a longer period of time. The values of permeability calculated from the rates of inflow during the tests varied from 0.9×10^{-4} cm/s- 1.2×10^{-6} cm/s. It was difficult to determine whether there was a correlation between the permeabilities of the samples and the hydraulic fracturing pressures, owing to difficulties in isolating the effects of density and water content.

Effect of Preexisting Fracture.—In Fig. 8 results are shown for a test on an undisturbed sample of Teton Dam soil in which the water pressure was increased to cause fracturing, then reduced to atmospheric pressure. After a period of 24 h, during which the externally applied lateral pressures were

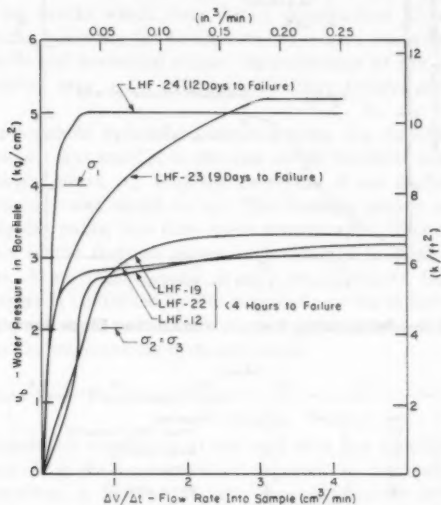


FIG. 7.—Effect of Duration of Tests

maintained, the borehole water pressure was again increased to cause refracturing. It may be seen that although the initial value of the water pressure required to cause fracturing was 5.5 kg/cm^2 , refracturing occurred when the water pressure reached a value equal to the minor principal stress, indicating that only this stress was available on the previous plane of separation to prevent fracturing from recurring. In other words, where a crack exists in the soil before water pressure is introduced, the value of m in Eq. 2 becomes equal to unity and $\sigma_t = 0$.

A second refracturing test was performed on a recompacted sample from the Group I series of tests. The results from this test are shown in Fig. 9. Initially, the sample was found to have fractured at a borehole water pressure of 3.2 kg/cm^2 with the horizontal stress equal to 1.0 kg/cm^2 . The borehole

water pressure was then reduced to atmospheric pressure, and the horizontal stress was increased to 2.0 kg/cm^2 . This procedure was considered to roughly simulate a crack formed during construction and then subjected to higher pressures

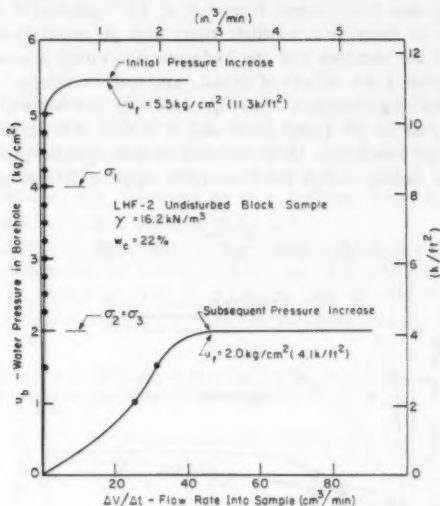


FIG. 8.—Refracturing Test on Undisturbed Block Sample

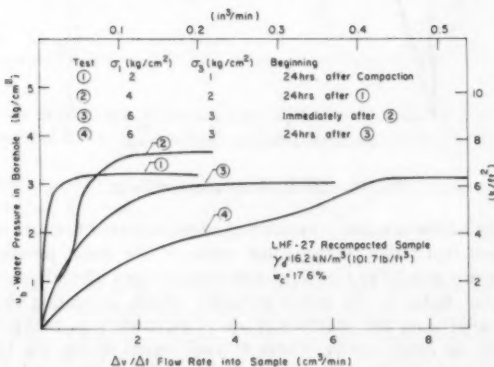


FIG. 9.—Refracturing Sample after Increasing Confining Pressures

as additional fill is placed. After the sample had remained at this higher pressure overnight, the borehole water pressure required to cause hydraulic fracturing was found to be 3.7 kg/cm^2 . The borehole water pressure was then reduced

to atmospheric pressure and the horizontal stress was increased to 3.0 kg/cm^2 . Immediately following this, the borehole water pressure was incrementally increased to cause hydraulic fracturing, which was found to occur when the borehole water pressure was equal to the horizontal stress. The borehole water pressure was returned to atmospheric pressure and the sample remained in the cubical stress apparatus overnight with the horizontal stress at 3.0 kg/cm^2 . The following day the borehole water pressure was incrementally increased, and it was found that the pressure required to cause hydraulic fracturing was again equal to the horizontal stress.

The results of these tests show that the presence of an existing crack in a soil substantially reduces the hydraulic fracturing pressure. However, the results also indicate that if stresses are increased after a crack has formed, the crack may heal to some extent over a period of time. This is an important consideration for cracks which form during construction. Cracks which form after construction, however, can be expected to reopen when the water pressure becomes equal to the horizontal stress. Determination of the conditions under which such healing may occur offers a potentially fruitful avenue for further investigation.

In all of the borehole hydraulic fracturing tests, the direction of the major principal stress, σ_1 , was parallel to the axis of the borehole and equal to twice the minor principal stress, σ_3 . With the exception of one test, the intermediate principal stress, σ_2 , was equal to σ_3 . The fracture planes usually followed somewhat irregular paths, but they were always approximately vertical with the orientations of the fracture planes most often across the diagonal of the cubical sample. From these results, it may be concluded that the hydraulic fracturing pressure is controlled by the magnitude of the minor principal stress, though the orientation of the fracture plane may be influenced to some extent by the value of the intermediate principal stress.

LABORATORY "ROCK JOINT" FRACTURING TESTS

In order to simulate conditions at the wall of a key trench in jointed rock, where the backfill might be compacted adjacent to the trench wall without an intervening filter, a number of tests were performed in which soil was compacted into the cubical test cell with a slot on one side simulating a rock joint $1/2$ in. wide and 4 in. high. Subsequently, the water pressure in the "joint" was increased to cause fracturing.

As shown in Fig. 10, attempts to compact the soil adjacent to the open slot or joint led to the formation of a loose zone of soil in this region. When water under pressure was introduced into the slot, it quickly penetrated the loose zone and acted to wedge the soil apart and cause hydraulic fracturing. As shown in the lower part of Fig. 10, fracturing did occur at a water pressure (u_f) which exceeded the value of σ_3 by 1.4 kg/cm^2 . This is within the range of values measured in the borehole fracturing tests. The observed fracture coincided with the loose zone adjacent to the simulated rock joint and followed the σ_3 plane across the sample. Similar failures were found in other tests where similar discontinuities were created on the side of a test sample.

In another rock joint test it was found that when water was introduced into the simulated rock joint, the loose soil sloughed into the joint, as shown in

Fig. 11. The size of the sloughed zone increased progressively, eventually involving well-compacted as well as poorly-compacted soil, and working its way inward and up to the top of the sample. This observation seems quite significant, because it indicates that the size of a discontinuity resulting from a rock joint can be many times the dimensions of the joint if the soil sloughs as shown in Fig. 9. Clearly not all soils will be vulnerable to sloughing in

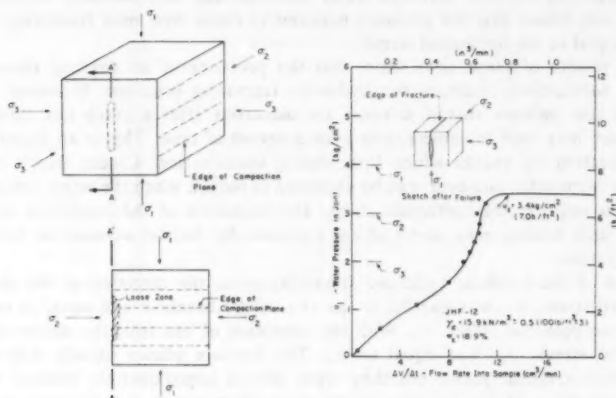


FIG. 10.—Joint Hydraulic Fracturing Test Conditions and Result

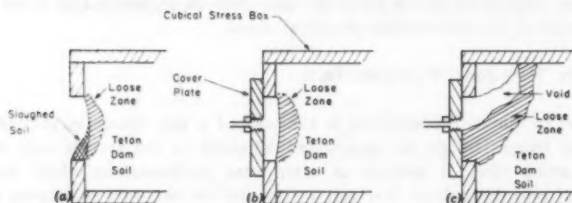


FIG. 11.—Sloughing Adjacent to Simulated Rock Joint: (a) After Compaction; (b) Start of Test; (c) After Test

this way, but some samples of the aeolian silt which formed the core of Teton Dam have this characteristic.

LABORATORY "TRANSITION ZONE" FRACTURING TESTS

The observations made during the testing program lead to the hypothesis that hydraulic fracturing can occur only if there is some discontinuity, such as a borehole or a loose zone adjacent to a rock joint, within which the water pressure can act to develop tension in the soil by wedging action. If this hypothesis is correct, hydraulic fracturing should not occur where water pressure impinges

on a flat face of homogeneous soil, no matter how high the water pressure might become.

As a final phase of the experimental program, tests were conducted to examine this hypothesis and the potential for hydraulic fracturing when water pressures are applied to a uniformly compacted and continuous face of core material in an earth dam. These tests were intended to simulate conditions at the upstream

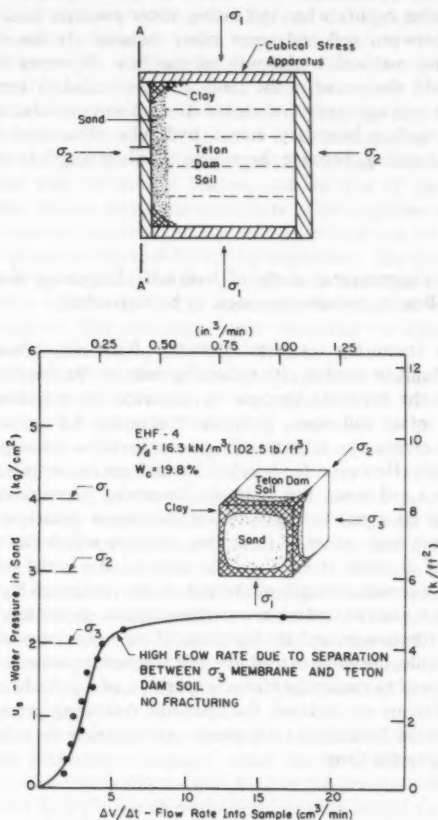


FIG. 12.—Transition Zone Hydraulic Fracturing Test Conditions and Results

face of the core of a dam, adjacent to a filter zone. As shown in Fig. 12, the filter material was sand. A plastic clay was used as a seal between the sand and the faces of the box. The results of this test are shown in Fig. 12. As the water pressure was increased, leakage developed between the sample and the side of the cubical cell soon after the water pressure reached the value

of σ_3 , but no fracturing occurred in the soil. Because the water pressure in this test was not much higher than σ_3 when leakage developed at the sides of the test specimen, the result shown in Fig. 12 neither proves nor disproves the hypothesis that a discontinuity and wedging action are necessary for hydraulic fracturing to develop.

The test results shown in Fig. 12, however, demonstrate a phenomenon which may be termed "hydraulic separation." Closely related to hydraulic fracturing, hydraulic separation occurs when increasing water pressure leads to separation at a boundary between soil and some other material. In the case shown in Fig. 12, the other material is the wall of the box. It seems likely that this phenomenon could also occur in the field, along a boundary between soil and rock, or between soil and structural materials such as concrete, steel, or wood. In cases where such a boundary exists, hydraulic separation is more likely than hydraulic fracturing, because there is no tensile strength to resist hydraulic separation.

CONCLUSIONS

Based on the experimental study of hydraulic fracturing described in the preceding, the following conclusions seem to be warranted:

1. In borehole fracturing tests the hydraulic fracturing pressure is highly variable and difficult to predict. Its value depends on the localized conditions in the soil which the borehole happens to penetrate. It was observed that for a homogeneous, intact soil mass, hydraulic fracturing did not occur until the borehole water pressure was substantially greater than the minor principal stress around the borehole. However, for boreholes which encounter preexisting cracks or weaknesses in a soil mass, the hydraulic fracturing pressure is substantially reduced and may be equal to the value of the minor principal stress acting in the soil. The minimum value of fracturing pressure which can be anticipated in the absence of a crack is equal to the sum of the initial minor principal total stress and the tensile strength of the soil. However, much higher fracturing pressures may be measured under some circumstances, depending on the extent of pressure redistribution around the borehole. If the behavior of the soil around the borehole is ductile, the value of the hydraulic fracturing pressure may approach the pressure required to cause the plastic expansion of a cylindrical cavity.

2. If all other factors are isolated, the hydraulic fracturing pressure is a linear function of the initial horizontal total stress. An equation describing the linear function would have the form

$$u_f = m\sigma_H + \sigma_{ta} \quad (3)$$

in which σ_{ta} = the apparent tensile strength of the soil available to resist cracking at the fracture pressure; m = the slope of the linear function of fracture pressure with horizontal stress; and σ_H = the minor principal total stress prior to the advancement of the borehole. The slope of the linear function and its intercept at zero horizontal stress appears to be dependent primarily on the strength of the material and the manner in which stresses redistribute themselves as a result of decreasing effective stress.

3. The values of m for different groups of samples tested varied about 1.5–1.8.

It is believed that these values are primarily dependent on the manner in which stresses redistribute themselves around the borehole, as proposed by Vaughan (14). According to Vaughan's criteria, the values of m may vary from 1 to 2 and they may be determined if the total stress path is known. For the case of a preexisting crack formed after construction, a minimum value of unity may be anticipated.

4. The values of σ_{ta} in Eq. 3, which were determined from the borehole hydraulic fracturing tests, varied from 0.2 kg/cm^2 – 2.7 kg/cm^2 . These apparent tensile strengths are, in general, much larger than values of tensile strength measured in indirect split tensile strength tests. However, it is believed that besides the actual tensile strength of the soil, the values of σ_{ta} also reflect the special conditions inherent in a borehole fracturing test, and the effects of stress redistribution. Thus, σ_{ta} is referred to as an apparent tensile strength. Haimson (4) showed that the tensile strength of the rock measured under these conditions varied with the rate of loading and the size of the borehole. It is possible that other factors could also contribute to this apparent tensile strength. The maximum value of apparent tensile strength which can be anticipated will be equal to the pressure required for cavity expansion. The minimum apparent tensile strength to be expected is zero, which was measured for samples with preexisting cracks, and for hydraulic separation between the soil and the wall of the test apparatus. The minimum value measured for intact samples was about 0.2 kg/cm^2 for the Group III series of tests.

5. For the 25 samples tested in this program, the minimum value of the hydraulic fracturing pressure observed was equal to the value of the minor principal stress plus 0.6 kg/cm^2 . Presumably somewhat lower values than this might be anticipated for the same soil under field conditions.

6. The significance of various soil parameters was not sufficiently isolated in the experimental study to determine the individual effects of each, although the results show clearly that the pressure at which hydraulic fracturing occurs is significantly affected by changes in water content and compactive effort. Presumably, this occurs because of changes in the strength and deformation characteristics of the soil as the compaction conditions are changed.

7. Hydraulic fracturing could readily be induced in soil samples which were compacted adjacent to an open slot, in the compaction mold, due to the fact that the soil adjacent to the slot was in a loose condition and permitted the entry of water under pressure so that a wedging action, similar to that in a borehole, could develop.

8. Teton Dam core material is particularly vulnerable to the type of fracturing described in the preceding paragraph, since soil in a loose zone adjacent to a slot or joint is also vulnerable to sloughing in the presence of water, thereby creating a sizeable cavity in which water pressures can develop a wedging action.

Based on the observations made during the tests and inferences from these, the following are suggested as useful tentative hypotheses relating to the occurrence of hydraulic fracturing:

1. Hydraulic fracturing is a "weak link" phenomenon in the sense that fracturing will develop at the point of least resistance. The larger the zone affected by the water pressure, the lower is likely to be the pressure required

to cause fracturing, all other conditions being equal. This is because the larger the affected zone, the more likely it is to contain an area of weakness.

2. Hydraulic fracturing is promoted by, and may, in fact, require the presence of a discontinuity, such as a borehole, an existing crack, or loose soil adjacent to a rock joint, within which the water pressure can act to develop tensile stresses through a wedging action in the soil. Although it cannot be proven conclusively at present, that such a discontinuity is required for hydraulic fracturing, no instances of hydraulic fracturing have been observed in the absence of such discontinuities.

3. Hydraulic separation can occur at an interface between soil and an adjacent dissimilar material such as concrete or rock as soon as the water pressure reaches the same magnitude as the normal stress across the interface. Hydraulic separation is not resisted by tensile resistance.

4. It appears that the mechanism by which hydraulic fracturing occurs requires that the effective stress becomes tensile and equal in magnitude to the tensile strength of the soil. However, the way in which the effective stress becomes tensile is complicated by stress redistribution which can lead to wide variations in the observed value of the fracturing pressure. An increase in pore water pressure results in three simultaneous effects: (a) The effective stresses decrease; (b) a zone of wetting is created within which pore pressures may vary; and (c) the total stresses may increase as a result of swelling, or it may decrease as a result of wetting.

5. A uniform increase in the pore water pressure in a continuous and homogeneous soil mass will not result in tensile stresses and will therefore not lead to hydraulic fracturing. The effective stress can only become tensile as a result of nonuniform changes in total stress, or water pressure, or both, and it is believed that these conditions are most likely where water pressure acts in discontinuity to split the soil through wedging action. Examples of features which produce this type of wedging action include boreholes, preexisting cracks, selective seepage paths, and zones of poor compaction adjacent to discontinuities in the foundation of a dam, such as at an open rock joint or a rock overhang.

6. Tensile stresses due to wedging only occur in a zone where the soil is subjected to extensional strains as a result of high water pressures in an adjacent discontinuity. If the water pressure increases slowly enough so that the water pressures in the adjacent soil mass also increase at the same rate as a result of seepage from the discontinuity, then the degree of wedging will be reduced. Thus, the potential for hydraulic fracturing decreases with increasing permeability and decreasing rate of reservoir filling. The effects of increasing permeability and rate of water pressure application have not been satisfactorily explained in any of the theories so far advanced for predicting the onset of hydraulic fracturing.

7. It is believed that hydraulic fracturing occurs in a borehole because of the wedging action of the water acting on the walls of the hole or the wetted zone around the hole. Without the presence of such a discontinuity, a uniform increase in the pore pressure would not provide the wedging action necessary to create a fracture. At the upstream side of an embankment dam, discontinuities along which a wedging action may develop include differential settlement cracks and selective seepage paths. However, if there are no discontinuities present, then there would be no possibility for developing this same wedging action.

Thus, the occurrence of hydraulic fracturing in boreholes is not necessarily indicative of a potential for hydraulic fracturing at the upstream face of the core of a dam.

8. It may be noted that the water pressure used to cause hydraulic fracturing around a borehole acts in an extremely small test section by comparison to the size of the dam, and the rate of pressure application may be quite different for a borehole test than the water pressure application on the core of a dam. Thus, only local stress redistribution and changes in water content can be expected to occur in borehole tests, while impoundment of a reservoir will probably cause extensive stress redistribution and changes in water content in a relatively large portion of the dam; thus the pressures required to cause fracturing during reservoir filling may be different from those observed in borehole fracturing tests for this reason. Development of an appropriate theory to take this factor into account is highly desirable.

9. The fact that the in-situ borehole fracturing tests may provide a useful indication of the potential for hydraulic fracturing in any given embankment is not sufficient reason to recommend these tests as part of a design study. The fractures induced in such tests would serve to provide discontinuities which could then facilitate hydraulic fracturing in the embankment. In any case, defensive measures against the possible effects of hydraulic fracturing should be provided in all dams, thereby eliminating the need for such studies. However, existing dams, which do not include such defensive measures, may require careful evaluation of their hydraulic fracturing potential.

ACKNOWLEDGMENT

Financial support for these studies was provided by the United States Bureau of Reclamation and the United States Army Corps of Engineers Waterways Experiment Station. The writers are grateful to Ralph Peck and Stanley J. Johnson for their helpful comments on the results and their significance.

APPENDIX.—REFERENCES

1. Bjerrum, L., and Andersen, K. H., "In-Situ Measurement of Lateral Pressures in Clay," *Proceedings of the Fifth European Regional Conference*, International Society of Soil Mechanics and Foundations Engineering, 1972.
2. Bjerrum, L., Nash, J. K. T. L., Kennard, R. M., and Gibson, R. E., "Hydraulic Fracturing in Field Permeability Testing," *Geotechnique*, London, England, Vol. 22, No. 2, June, 1972, pp. 319-332.
3. Carneiro, F. L. L., and Barcellos, A., "Tensile Strength of Concrete," *Bulletin No. 13*, The International Union of Testing and Research Laboratory for Material and Construction, Paris, France, 1953, pp. 99-125.
4. Haimson, B., "Hydraulic Fracturing in Porous and Non-Porous Rock and Its Potential for Determining In-Situ Stresses at Great Depth," *Technical Report No. 4-68*, United States Army Corps of Engineers, Missouri Division, Omaha, Neb., 1968.
5. Hvorslev, M. J., "Time Lag in the Observation of Ground-Water Levels and Pressures," United States Army Waterways Experiment Station, Vicksburg, Miss., 1949.
6. "Report to United States Department of the Interior and the State of Idaho on Failure of Teton Dam," Independent Panel to Review Cause of Teton Dam Failure, United States Bureau of Reclamation, Denver, Colo., Dec., 1976.
7. "Failure of Teton Dam, A Report of Findings," Interior Review Group, United States Dept. of the Interior, Teton Dam Failure Group, Washington, D.C., Apr., 1977.

8. Jaworski, G. W., "An Experimental Study of Hydraulic Fracturing," thesis presented to the University of California at Berkeley, Calif., in 1979, in partial fulfillment of the requirements for the degree of Doctor of Philosophy.
9. Kjaernsli, B., and Torblaa, I., "Leakage Through Horizontal Cracks in the Core of Hyttejuvet Dam," *Publication No. 80*, Norwegian Geotechnical Institute, Oslo, Norway, 1968.
10. Nobari, E. S., Lee, K. L., and Duncan, J. M., "Hydraulic Fracturing in Zoned Earth and Rockfill Dams," *Report No. TE 73-1*, Vol. 9, No. 8, Office of Research Services, Univ. of California, Berkeley, Calif., 1973, pp. 17-23.
11. Penman, A. D. M., "Earth Pressures Measured with Hydraulic Piezometers," *Ground Engineering*, London, England, Nov., 1976.
12. Sherard, J. L., "Embankment Dam Cracking," *Embankment Dam Engineering—The Casagrande Volume*, John Wiley and Sons, Inc., New York, N.Y., 1973.
13. Sherard, J. L., Decker, R. S., and Ryker, N. L., "Hydraulic Fracturing in Low Dams of Dispersive Clay," *Performance of Earth and Earth-Supported Structures*, ASCE, Vol. 1, 1972, pp. 653-689.
14. Vaughan, P. R., "The Use of Hydraulic Fracturing Tests to Detect Crack Formation in Embankment Dam Cores," *Interim Report*, Department of Civil Engineering, Imperial College, London, England, 1971.
15. Vaughan, P. R., Kluth, D. J., Leonard, M. W., and Pradowa, H. H. M., "Cracking and Erosion of the Rolled Clay Core of Balderhead Dam and the Remedial Works Adopted for Its Repair," *Proceedings, 10th International Congress on Large Dams*, Vol. 3, 1970, pp. 73-93.

HYDROCONSOLIDATION POTENTIAL OF PALOUSE LOESS

By Gary T. Lobbell,¹ A. M. ASCE

INTRODUCTION

Loessial soil found in many parts of the United States is typically considered to be unstable as a foundation material because of its potential for large settlements due to inundation or rise in ground-water levels near hydraulic structures (1,6,7,11). A substantial loess deposit covers the majority of Southeastern Washington State and parts of Northwestern Idaho. Heavy construction projects founded on this type of soil are often founded on pile or caisson foundations rather than spread footings. Because spread footings are usually less expensive than pile foundations, they are economically preferable to deep foundations.

Observations of structures built on Palouse loess at Washington State University indicate that loess of the Pullman area may possess structural characteristics different from midwest loess. Several large structures which are over 50 yr old, some of which have been inundated, show no signs of physical damage.

This paper presents the results of a study undertaken to determine if spread footing foundations on Palouse loess would experience structural collapse due to increases in moisture contents. A detailed description of Palouse loess is given to familiarize the reader with the physical and chemical characteristics of this soil. Hydroconsolidation testing was used to compare the reaction of Palouse loess under load for natural and field saturated moisture conditions.

DESCRIPTION OF PALOUSE LOESS

Geographical Distribution of Palouse Loess.—Loessial deposits cover most of southeastern Washington and extend into Idaho as shown in Fig. 1. These soils are comprised of four formations: (1) The Ritzville loess; (2) the Walla Walla loess; (3) the Nez Perce loess; and (4) the Palouse loess (3). The Palouse loess formation covers portions of Spokane, Whitman, Adams, Columbia, Asotin, and Garfield counties in Washington, and Lewis, Latah, and Nez Perce counties in Idaho (9). Thickness of the formation varies substantially because of the wind-blown nature of the material and is known to be as great as 75 ft (23 m) in depth in the Pullman area (12).

Origin of Palouse Loess.—Many theories have been presented over the years

¹Geotechnical Engr., Rittenhouse-Zeman & Assoc., Inc., Bellevue, Wash.

Note.—Discussion open until November 1, 1981. To extend the closing date one month, a written request must be filed with the Manager of Technical and Professional Publications, ASCE. Manuscript was submitted for review for possible publication on September 24, 1980. This paper is part of the Journal of the Geotechnical Engineering Division, Proceedings of the American Society of Civil Engineers, ©ASCE, Vol. 107, No. GT6, June, 1981. ISSN 0093-6406/81/0006-0733/\$01.00.

as to the origin of loess and, in particular, Palouse loess. The generally accepted theory is that it is wind-transported material of glacio-fluvial origin (5). Continental and large mountain glaciers ground bedrock to a fine powder by abrasive action. The retreat of the ice sheets left this fine material deposited on outwash plains, subject to erosion by wind and water.

Geomorphology of the Palouse hills reinforces the idea of eolian transport. The alignment of hills, thickening of deposits behind bedrock knolls, and a decrease in grain size to the northeast all indicate a southwesterly source. It

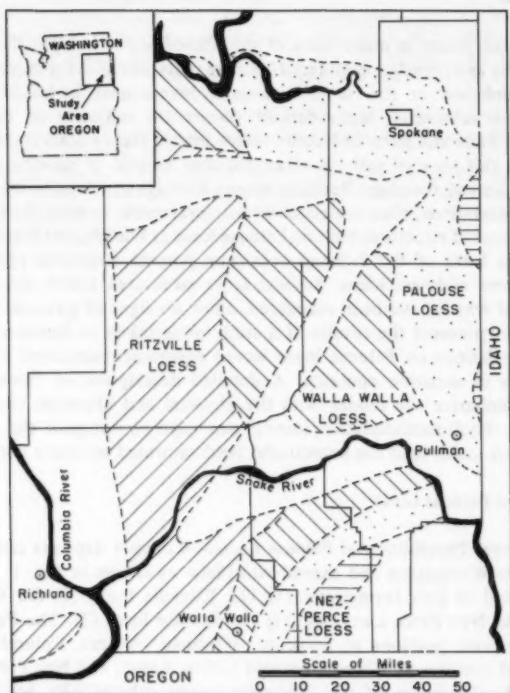


FIG. 1.—Loess Deposits in Southeastern Washington

has been suggested that the major source of the loess is the Ringold Formation in south-central Washington (4).

General Characteristics.—Typical midwest loess is a quartzose, somewhat feldspathic, clastic sediment composed of a mixture of fine sand, silt, and clay particles. The soil is uniformly sorted and arranged in an open, cohesive fabric (8).

Palouse loess has some important differences from midwest loess. Soil of the Pullman area is a uniformly sorted mixture of silt and clay but contains

very little sand. It is cohesive in nature but does not display the open fabric common to other loessial soils. The higher dry densities, γ_d , of Palouse loess may be attributed to its close fabric. Dry densities of samples used in this study ranged from 95 pcf–98 pcf ($1,520 \text{ kg/m}^3$ – $1,568 \text{ kg/m}^3$) at porosities of 42%–44%, as compared to 70 pcf–90 pcf ($1,120 \text{ kg/m}^3$ – $1,440 \text{ kg/m}^3$) for midwest loess (5).

The natural moisture contents for the field samples varied between 23% and 28%. This converts (on a volumetric basis) to a degree of saturation of 85%–96% at a specific gravity of 2.68.

Loess deposited under humid conditions is thought to develop a dense matrix as a result of structural collapse along grain boundaries. It is postulated that this is probably caused by softening of the clay cementing material by the

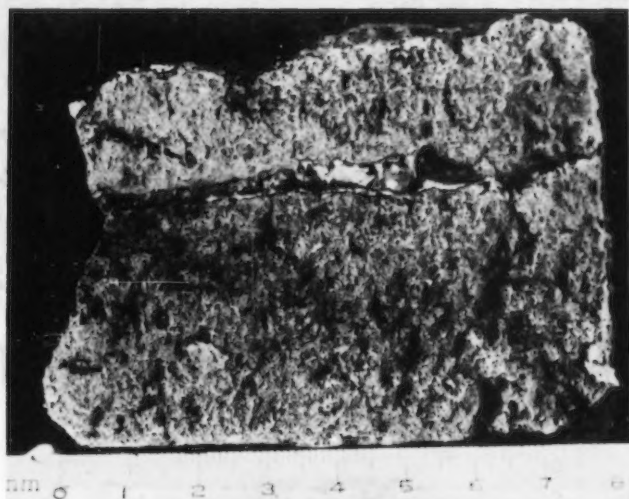


FIG. 2.—Vertical Root Tube in Palouse Loess (Cross-Sectional View)

action of soil water (5). It is the writer's opinion that the dense fabric may, in part, have resulted from repeated wetting and desiccation during deposition.

Type of Matrix.—The matrix of Palouse loess is typically clayey, although some secondary calcite may be present. For the most part, granular components are connected along grain boundaries by illite; however, in some places, the individual grains do not touch but are separated by the clay cement. The close packing of these grains gives rise to a fairly high dry density, commonly 95 pcf ($1,520 \text{ kg/m}^3$) but sometimes as high as 108 pcf ($1,728 \text{ kg/m}^3$) (13).

Even with this high dry density, large voids can be found randomly distributed in the matrix. These voids occur as tubes left empty by the decomposition of plant roots and were observed throughout the entire 30 ft (9.1 m) of exposed

stratum. The larger holes are essentially vertical whereas the smaller holes branch off from the main tubes in dendritic patterns. Some smaller individual root holes are scattered randomly within the matrix but do not account for an appreciable void space. Well-formed tubes may be as large as 0.16 in. (4 mm) in diam and extend vertically for several inches. Fig. 2 shows a cross-sectional view of a large vertical root tube and Fig. 3 shows a top view of a typical sample of Palouse loess. The root holes show up as black areas on the photos. This natural "plumbing" system accounts for the high vertical permeability of soils in the Palouse area, typically on the order of 9×10^2 ft/yr (9×10^{-4} cm/s).

Particle Shape.—Microscopic examination of Palouse loess revealed that the

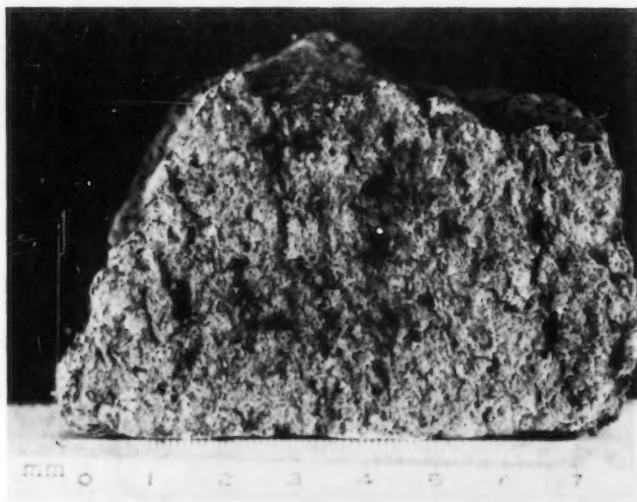


FIG. 3.—Root Holes in Palouse Loess (Top View)

shape of individual grains varies depending on the mineral. Quartz and feldspar are mostly irregular in form. The micas, on the other hand, are platy because of their cleavage. Minor constituents appear prismatic or irregular. Calcite accounts for a small percentage of the matrix, occurring as irregularly-shaped detrital silt-size grains, euhedral crystals, and precipitates in former void spaces. Clay minerals occur as cemented aggregates in the spaces between the quartz and feldspar particles and as films surrounding silt grains. The majority of clay particles are so fine-grained that they are not distinguishable under the petrographic microscope.

The granular components comprise about 80% of the total solid volume of Palouse loess. x-ray diffraction by McCreery (10) and petrographic analysis

HYDROCONSOLIDATION TESTING OF PALOUSE LOESS

Testing Procedure.—The standard test procedure for evaluation of the hydroconsolidation (or hydrocompaction) potential involves prestressing the soil to some level, and then adding water to the specimen at that level. This procedure is repeated at increased stress levels using a different specimen each time. The results are used to predict the settlement of a soil (at any prestressed level) due to increases in water contents from either inundation or a rise in ground-water levels (2).

This standard procedure was modified because of the large number of

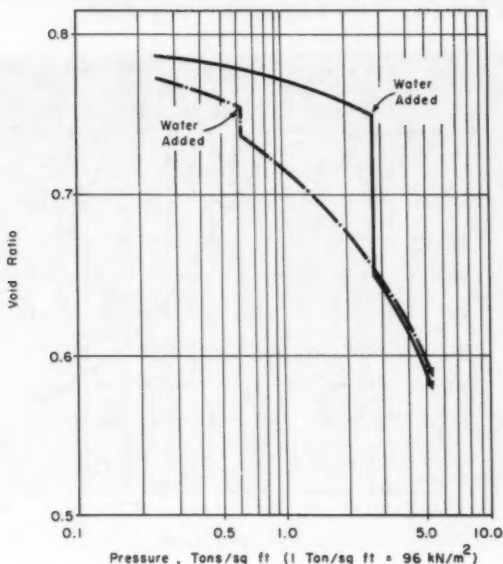


FIG. 5.—Paired Consolidation Tests Showing Effect of Load at Time of Moisture Content Increase

undisturbed specimens required (20–30) to define the hydroconsolidation potential in this manner. The modified procedure followed in this study involved the addition of water to the specimen at the beginning of the test. Since increasing the water content of the soil by the upward movement of water would tend to lessen the chance for air entrapment and thus increase the water to grain surface ratio, test specimens were brought to field saturation in this manner. Time was allowed for the specimen to come to field saturation before consolidation loads were applied. The length of time required to achieve field saturation was determined by comparing moisture contents of specimens after various periods of time. The minimum length of time required to reach field saturation was

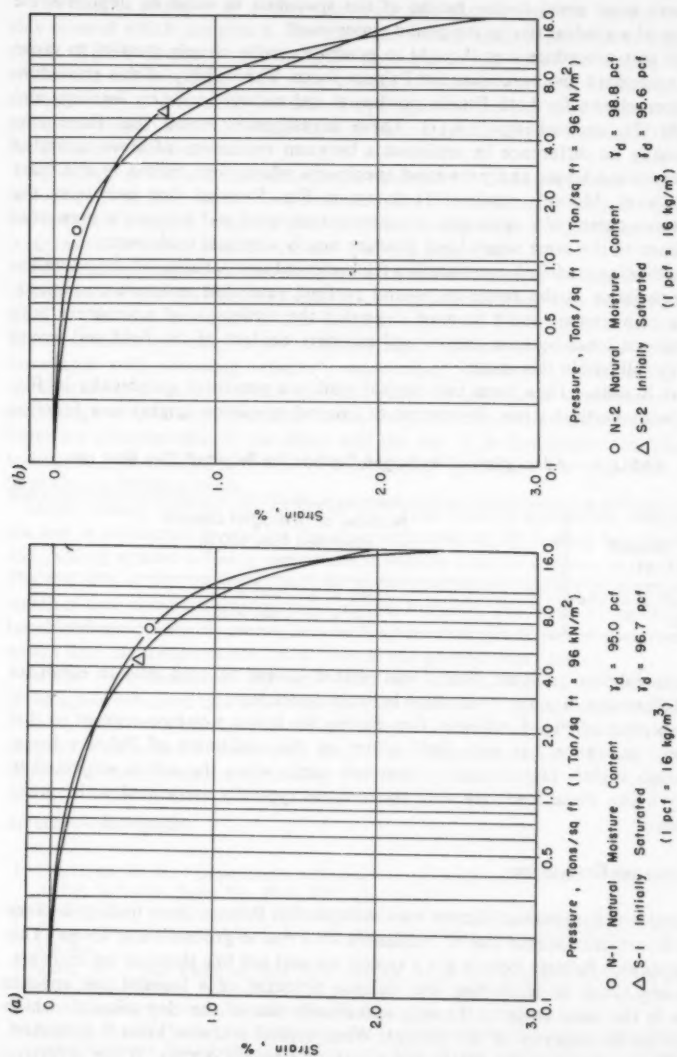


FIG. 6.—Typical Hydroconsolidation Test Results of Palouse Loess: (a) Tests N-1 and S-1; (b) Test N-2 and S-2

taken as that point at which no further increase in moisture content was observed. During this time, water was supplied to the base of the consolidometer at a pressure head equal to the height of the specimen in order to duplicate the effects of a gradual rise in the ground-water level.

This test procedure was thought to produce results closely parallel to those of the standard test procedure for Palouse loess. The validity of this procedure has been shown for both Pacific northwest and midwest soils by Jennings and Knight (7), and others, (1,6,11). These investigators found that there was essentially no difference in settlements between specimens of loess saturated at prestressed levels and prewetted specimens which were raised to the same stress level. Moore's results (11) shown in Fig. 5 reveal that increasing the moisture content of a specimen at a prestressed level and bringing a prewetted specimen to the same stress level produce nearly identical settlements.

Conducting modified consolidation tests allowed comparisons of consolidation characteristics in the range of natural to field saturated moisture conditions. These comparisons could be used to predict the settlement of a structure built on Palouse loess because the natural moisture content of the field soil would usually fall within this range.

Test Results.—Data from two typical tests are presented graphically in Fig. 6 showing vertical strain (in percent of original specimen height) as a function

TABLE 1.—Adsorption of Hydrogen Cations for Selected Clay Minerals

Mineral (1)	Number of hydrogen cations adsorbed (per 100 g) (2)
Montmorillonite	360×10^{20} – 500×10^{20}
Illite	120×10^{20} – 240×10^{20}

of consolidation pressure. Strain was plotted instead of void ratio to eliminate the differences in initial void ratios between specimens.

Inspection of Fig. 6 indicates that raising the initial moisture content to that of field saturation has very little effect on the settlement of Palouse loess. Although slightly larger strains sometimes occur when the soil is subjected to heavy loads, these loads are well above those typically associated with spread footings.

ANALYSIS AND CONCLUSIONS

Results of hydroconsolidation tests indicate that Palouse loess undergoes very little structural collapse due to inundation or a rise in ground-water levels. This suggests that Palouse loess is not a typical loessial soil like those of the midwest.

A key factor in evaluating the collapse potential of a loessial soil appears to lie in the mineralogy of the soil, specifically that of the clay minerals which comprise the majority of the cement. When typical midwest loess is saturated, the clay cement adsorbs water and a loss of strength occurs. If the effective stress is sufficient, the weakened clay will fail in shear at points of contact between grains. Destruction of the intergranular supports allows the grains to

move into void spaces yielding a net decrease in volume and a permanent settlement.

The loss in strength of a clay-cemented soil depends on the nature of the clay mineral which cements it. The chief cementing agent in most loess deposits of the United States is montmorillonite, whereas the chief cementing agent of Palouse loess is illite, with only a trace of montmorillonite. Different clay minerals vary in their ability to adsorb hydrogen cations and thus in their ability to adsorb water. Table 1 (14) gives the relative adsorption of hydrogen cations for these two minerals.

As shown in Table 1, montmorillonite adsorbs 1-1/2-4 times more hydrogen cations (water) than illite. Since Palouse loess is cemented by illite as opposed to montmorillonite, it displays little or no softening when the moisture content is increased and thus possesses a low collapse potential.

Although laboratory studies do provide reliable means to access the hydroconsolidation potential of loess deposits, other factors must also be considered from a practical standpoint. The costs involved in conducting a laboratory hydroconsolidation analysis are relatively high. The majority of these costs are associated with obtaining relatively undisturbed specimens, transporting the specimens in a manner which will not result in additional disturbance, and preparing the specimens once they reach the laboratory. More than often, these costs are unacceptable to the client and the use of in-situ hydroconsolidation testing may be utilized in lieu of the laboratory procedure for sites with light to moderate building loads.

In-situ testing may be accomplished with plate bearing equipment. Basically, the test is conducted by placing the plate apparatus at the footing bearing level and jacking against a heavy construction vehicle such as a dozer or backhoe. The test area is then inundated and the water level maintained for an appropriate length of time commensurate with the adverse hydraulic conditions being designed for. Field testing is, of course, not without its limitations and is not practical where field saturation occurs from rises in the ground-water table.

In-situ tests conducted by the writer in a loess deposit in Kennewick, Washington indicated that the soil on this site was not susceptible to hydroconsolidation. This resulted in recommendations for economical, shallow spread footings. Extensive soil reworking, which would have been required if collapsible soils were found, was not necessary.

APPENDIX.—REFERENCES

1. Clevenger, W. A., "Experiences with Loess as a Foundation Material," *Transactions, ASCE*, Vol. 123, Paper No. 2916, 1958, pp. 151-169.
2. Dudley, J. H., "Review of Collapsible Soils," *Journal of the Soil Mechanics and Foundations Division, ASCE*, Vol. 96, No. SM3, Proc. Paper 7278, May, 1970, pp. 925-946.
3. Eske, M., "The Value of Soil Test Data in Local and Regional Road Planning," *Proceedings of the Symposium on Application of Soil Testing in Highway Design and Construction*, American Society for Testing Material, STP 239, 1959, p. 75.
4. Fryxell, R., Cook, E., and McCreery, R. A., "A Field Guide to the Loess Deposits and Channeled Scablands of the Palouse Area, Eastern Washington," *Report of Investigations No. 22*, Washington State University Laboratory of Anthropology, Pullman, Wash., 1964.
5. Gibbs, H. J., and Holland, W. Y., "Petrographic and Engineering Properties of Loess,"

- Engineering Monographs No. 28*, United States Bureau of Reclamation, Denver, Colo., Nov., 1960.
6. Gibbs, H. J., and Holtz, W. G., "Consolidation and Related Properties of Loessial Soils," *Proceedings of the Symposium on Consolidation Testing of Soils*, American Society for Testing Materials, STP 126, 1951.
 7. Jennings, J. E., and Knight, K., "The Additional Settlement of Foundations Due to a Collapse of Structures of Sandy Soils on Wetting," *Proceedings of the 4th International Conference on Soil Mechanics and Foundations Engineering*, Vol. 3a/12, Aug., 1957, pp. 316-319.
 8. King, M. H., and Judd, W. R., "Loess, Its Petrography, Physical Behavior, and Relationship to Engineering Structures," presented at the Oct., 1952, Annual Meeting of the Geological Society of America, held at Boston, Mass.
 9. Luck, L. K., "An Investigation of the Shear Characteristics of Palouse Clay," thesis presented to the University of Minnesota, at Minneapolis, Minn., in 1951, in partial fulfillment of the requirements for the degree of Master of Science.
 10. McCreery, R. A., "Mineralogy of Palouse and Related Series," thesis presented to the State College of Washington, at Pullman, Wash., in 1954, in partial fulfillment of the requirements for the degree of Doctor of Philosophy.
 11. Moore, H. E., "The Engineering Properties of Silty Soils, Snake River Canyon, State of Washington," United States Army Corp of Engineers, Engineer District Walla Walla, July, 1967, pp. 1-31.
 12. "Rock Elevation Study," Department of Facilities Planning, Washington State University, Pullman, Wash., 1973, map.
 13. Schroeder, W. L., "An Evaluation of Palouse Clay as a Foundation Material," thesis presented to Washington State University, at Pullman, Wash., in 1963, in partial fulfillment of the requirements for the degree of Master of Science.
 14. Terzaghi, K., and Peck, R. B., *Soil Mechanics in Engineering Practice*, 2nd ed., John Wiley and Sons, Inc., New York, N.Y., 1967, p. 13.

CAISSONS SOCKETED IN SOUND MICA SCHIST

By Demetrious C. Koutsoftas,¹ A. M. ASCE

INTRODUCTION

Caissons socketed in rock are frequently used to support very high concentrated loads with small deflections. The design of these caissons is mostly empirical and is based on allowable or estimated average skin, or base resistances, or both (2,4,6,12,15). Because of the high cost associated with load tests on caissons socketed in rock, only in very rare occasions can such load tests be economically justified prior to construction. Allowable skin and base resistances, therefore, are usually selected based on building codes and local experience.

Until recently, the basic assumption in the design of rock sockets was that the mobilized skin resistance was constant along the entire length of the socket. However, it has been shown theoretically (3,9,10,11), assuming linear elastic behavior, that the skin resistance varies within the socket, being highest near the top of the socket and decreasing rapidly with depth. Recognizing this behavior, Rosenberg and Journeaux (12) proposed a new design procedure that accounts for the nonuniform distribution of mobilized skin resistance within rock sockets. Pells and Turner (11) developed design charts based on the concept of nonuniform distribution of shear stress within the socket. These charts can be easily used to predict the loads supported by skin and base resistances. Ladanyi (7) provided limited data from an instrumented caisson which served to support the new design procedure. However, there are no other published data on the distribution of shear stresses within rock sockets to allow evaluation of the new design procedure and the present design practices.

It therefore appears that there is a need for load test data on rock sockets with emphasis on the distribution of shear stresses within the socket. The purpose of this paper is to present the results of several load tests performed on caissons with relatively long sockets (length to diameter ratios, L_s/d , greater than 10), and to examine the distribution of skin resistance within the socket of a well-instrumented caisson.

The load test data were collected during the underpinning of a 22-story steel frame structure in Philadelphia. The structure was initially supported on large diameter caissons founded on medium hard mica schist as shown schematically

¹Sr. Engr., Dames & Moore, 1550 Northwest Hwy., Park Ridge, Ill. 60068.

Note.—Discussion open until November 1, 1981. To extend the closing date one month, a written request must be filed with the Manager of Technical and Professional Publications, ASCE. Manuscript was submitted for review for possible publication on June 26, 1980. This paper is part of the Journal of the Geotechnical Engineering Division, Proceedings of the American Society of Civil Engineers, ©ASCE, Vol. 107, No. GT6, June, 1981. ISSN 0093-6405/81/0006-0743/\$01.00.

in a later figure. Several of the caissons suffered large settlements which necessitated a remedial program to prevent further settlements. The remedial program consisted of installing two replacement caissons symmetrically about the center line of each column that needed underpinning. After installation of the replacement caissons, the load was transferred to the replacement caissons by jacking against the column.

The unexpected settlements of the original caissons are believed to be the result of founding these caissons within the soft mica schist, which had been subjected to varying degrees of weathering at different locations. Although the soft mica schist is considered a very competent foundation material, at many caisson locations it underwent considerable compression under the high design loads [556 psi (3,832 kPa)] applied by the caissons. The details of the settlement behavior of the caissons, as well as the details of the underpinning system, although of practical interest, are beyond the scope of this paper. The paper deals only with the behavior of the replacement caissons during and after the load transfer operation.

SUBSURFACE CONDITIONS AND CAISSON INSTALLATION

The caissons were constructed from the basement of an existing structure in downtown Philadelphia that is approx 20 ft (6.1 m) below street level. The subsurface conditions encountered below basement level are presented in Fig. 1 and are described in the following.

The top 50 ft (15.2 m) of subsoil consist of heterogeneous alluvium, interbedded fine to medium sand, silty sands, and occasional silt layers. A very dense sandy gravel layer was usually encountered in the bottom 5 ft–8 ft (1.5 m–2.4 m) of the alluvium. The underlying 20 ft–30 ft (6.1 m–9.1 m) of material consists of decomposed mica schist, a soil-like material with standard penetration resistances in the range of 15 blow/ft–50 blow/ft. This stratum generally becomes denser with depth and gradually grades into soft, then medium hard, and finally sound mica schist. A typical subsurface soil profile is shown in Fig. 1. Sound mica schist was normally encountered between elevations –70 ft and –75 ft [–21.3 and –22.9 m (Philadelphia Third Survey District datum)].

As shown in a later figure, the caissons were socketed into the sound mica schist, which is quite massive with tight joints spaced 2 ft–3 ft (0.6 m–1.0 m) apart. The foliation of the sound mica schist was relatively steep, between 45° and 60° to the horizontal. Fig. 2 plots the tangent modulus versus the unconfined compressive strength of sound mica schist obtained from uniaxial compression tests. As seen in Fig. 2, most of the data fell within the envelope defined by Deere (1) for schist with steep foliation. It is interesting to note that in some instances the sound mica schist had unusually high strengths and high moduli. The material which exhibited these very high strengths was very fine-grained and gneissic in nature. This material was encountered randomly in thin layers, each about 3 ft–6 ft (1 m–2 m) thick, within the sound mica schist.

Caisson Installation.—The caissons were installed by first driving open-ended casing to the top of the decomposed mica schist using a double-acting air hammer with rated energy of 15,000 ft-lb (8,000 J). The casings were 24 in. or 30 in. (60.96 mm or 76.2 mm) in outside diameter (OD) with a 0.5-in. (12.7-mm) wall

thickness. The casing was then cleaned all the way to the tip. From there on, a churn drill was used to drill a hole usually 10 ft–12 ft (3.1 m–3.7 m)

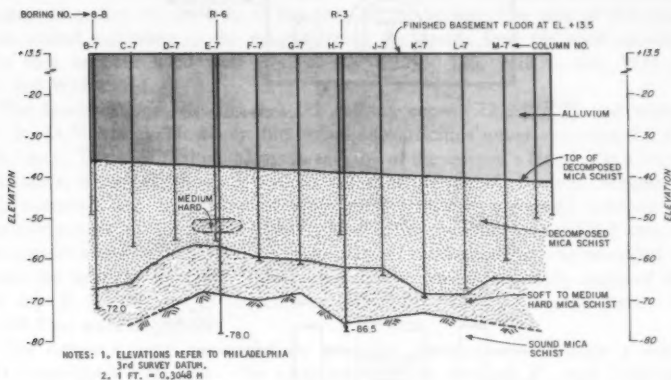


FIG. 1.—Generalized Subsurface Section at Col. Line 7

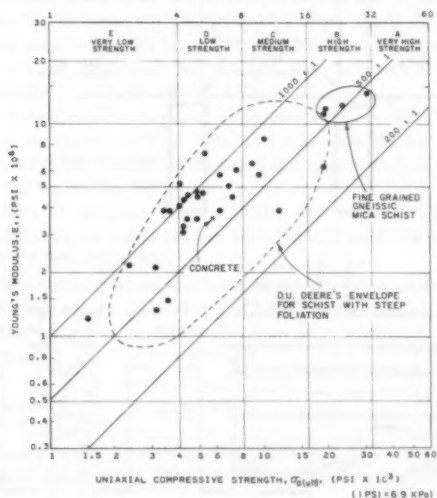


FIG. 2.—Young's Modulus Versus Uniaxial Compressive Strength for Sound Mica Schist

below the pipe tip. The pipe was then driven to the bottom of the drilled hole using a free-falling impact hammer. Following this, the casing was cleaned out using an airlift pump. This procedure of alternate drilling, pipe driving, and

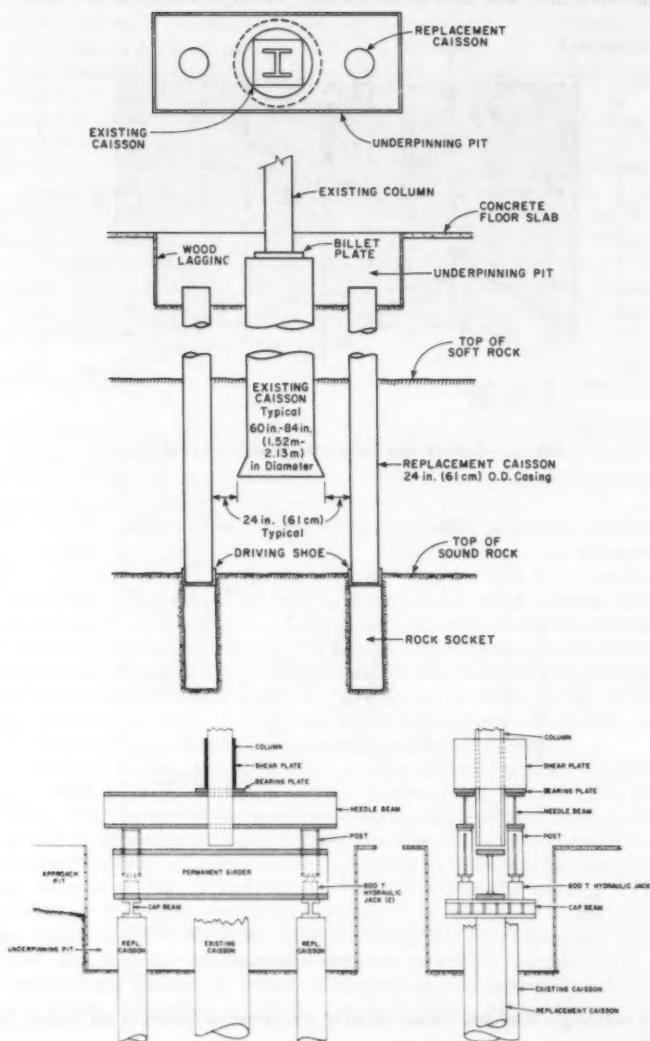


FIG. 3.—(a) Plan and Elevation of Underpinning System; (b) Load Transfer System

cleaning was repeated until the pipe reached the top of sound rock. Finally, the socket was drilled with the churn drill to the desired depth.

A steel core beam of selected standard W section was installed inside the casing, extending all the way to the base of the socket. The size of the steel core varied according to the magnitude of the design load for each caisson. The core sections used were W12 \times 92, W12 \times 120, W12 \times 190, W14 \times 36, and W14 \times 314.

The specifications required that the caisson eccentricities be limited within ± 3 in. (± 76.2 mm). However, the actual eccentricities never exceeded 1.5 in. (38.1 mm). The specified plumbness was 2.0% of the caisson's length. On several occasions, the out-of-plumb deviations exceeded the specified values. Whenever this occurred, the caissons were analyzed for bending moments induced by the component of the vertical load perpendicular to the longitudinal axis of the caissons and, if necessary, additional steel reinforcement was provided to resist the bending moments. This reinforcement was usually only required for the top 35 ft (10.7 m) of the caisson, since the bending moments below 35 ft (10.7 m) were negligible.

The caissons were concreted by pumping the concrete through a 4-in. (10.2-mm)-diam steel pipe. The specified concrete strength, f'_c , was 5,000 psi (32,585 kPa). However, the contractor elected to use a concrete mix which would provide a 28-day strength of 6,000 psi (39,102 kPa). The maximum aggregate size was 3/8 in. (9.5 mm), and the specified slump was 6 in. \pm 1 in. (15.2 mm \pm 2.5 mm). Three concrete test cylinders were made for each caisson. One cylinder was prepared at the beginning, one at the middle, and one towards the end of the pouring operation. All the test cylinders exhibited strengths in excess of the specified 5,000 psi (32,585 kPa).

The caissons were installed in pairs, symmetrical about the existing columns of the structure, as shown in Fig. 3(a), and were loaded by jacking against the column to transfer the load from the existing foundation to the new caissons, using the setup shown in Fig. 3(b).

In total, 14 pairs of caissons were installed and were all load tested using the same procedure. Axial loads for the replacement caissons varied from 400 kip–2,000 kip (1,779 kN–8,896 kN).

The caissons were designed on the basis of an allowable uniform bond stress of 69.5 psi (479 kPa) and an allowable end bearing pressure of 556.2 psi (3,832 kPa). The required length of socket could thus be determined once the socket diameter was selected.

CAISSON INSTRUMENTATION

During the load-transfer operation, the loads and deflections at the top of each caisson were monitored. Thus, a load-deflection diagram was obtained for each caisson.

One of the 30-in. (762-mm) caissons was provided with a tell-tale rod to measure the deflection at the top of the socket.

One of the 24-in. (610-mm) caissons was instrumented with Carlson-type strain meters to evaluate the load transfer behavior of the caisson. The locations of the instruments are shown on Fig. 4. The Carlson strain meters were attached to the core beam by welding holding brackets on the web of the core beam

and fastening the strain meters to those brackets.

As shown in Fig. 4, strain meters were installed at six locations within the 31-ft (9.45-m) long socket. At each of these locations, two strain meters were installed, one on each side of the web of the core beam. One strain meter was located at the tip of the casing, and three others were placed intermittently within the cased portion of the caisson.

The top two strain meters within the cased portion of the caisson were damaged during concreting, and one of the strain meters in the socket malfunctioned. The rest of the strain meters functioned properly throughout the test period. It is interesting to note that at the five locations within the socket where the

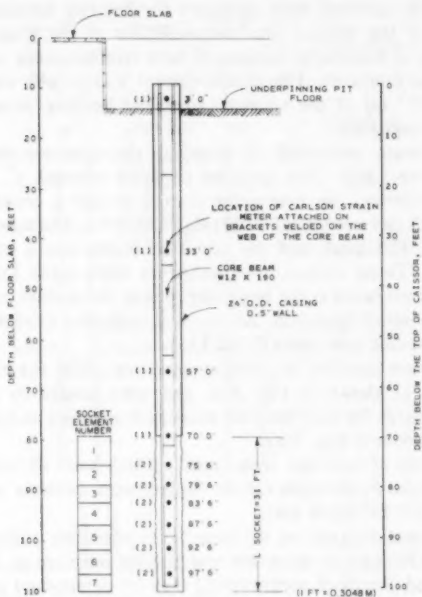


FIG. 4.—Caisson Instrumentation

pairs of strain meters functioned properly, the loads measured with the two strain meters did not differ by more than 10 kip (44.5 kN) to 30 kip (133.4 kN).

TEST RESULTS

Fig. 5 presents load deflection data from a pair of 30-in. (762-mm) diam caissons. As mentioned earlier, one of these caissons was provided with a tell-tale rod to measure the deflections at the top of the socket. The socket deflections are also plotted versus the applied butt load in Fig. 5. From the measured

deflections at the top of the socket and at the butt of the caisson, it was possible to compute the compression of the cased portion of the caisson, which is also plotted versus the butt load in Fig. 5. The theoretical elastic compression of the cased part of the caisson is computed as

$$\delta = \frac{PL}{AE_{eq}} \dots \dots \dots (1)$$

in which δ = the elastic compression; L = the length of the cased portion of the caisson; A = the gross area of the caisson; E_{eq} = the equivalent modulus, assuming the caisson consists of a single material; and P = is the applied butt load. From the theoretical elastic compression lines shown in Fig. 5, it is seen that the west caisson is stiffer. This is because the west caisson was provided with additional steel reinforcement (as shown on the lower left-hand portion

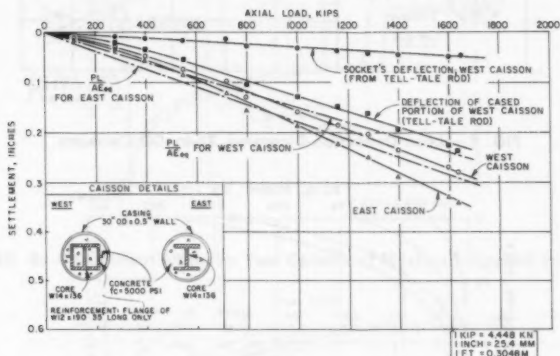


FIG. 5.—Load-Deflection Diagram, 30-in. OD Caissons

of Fig. 5) to resist bending moments induced by the out-of-plumb deviation of this caisson.

The data shown in Fig. 5 clearly demonstrate that the compression of the socket was very small, about 0.05 in. (1.27 mm), and that it increased linearly with increasing butt load. The settlement of the caissons, 0.28 in.–0.34 in. (7.1 mm–8.6 mm), is primarily attributed to the elastic shortening of the cased portion of the caisson. The measured compression of the cased portion of the caisson is slightly smaller than the theoretical elastic shortening, which means that a small part of the applied butt load is perhaps resisted by skin friction along the casing.

Fig. 6 presents the load deflection diagrams for a pair of 24-in. (610-mm) diam caissons. One of these caissons was instrumented with strain meters, as shown in Fig. 4, to study its load-transfer characteristics. The strains measured within the socket, at various magnitudes of the applied butt load, are presented in Fig. 7. Integration of these strains over the length of the socket provides the deflections at the top of the socket. The computed deflections at the top

of the socket are plotted in Fig. 6 as a function of the applied butt load. Again, the deflection of the socket is very small, as was the case for the 30-in. (762-mm) caissons shown in Fig. 5.

The deflections of the two caissons were for all practical purposes identical and only slightly greater than the theoretical elastic shortening of the cased

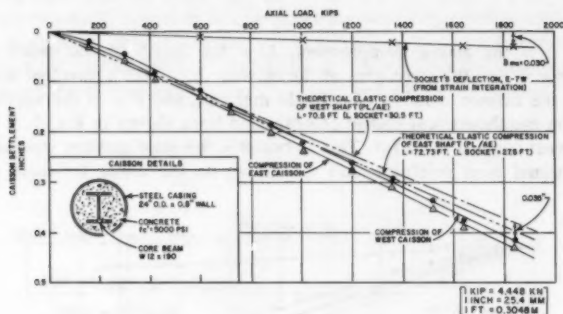


FIG. 6.—Load-Deflection Diagrams, 24-in. OD Caissons

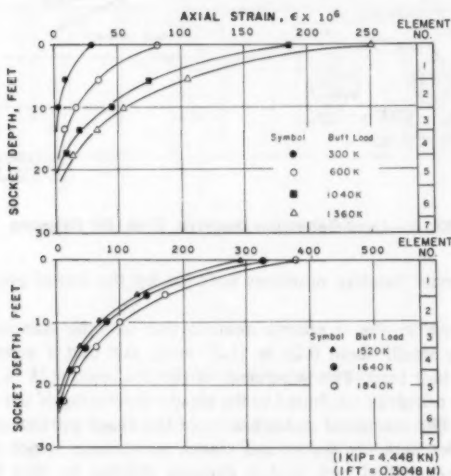


FIG. 7.—Distribution of Axial Strain within Socket at Various Load Levels

portion of the caissons. This behavior was typical of the other 12 pairs of caissons.

The measured axial strains were used to compute axial loads at the level of each measurement. The computations were based on the assumption that

the entire cross-sectional area of the caisson was subjected to a uniform strain; i.e., it was assumed that the steel core and the concrete deformed without slippage. Likewise, it was assumed that there was no slippage between the

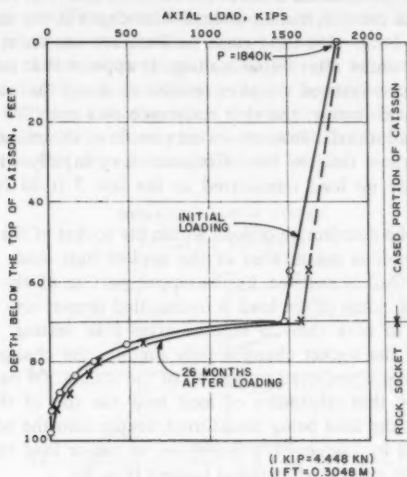


FIG. 8.—Load Distribution for Test Caisson at Maximum Applied Load

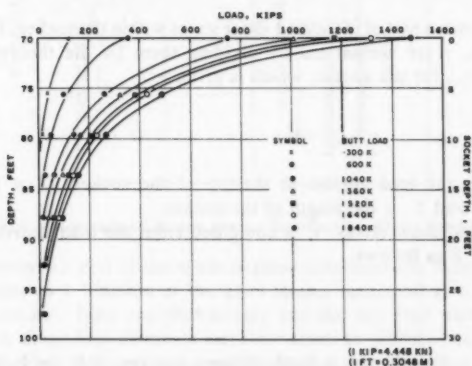


FIG. 9.—Load Distribution within Socket at Various Stages of Loading

concrete and the surrounding rock. The total axial load at any level at which strain measurements were taken was therefore computed as

$$Q = (E_c A_c + E_s A_s) \times \epsilon \quad (2)$$

in which Q = the total axial load; E_c = the Young's modulus of concrete determined from compression tests to be 3.6×10^6 psi (25.5×10^6 kPa); E_s = the Young's modulus of steel taken as 29×10^6 psi (200×10^6 kPa); and A_c and A_s = the cross-sectional areas of the concrete and steel core, respectively.

Fig. 8 represents the distribution of load with depth at the maximum applied butt load for the 24-in. (610-mm) caisson. Data are shown at the end of the load test and 26 months after initial loading. It appears that initially about 350 kip (1,557 kN) were resisted by skin resistance along the casing. However, 26 months after load testing, the skin resistance was only 265 kip (1,179 kN), indicating some load transfer from the cased portion of the caisson to the socket. The data clearly show that the load dissipates very rapidly within the socket. There is practically no load transferred to the last 7 ft–10 ft (2.1 m–3.1 m) of the socket.

Fig. 9 presents the distribution of load within the socket of the 24-in. (610-mm) diam caisson at various magnitudes of the applied butt load. At small values of butt load, the load is resisted by the upper portion of the socket. As the butt load increases, some of the load is transmitted deeper into the socket.

It is important to note that 26 months after load testing, the distribution of the load within the socket changed only slightly; the change corresponding to the increased load transferred to the top of the socket. Of particular concern was the possibility that relaxation of load near the top of the socket might occur, resulting in the load being transferred deeper into the socket. One such case was described by Ladanyi (7). However, no major load redistribution can be detected even 26 months after initial loading (Fig. 8).

ANALYSIS OF LOAD-TRANSFER DATA

Fig. 10 presents a plot of mobilized shear stress within the socket. The mobilized shear stresses, τ are normalized by dividing them by the theoretical average shear stress, τ_{av} , for the socket, which is given as

$$\tau_{av} = \frac{P_s}{\pi D_s L_s} \dots \dots \dots (3)$$

in which P_s = the load applied at the top of the socket; D_s = the diameter of the socket; and L_s = the length of the socket.

The mobilized shear stress, τ , is computed from the load distribution curves shown on Fig. 8 as follows:

$$\tau = \frac{\Delta p}{\pi D_s \Delta L} \dots \dots \dots (4)$$

in which Δp = the change in load between the top and the bottom of each element; and ΔL = the length of each individual element, identified in Figs. 7 and 11(a).

Theoretical solutions provided by Mattes and Poulos (9) and Poulos (personal communication, 1979) are also shown in Fig. 10. The distribution of the normalized shear stress is a function of the relative pile stiffness, K , defined as the ratio of the equivalent modulus of the socket to the modulus of the rock. At normalized depths, Z_s/L_s , greater than 0.25, the experimental data are practically identical

to the theoretical distribution for a relative stiffness of about 10, in which Z_s = the depth below the top of the rock socket. Near the top of the socket (Z_s/L_s less than 0.20), the mobilized shear stresses are higher than the predicted values from the elastic solutions. As a practical matter, however, the elastic solutions for relative stiffness coefficients between 10 and 50 would provide good estimates of shear stresses within the socket.

The significance of this observation is that the use of elastic solutions to design caissons socketed in rock may not require a precise knowledge of the relative stiffness coefficients. Furthermore, the elastic solutions have the potential of providing useful insight with respect to the load distribution, viewed as a more rational approach to the selection of socket lengths.

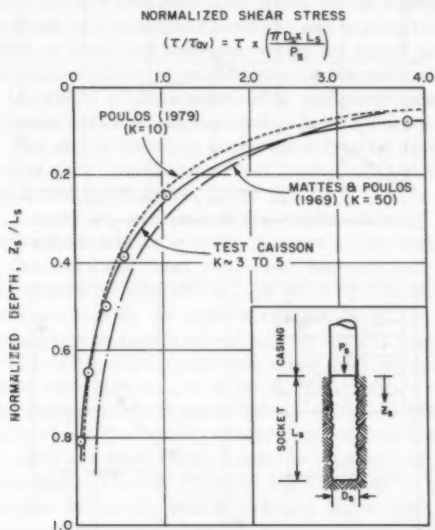


FIG. 10.—Normalized Shear Stress Distribution Along Socket

Fig. 11(a) presents a plot of the shear stresses determined at various locations within the socket as a function of the axial strains measured at corresponding points in the socket. Data are shown only for the top four elements, since the loads below these four elements were too small to mobilize any significant skin resistance. Fig. 11(b) presents mobilized shear stresses versus the axial deflections at the top of each element. The axial deflections were obtained by integrating the measured strains (see Fig. 7).

The data show a linear relationship between the mobilized shear stress and axial strain (or vertical deflection), even up to the maximum measured shear stress of 219 psi (1,509 kPa). The first element appears to be much stiffer than the other three elements, which shows a unique relationship between shear stress and compressive strain (or vertical deflection). This observation was quite

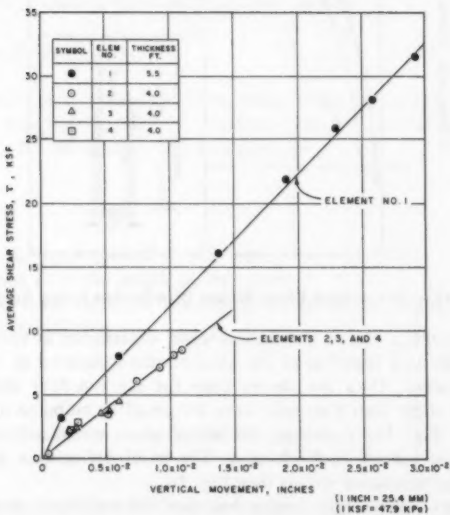


FIG. 11.—(a) Side Shear Stress Versus Compressive Strain; (b) Mobilized Shear Stress Versus Vertical Movement

surprising at first, but examination of the drilling records showed that drilling was much harder near the top 5 ft (1.2 m–1.5 m) of the socket, apparently caused by the presence of a harder layer of mica schist. This behavior could not be detected by simple examination of the data shown in Fig. 9, but it is in general agreement with analytical solutions presented by Gill (3), which demonstrate that in stratified rocks the stiffer layers support a greater proportion of load than the less stiff layers.

It is perhaps of interest to note that the maximum measured bond stress of 219 psi (1,509 kPa) is slightly greater than the maximum bond stress of 200.3 psi (1,380 kPa) allowed by the building code of the City of New York for sound rock. Other codes allow smaller values of bond stress. It should be remembered, however, that the sockets were designed with an allowable bond stress of 69.5 psi (479 kPa) only. This points out the limitations of present design practices based on presumptive bond and end bearing stresses.

The applicability of analytical solutions, which are based on elastic theory, for data interpretation, or for design, or both, must be tempered with the designer's judgment as to the ability of these solutions to realistically model the existing in-situ rock conditions and the interactions between the caisson and the surrounding rock mass. The elastic solutions gave relatively good results in this case because the sockets were formed in excellent quality rock, which had relatively few widely-spaced, and tightly-closed joints.

Horvath and Kenney (4) summarized the results of many field load tests on large diameter piers socketed in rock. It appears from these data that, for straight shafts, the mobilized bond stress was between 0.05 and 0.10 times the unconfined compressive strength, σ_{ult} , of the rock. Using this correlation, the gneissic mica schist with the highest strength of $\sigma_{ult} = 20,000$ psi (138 MPa) would be expected to mobilize bond stresses ranging from 1,000 psi–2,000 psi (6.89 MPa–13.8 MPa). The sound mica schist with strengths in the lower range of measured values, say $\sigma_{ult} = 4,000$ psi (27.6 MPa), would be expected to mobilize bond stresses in the range of 200 psi–400 psi (1.38 MPa–2.76 MPa). There is obviously a large discrepancy between presumptive bond stresses given by many local codes and bond stresses that the presently available field load test data would suggest. The use of higher bond stresses would lead to more economical designs. However, before adopting higher stresses for design, additional data on well-instrumented prototype caissons are required to establish the validity of the new procedures and to further substantiate the high bond stresses.

CONCLUSIONS

The results of load tests on long sockets in sound mica schist lead to the following conclusions:

1. Very high shear stresses were mobilized along the periphery of the socket. Despite the fact that the sockets were conservatively designed, the maximum mobilized shear stress was in excess of allowable values given by many codes. These high shear stresses were mobilized at extremely small deflections.
2. The distribution of the mobilized shear stresses within the socket decreased rapidly with depth, as could be predicted from the theory of elasticity. The

lower 7 ft–10 ft (2.1 m–3.0 m) offered practically no resistance, since no load was transferred to that depth.

3. The load test data provide limited support for the new design procedure proposed by Rosenberg and Journeaux (13) and Pells and Turner (11), which accounts for the nonuniform distribution of shear stresses within the socket.

4. The good agreement between theory and experimental data is believed to be the result of the good quality of the rock, which was basically free of major defects, with only widely-spaced, tightly-closed joints.

ACKNOWLEDGMENTS

Dames & Moore provided financial assistance for the instrumentation of the caissons and for the preparation of this paper. V. Miller of the Port Authority of New York and New Jersey (formerly of Dames & Moore) provided valuable assistance with the instrumentation. The writer acknowledges, with appreciation, the cooperation of the contractor, Underpinning & Foundation Constructors Inc., who provided all skilled and unskilled labor that was necessary for instrumentation and load testing. Duncan Wood of Schiavone Construction, Inc. (formerly of Underpinning & Foundation Constructors Inc.) was in charge of the project and developed the underpinning system. His careful and conscientious efforts in the field were the key to the success of the project. Edward McNamara, James Reilly, Eugene Currie, and Edward Ribachoneck of Underpinning & Foundation Constructors, Inc., provided valuable assistance throughout the project. H. G. Poulos of the University of Sydney, Australia kindly provided some unpublished elastic solutions for the instrumented caisson. T. M. Gates of Acres American, Inc. (formerly of Dames & Moore) was the principal in charge for the project. His continuous support is acknowledged with appreciation. Colleague Robert D. Darragh kindly reviewed the paper and offered many useful comments.

APPENDIX I.—REFERENCES

1. Deere, D. U., "Geological Considerations," *Rock Mechanics in Engineering Practice*, K. G. Stagg and O. C. Zieniewicz, eds., John Wiley and Sons, Inc., New York, N.Y., 1968, Chapter 1.
2. Freeman, C. F., Klajnerman, D., and Prasad, G. D., "Design of Deep Socketed Caissons into Shale Bedrock," *Canadian Geotechnical Journal*, Toronto, Ontario, Canada, Vol. 9, No. 1, 1972, pp. 105–114.
3. Gill, A. S., "Load Transfer Mechanism for Caissons Socketed into Rock," thesis presented to Northwestern University, at Evanston, Ill., in 1970, in partial fulfillment of the requirements of the degree of Doctor of Philosophy.
4. Horvath, R. G., and Kenney, T. C., "Shaft Resistance of Rock-Socketed Drilled Piers," presented at the October 22–26, 1979, ASCE Convention and Exposition, held at Atlanta, Ga. (Preprint 3698).
5. Jackson, W. T., Perez, J. Y., and Lacroix, Y., "Foundation Construction and Performance for a 34 Story Building in St. Louis," *Geotechnique*, London, England, Vol. 24, No. 1, 1976, pp. 63–90.
6. Kenney, T. C., "Factors to be Considered in the Design of Piers Socketed into Rock," *Proceedings of the Conference on the Design and Construction of Deep Foundations*, Feb., 1977, pp. 11–39.
7. Ladanyi, B., discussion of "Friction and End Bearing Tests on Bedrock for High Capacity Socket Design," *Canadian Geotechnical Journal*, Toronto, Ontario, Canada, Vol. 14, No. 1, 1976, pp. 153–155.

8. Matich, M. A., and Kozicki, P., "Some Load Tests on Drilled Cast-in-Place Concrete Caissons," *Canadian Geotechnical Journal*, Toronto, Ontario, Canada, Vol. 4, 1967, pp. 357-375.
9. Mattes, N. S., and Poulos, H. G., "Settlement of a Single Compressible Pile," *Journal of the Soil Mechanics and Foundations Division*, ASCE, Vol. 95, No. SM1, Proc. Paper 6356, Jan., 1969, pp. 189-207.
10. Osterberg, J. O., and Gill, S. W., "Load Transfer Mechanism for Piers Socketed in Hard Soils or Rock," *Proceedings of the 9th Canadian Symposium on Rock Mechanics*, 1973, pp. 235-262.
11. Pells, P. N. J., and Turner, R. M., "Elastic Solutions for the Design and Analysis of Rock-Socketed Piles," *Canadian Geotechnical Journal*, Toronto, Ontario, Canada, Vol. 16, No. 3, 1979, pp. 481-487.
12. Rosenberg, P., and Journeaux, N. L., "Friction and End Bearing Tests on Bedrock for High Capacity Socket Design," *Canadian Geotechnical Journal*, Toronto, Ontario, Canada, Vol. 13, No. 3, 1976, pp. 324-333.
13. Spanovich, M., and Garvin, R. G., "Field Evaluation of Caisson-Shale Interaction," *ASTM STP 670, Behavior of Deep Foundations*, American Society of Testing and Materials, 1978, pp. 537-557.
14. Vogan, R. W., discussion of "Friction and End Bearing Tests on Bedrock for High Capacity Socket Design," *Canadian Geotechnical Journal*, Toronto, Ontario, Canada, Vol. 14, No. 1, 1977, pp. 156-158.
15. Winterkorn, H. F., and Fang, H-Y., "Drilled Piers," *Foundation Engineering Handbook*, Van Nostrand Reinhold Company, New York, N.Y., pp. 601-615.

APPENDIX II.—NOTATION

The following symbols are used in this paper:

- A = cross-sectional area;
 D_s = diameter of socket;
 E_{eq} = equivalent modulus of elasticity for socket;
 E_r = tangent modulus of rock;
 f'_c = unconfined compressive strength of concrete;
 K = relative pile stiffness = E_{eq} / E_r ;
 L = length of cased portion of caisson;
 L_s = length of socket;
 P_s = axial load at top of socket;
 q = uniaxial compressive strength of rock;
 Z_s = depth below the top of rock socket;
 δ = elastic shortening of cased portion of caisson;
 σ_{ult} = uniaxial compressive strength of rock; and
 τ_{av} = average skin resistance along socket.

PREDICTION OF MOVEMENTS FOR BRACED CUTS IN CLAY

By Abdulaziz I. Mana,¹ A. M. ASCE and G. Wayne Clough,² M. ASCE

INTRODUCTION

The basic functions of excavation support systems are to provide stability and minimize movements of the adjacent ground. Methods for predicting system stability are reasonably well established; however, this is not the case for movements. The movements of the support system and the adjacent ground are, in fact, a more involved problem than stability, since movements are influenced by more factors than stability. For example, overall stability is not necessarily affected by support system stiffness, method of support installation or soil stiffness, but movements are. In this paper, a simplified method for predicting movements of braced excavation in clay is presented, and tested against observed behavior. The method is based upon behavior measured in the field, and supplemented with results from finite element analyses developed to closely simulate the field response.

The predictive methodology developed allows a designer to estimate wall deflections and soil settlements for crosslot braced systems in soft to medium clay deposits. Effects of important structural system variables are considered explicitly. The basic soil parameters needed to make the predictions can be defined from the results of high quality triaxial tests or vane tests and a knowledge of the site geology and expected construction procedures.

PATTERNS OF BEHAVIOR EVALUATED FROM FIELD DATA

Settlements of the ground behind an excavation and the lateral movements of the support walls in clays are a function of many factors. It is possible, however, to define certain basic trends from projects where differences in support system and loading are not too great. Previous efforts of this type have been presented by Peck (23), D'Appolonia (9), and Goldberg, Jaworski, and Gordon

¹Asst. Prof. Dept. of Civ. Engrg., Univ. of Petroleum and Minerals, Dhahran, Saudi Arabia.

²Prof., Dept. of Civ. Engrg., Stanford, Univ., Stanford, Calif. 94305.

Note.—Discussion open until November 1, 1981. To extend the closing date one month, a written request must be filed with the Manager of Technical and Professional Publications, ASCE. Manuscript was submitted for review for possible publication on September 17, 1980. This paper is part of the Journal of the Geotechnical Division, Proceedings of the American Society of Civil Engineers, ©ASCE, Vol. 107, No. GT6, June, 1981. ISSN 0093-6405/81/0006-0759/\$01.00.

(12). Their work is extended herein by using a somewhat different approach and field data not previously available.

Relationship Between Maximum Lateral Movements and Potential for Basal Heave.—In establishing a correlation between movements and the potential for basal heave, the present work deviates from earlier efforts in three ways:

1. Case histories with unusual construction effects are not used. That is, data are incorporated only from projects where average prudent construction procedures were employed and where movements were generated primarily by the excavation stress relief. Thus, effects such as consolidation due to dewatering and displacements due to pile driving within the excavation are excluded. Furthermore, no projects are included where the first strut was placed at a depth greater than twice the undrained shear strength divided by the total unit weight, i.e., $2 s_u/\gamma$. As noted by Peck (23), and Clough and Davidson (5) late placement of the first strut typically leads to unnecessarily large movements. Some 130 case histories were reviewed for this effort, but only 11 were selected which met the criteria required, and which had suitable soil data.

2. Only sheetpile or soldier pile walls supported primarily by crosslot braces are considered. This helps keep the potentially large number of variables involved in the support system to a minimum.

3. Potential for basal heave is defined in terms of factor of safety against basal heave rather than stability number. The stability number approach is not used since it does not account for the stabilizing influence of underlying strong layers nor the presence of noncohesive layers in the soil profiles above the bottom of the excavation.

The factor of safety against basal heave is calculated using the approach set out by Terzaghi (26), and summarized for isotropic clays in Fig. 1. While the factor of safety obtained in this manner is not rigorously correct for all conditions (see Bjerrum and Eide, Ref. 2), it serves as a consistent index for a wide range of soil conditions. The special circumstances applicable for strongly anisotropic clays are considered in a later section of this paper.

The 11 case histories from which data were obtained are characterized in Table 1; basic soil data as well as minimum factors of safety against basal heave and maximum lateral wall movement and surface settlement are given. The predominate soil type for each project is a saturated soft to medium clay with a low to medium plasticity. Sensitivities of the clays range primarily from 2 to 8, with one case in San Francisco reaching as high as 20.

In order to maximize the utility of the case histories, the data from all but the first, or cantilever, stage of the excavation are used. The movements from intermediate stages are plotted against the appropriate basal heave factors of safety for each of the stages, not that for the maximum depth. Where time-dependent movements were observed at any excavation depth, the final values reported are used; in the following section of the paper details are given on this special behavior.

In Fig. 2, the maximum observed lateral movements for the case histories are divided by the excavation depth at which they were measured, and plotted versus factor of safety against basal heave. While there is some scatter to the data, it is apparent that there is a strong correlation between factor of

safety and movement. The scatter results from a number of factors such as differences in timing of strut placement, strut stiffness and spacing, difficulties in knowing the actual shear strength, and effects of differences in plan dimensions of the projects. From the trends in Fig. 2, however, it is apparent that the movements increase rapidly below a factor of safety of 1.4–1.5, while at higher factors of safety, the nondimensional movements are roughly constant at a value of 0.5%. Interestingly, Goldberg, Jaworski, and Gordon (12) have shown that lateral movements of braced walls in stiff clays with very high basal heave factors of safety are typically also about 0.5%, confirming the trend indicated in Fig. 2 for high factors of safety. The fact that the nondimensionalized movements are constant at high factors of safety is indicative of a largely elastic soil response. The rapid increases in movements at lower factors of safety are a result of yielding in the subsoils.

An additional behavior pattern of interest in Fig. 2 is the relative lack of difference in lateral movements for sheetpile walls whose tips are embedded in an underlying stiff layer and those whose tips remain in the moving clay mass. Typically, the maximum lateral movement occurs at or just below the bottom of the excavation, regardless of wall penetration depth although there

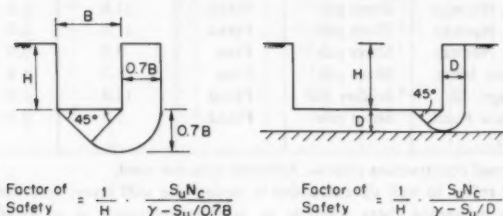


FIG. 1.—Method of Basal Heave Analysis, After Terzaghi (26)

is a tendency for it to move deeper as the factor of safety decreases. The trends in Fig. 2 suggest that for the case histories considered, amount of sheetpile wall penetration below excavation has relatively little influence on the level of lateral movements which occur.

In summary, Fig. 2 demonstrates that the factor of safety against basal heave is a significant index to lateral wall movements. For wall and soil systems similar to those used in Fig. 2, the data may be employed directly to estimate expected levels of movement. The amount of scatter in the data gives the designer information as to the level of confidence which can be obtained in wall movement predictions.

Time Effects on Lateral Wall Movements.—As noted previously, data for several of the case histories were detailed enough that changes in wall movement could be observed over periods of time while the excavation depth was not changed. All of the projects where time data were available were located in the San Francisco Bay Area. It is presumed that the time dependent effects are due primarily to undrained creep in San Francisco Bay Mud.

In Fig. 3 the logarithm of the rate of the observed lateral movements, defined as $\Delta\delta/\Delta t$, is plotted versus the logarithm of time. A linear trend results, with

TABLE 1.—Pertinent Data for Case Histories

Case No. (1)	Location (2)	Wall type (3)	Wall end condition ^b (4)	Final depth of excavation, in meters (5)	Clay Prop	
					Average S_u , in tons per square meter (6)	w_p , as a percentage (7)
1	San Francisco Calif.	Sheet pile	Fixed	13.5	3.5	15-40
2	San Francisco, Calif.	Sheet pile	Fixed	14.0	3.5	15-40
3 ^a	San Francisco, Calif.	Sheet pile	Fixed	14.0	3.5	15-40
4	San Francisco, Calif.	Sheet pile	Free	9.1	2.4	35-60
5	San Francisco, Calif.	Sheet pile	Free	9.1	2.1	35-60
6	Oslo, Norway	Sheet pile	Fixed	11.0	2.5	15-30
7	Oslo, Norway	Sheet pile	Fixed	11.0	3.0	10-35
8	Oslo, Norway	Sheet pile	Free	9.2	3.0	10-35
9	Boston, Mass.	Sheet pile	Free	15.2	6.6	11
10	Chicago, Ill.	Soldier pile	Fixed	13.4	1.9	10-20
11	Bowline Point, N.Y.	Sheet pile	Fixed	9.8	3.9	10-40

^a Local unusual construction effects. Affected data not used.

^b Fixed end refers to wall tip embedded in underlying stiff layer; free end, tip in soft

Note: S_u = undrained shear strength; w_p = plasticity index; w = water content; S ,

the rate of movement decreasing rapidly with increasing time. This behavior is similar to that observed for results of undrained creep tests in the laboratory (20). The data in Fig. 3 also suggest that there is a tendency for higher creep rates to be associated with lower factors of safety, as would be expected. The utility of the results indicated by Fig. 3 lies in knowing that short-term, time-dependent movements are common for braced excavations, especially if the factor of safety is low. Instrumentation programs should be designed to pick up movements so as to identify the time related trends or to record the final, stabilized values. Such information will aid in reducing data scatter for correlations as defined in Fig. 2.

Relationship Between Maximum Surface Settlements and Maximum Lateral Wall Movements.—The designer of an excavation support system typically needs to know surface settlements as well as lateral wall movements, but settlements for the case histories of Table 1 are not as well documented. However, an approximate relationship between settlement and lateral wall movement can be established which can indirectly link settlements and factors of safety via Fig. 2. In Fig. 4 the available maximum settlement data are plotted versus lateral wall movements, and it can be seen that settlements range from 0.5-1.0 times the lateral wall movements. It should be re-emphasized here that cases

used in Field Response Plots

erties

w, as a per- centage (8)	S_r (9)	Minimum factor of safety, FS (10)	Movement, in centimeters		Reference (13)
			δ_H (11)	δ_V (12)	
45-60	4-8	1.3	19.3	15.2	25
45-60	4-8	1.3	15.0	14.4	Personal files
45-60	4-8	1.3	10.2	—	Personal files
55-90	4-8	1.3	3.8	—	24
75-100	8-20	1.0	25.4	—	24
20-45	2-6	1.0	23.5	23.3	19
20-45	2-6	1.1	14.2	14.0	20
20-45	3-7	1.3	18.5	11.6	21
30	—	1.6	11.5	—	14
20-40	—	1.2	8.9	8.0	22
35-65	4-8	2.4	5.1	—	18

to medium clay.
= sensitivity.

with unusual construction effects are not used since settlements in such instances can easily exceed the lateral wall movements. Considering only the data in Fig. 4, it would appear to be a useful and conservative design expedient to say that settlements will equal lateral wall movements. If such is the case, then Fig. 2 demonstrates the relationship between either maximum ground settlements or lateral wall movements and factor of safety against basal heave.

FINITE ELEMENT STUDIES

The finite element analyses are devoted towards defining effects of detailed parameters including wall stiffness, strut spacing and stiffness, excavation width, preloading, depth to an underlying stiff layer, and soil stiffness and strength distribution. It is beyond the scope of this paper to describe in detail the finite element procedures used in the studies. They have been developed and refined over a period of 8 yr (4,8,13,16,27), and have been shown to produce predicted behavior which is consistent with observed field response (4,5,6,21).

A number of versions of programs were used to produce the results for this paper. All of them allow for nonlinearity in the soil stress-strain curve, realistic variations in soil strength profiles, and simulation of the actual staged

sequence of construction of a braced wall. For purposes of simplicity, the primary program used in this work employed an isotropic stress-strain soil model which assumes a linear response prior to yield, and a perfectly plastic behavior, as defined by the von Mises criterion, after yield. This model is known to be

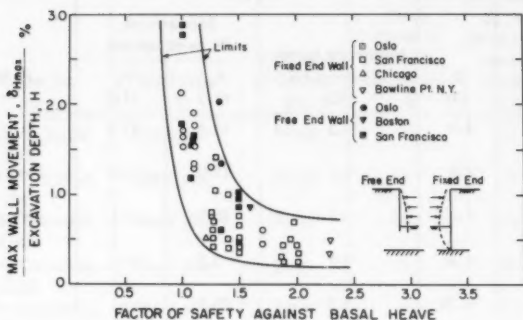


FIG. 2.—Relationship Between Factor of Safety Against Basal Heave and Nondimensionalized Maximum Lateral Wall Movement for Case History Data

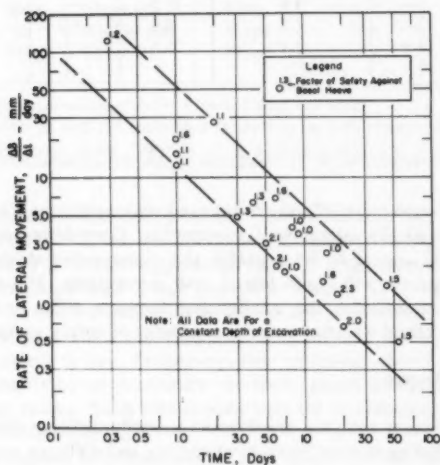


FIG. 3.—Observed Rate of Time Dependent Lateral Wall Movements in San Francisco Bay Mud

reasonably well suited for the undrained response of soft to medium clays. The program utilizes eight-node isoparametric elements for soil and wall materials, six-node slip elements for the interface between the wall and the soil, and two-node spring elements for struts. Plane strain conditions are assumed to

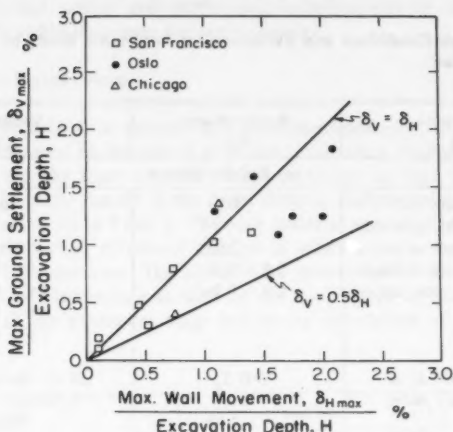


FIG. 4.—Relationship Between Maximum Ground Settlements and Maximum Lateral Wall Movements—Case History Data

exist. An elastic-plastic response is assigned for the load-deformation behavior of the slip elements.

PARAMETRIC STUDY PROBLEMS

Over 70 different analyses were made simulating braced wall excavations in homogeneous clay deposits. The variations considered in soil shear strength, soil stiffness, wall and strut properties, and excavation geometry are typical of those which could occur for braced walls in clay. Details of the parameters used in the analyses are given in Table 2. The primary variables are the magnitude and distribution of the undrained shear strength, the Young's modulus, support conditions, and depth to a rigid underlying layer. Basic values listed in Table 2 are those used in most of the analyses. Variations relative to the basic values are given in the last column of the table. Soil parameters are varied over ranges reported in the literature for soft to medium clays (1,8,10,11).

The different wall end conditions modeled are termed free or fixed consistent with those used for the field behavior. In most of the analyses, the wall stiffness is set equal to that of a PZ-38 steel sheetpile section. Three other wall sections are considered: a PZ-27 steel sheeting, a 0.5-m (20-in.) thick, and 1.0-m (39-in.) thick concrete diaphragm walls.

One to four crosslot strut levels are used in the analyses, with the first strut placed at a depth of 2.5 m (8.3 ft). Vertical spacings between the lower level struts are varied from 2.5 m–5.0 m (8.3 ft–16.5 ft). Depending upon the shear strength used, the lower strut spacings range from 0.2–2.0 times $2 S_u/\gamma$. The basic value of the strut stiffness is taken to be 2,000 t/m/lin m; values of 900 t/m/m, 8,000 t/m/m, and 25,000 t/m/m are used as the variations. Hansen

TABLE 2.—Basic Conditions and Variations for Parametric Study of Braced Excavations in Soft Clay

Parameter (1)	Basic values (2)	Variations (3)
(a) Soil Conditions		
Initial stress ratio, K_0	0.6	None
Total unit weight, γ , in tons per cubic meter	2.0	None
Undrained shear strength, S_u , in tons per square meter	$2.9 + 0.2\sigma'_v$ $0.9 + 0.2\sigma'_v$	$2.9 + 0.3\sigma'_v$ $1.9 + 0.2\sigma'_v$ $4.9 + 0.2\sigma'_v$ $7.9 + 0.2\sigma'_v$ 5.9
Young's modulus, E , in tons per square meter	$300 S_u$	$150 S_u$, $200 S_u$, $600 S_u$, $1,200 S_u$
Poisson's ratio, ν	0.48	None
Soil-to-wall adhesion, in tons per square meter	0.0	0.5, ∞ (inactive interface)
(b) Support Conditions		
Wall stiffness, EI , in tons-square meter per meter	8,088 (PZ-38)	5,310 (PZ-27) 22,200 (0.5 m slurry wall) 183,000 (1.0 m slurry wall)
Effective strut stiffness, in tons per meter per meter	2,000	900, 8,000, 25,000
Number of strut levels	4	1, 2, 3
Vertical strut spacing, per meter	3.5	2.5 m, 5.0 m ^b
Prestressing load (design values expressed as a percentage ^a)	0.0	50%, 100%
(c) General Conditions		
Depth to firm layer, in meters	30	15, 21, 25
Final depth of excavation, in meters	15	10, 20
Width of excavation, in meters	12	20, 48
Depth of wall penetration below final excavation depth, H_w , in meters		
(a) Free wall	2.5	6, 10
(b) Fixed wall	The wall was assumed to be driven into the firm layer and fixed against translation but free to rotate (hinged support).	

^aDesign values refer to strut loads calculated from the usual apparent pressure diagrams.

^bDepth to first strut level does not exceed 2.5 m.

Note: $1 \text{ t/m}^2 = 9.81 \text{ kN/m}^2$.

(13) has shown that actual strut stiffnesses, including effects of connections and wedges fall within this range for most projects.

RESULTS OF FINITE ELEMENT STUDIES

The review of field data showed that nondimensionalized maximum lateral wall movements could be correlated with factor of safety against basal heave. A similar plot for the finite element results is shown in Fig. 5. The data in the plot come from the results of the finite element analyses using basic values of the parameters listed in Table 2. The only material parameter which is varied is shear strength profile; effects of changes in other important parameters are considered in later sections. The lateral wall movements used in Fig. 5 are taken both at the intermediate as well as the final stages of excavation, with the exception of the cantilever stage before the installation of the first strut level.

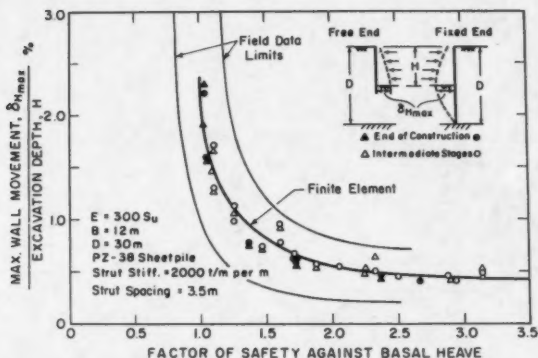


FIG. 5.—Analytically Defined Relationship Between Factor of Safety Against Basal Heave and Nondimensionalized Maximum Lateral Wall Movement

As is the case with the field data, there is a well-defined relationship between the basal heave factor of safety and maximum lateral movement showing that movements occur as a fixed percentage of excavation depth for large factors of safety, but increase very rapidly below a factor of safety of 1.5. There is a small scatter in the finite element points, produced by the fact that both free and fixed end wall data are used as well as data from the intermediate stages. Interestingly, there seems to be little effect of amount of wall penetration or wall end condition, a trend also observed with the field data.

Superimposed onto Fig. 5 are the ranges defined from the field data correlation established in Fig. 2. The ranges nicely band the finite element trend curve. This excellent agreement suggests that:

1. The finite element model and the soil parameters used, produce realistic

behavior over a wide range of conditions, spanning that of the 11 case histories in Table 2.

2. The correlation between movement and factor of safety can be verified theoretically or using field data.

Relationship Between Maximum Lateral Wall Movements and Maximum Settlements.—From the field data it was found that the maximum ground settlements behind the wall were from 0.5 to equal to the lateral wall movements. In the finite element results, the settlements range from 0.4–0.8 of the maximum lateral wall movements. As can be seen in Fig. 6, the settlements become a larger percentage of the lateral movements at lower factors of safety. The slightly larger ratio of settlement to lateral movement observed for some of the field cases is probably due to the effects of small amounts of consolidation or traffic or surcharge loading behind the wall.

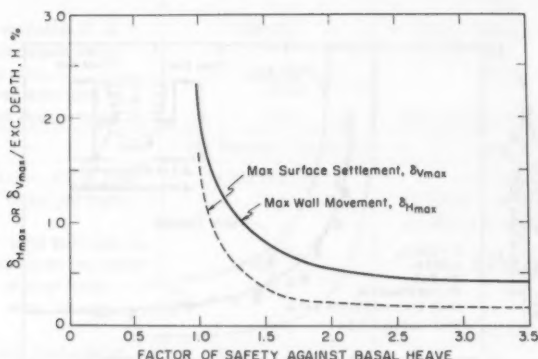


FIG. 6.—Analytically Defined Relationship Between Maximum Surface Settlement and Maximum Wall Movement as Function of Factor of Safety

Effects of Specific Parameters.—In Figs. 7–12 results are presented for the finite element analyses performed to quantify effects of important design parameters on maximum movements. For each case, the movement is expressed as a ratio of that which would occur using the basic parameter values listed in Table 2. The ratios are assigned symbols which reflect the effect of the parameter against which it is plotted:

1. α_w : wall stiffness and strut spacing (Fig. 7).
2. α_s : strut stiffness and spacing (Fig. 8).
3. α_D : depth to an underlying firm layer (Fig. 9).
4. α_B : excavation width (Fig. 10).
5. α_P : strut preload (Fig. 11).
6. α_m : modulus multiplier, M (Fig. 12).

Naturally, all of the α values are one if the basic parameters are used. In this case, the maximum lateral wall movement is obtained directly from Fig.

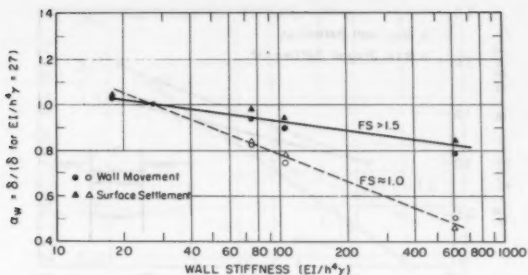


FIG. 7.—Effect of Wall Stiffness on Maximum Lateral Wall Movement (EI = Wall Bending Stiffness per Horizontal Unit of Length; h = Vertical Strut Spacing; γ = Total Unit Weight of Soil)

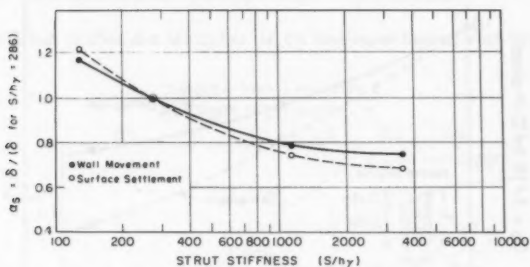


FIG. 8.—Effect of Strut Stiffness on Maximum Lateral Wall Movement (S = Strut Stiffness per Horizontal Unit of Length; h = Vertical Strut Spacing; γ = Total Unit Weight of Soil)

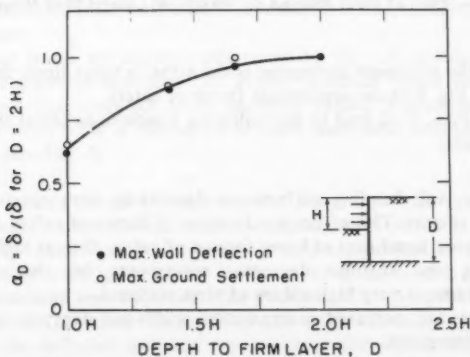


FIG. 9.—Effect of Depth to Underlying Firm Layer on Maximum Lateral Wall Movement

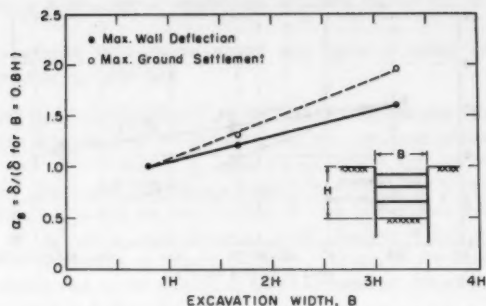


FIG. 10.—Effect of Excavation Width on Maximum Lateral Wall Movement

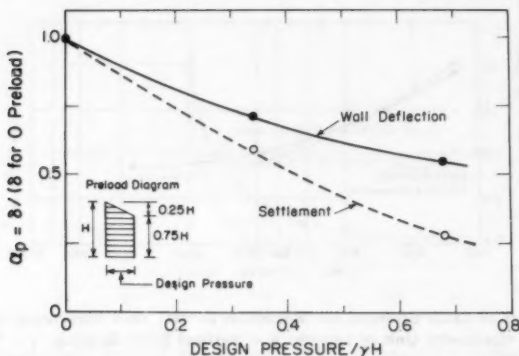


FIG. 11.—Effect of Strut Preload on Maximum Lateral Wall Movement

5. Otherwise, the maximum movement is the actual α value times the movement obtained from Fig. 5 at the appropriate factor of safety.

The data in Figs. 7-12 lead to the following conclusions about the individual parameter effects:

1. Increasing wall bending stiffness or decreasing strut spacing, or both, decreases movements. This effect is a function of factor of safety against basal heave, being more significant at lower factors of safety than at higher ones.

2. Increasing strut stiffness decreases movements, but the effect shows diminishing returns at very high values of strut stiffness.

3. Movements are increased as excavation width and depth to an underlying firm layer are increased.

4. Use of preloads in the struts reduces movements, although there is a diminishing returns effect at higher preloads. Very high preloads may, in fact,

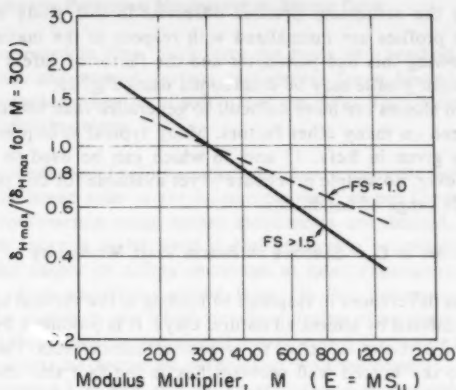


FIG. 12.—Effect of Modulus Multiplier, M , on Maximum Lateral Wall Movement

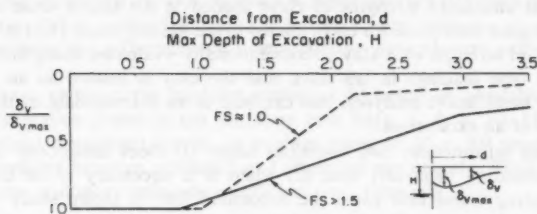


FIG. 13.—Envelopes to Normalized Ground Settlement Profiles

be counter-productive since local inward movements at support levels can damage adjacent utilities.

5. Movement levels are strongly influenced by the soil modulus, as characterized by the modulus multiplier, M . Higher modulus values lead to smaller movements and vice-versa for lower modulus values. Fortunately, for many cases a single value of $M = 300$ seems to yield reasonable results for predicted deformations (see Fig. 5).

Of the seven factors shown to influence movements, at least four are subject to designer control; namely, wall bending stiffness, strut stiffness, strut spacing, and preloading. These can be adjusted to hold movements to preset values, using the predictive methodology set out in a subsequent section of this paper.

Surface Settlement and Deflected Wall Profiles.—To this point, the primary emphasis has been on maximum levels of movement. In many cases, however, the shape of the deflected wall and the curvature and extent of the settlement trough are also important. This information can be quantified, using the results of the finite element analyses.

Envelopes to the settlement profiles observed in this study are presented in Fig. 13. The profiles are normalized with respect to the maximum vertical settlement. Knowing this one parameter and the factor of safety against basal heave, a settlement profile may be determined using Fig. 13.

Deflected wall shapes are more difficult to generalize than settlement profiles since they depend on many other factors. Many typical examples of deflected wall shapes are given in Refs. 13 and 16 which can be used to guide design estimates. However, no simple procedure is yet available for this purpose which works for a wide range of conditions.

EFFECT OF ANISOTROPY OF CLAY SUBSOILS ON BRACED WALL MOVEMENTS

Anisotropy, or differences in response to loading in the vertical and horizontal directions, is exhibited by almost all natural clays. It is produced by preferential orientation of soil particles as well as stress reorientation effects. The significance of anisotropy to the braced wall problem lies in the fact that the soil behind the wall, or on the active side, is loaded essentially by the vertical gravity stresses, while that on the passive side is loaded primarily horizontally by the lateral pressure exerted by the wall. For soft to medium clays, laboratory tests suggest that undrained strengths of clays loaded in the active sense are from 15%–80% higher than those for clays loaded in the passive sense (13,14). Because the undrained strength of a clay is conventionally evaluated using only active, or vertical type loadings in lab tests, and the clay is treated as an isotropic material in basal heave analyses, this can lead to an overestimate of the degree of stability of an excavation.

Given this information, two questions arise: (1) Does anisotropy in a clay affect deformation behavior? and; (2) when is it necessary to be concerned about anisotropy, and how can it be accounted for? A recent study reported by Clough and Hansen (7) addressed these questions. It was found that the primary effect of anisotropy is to lower the factor of safety against basal heave relative to its value determined by conventional procedures. No significant changes were observed in basic deformation patterns. This conclusion means that the data presented in this paper for isotropic soils may also be used for anisotropic soils, providing the proper factor of safety against basal heave is employed.

Based on the work of Clough and Hansen (7) it appears that unless the passive strength of a clay is less than 80% of the active strength, the basal heave factor of safety will be within 10% of its conventional value. Thus, only for the more strongly anisotropic clays or at low factors of safety will it normally be necessary to be concerned about anisotropy. A rigorous approach designed to include anisotropy would involve testing in the compression (active) and extension (passive) modes to determine the degree of anisotropy, and using this information in the Clough and Hansen (7) anisotropic bearing failure analysis. Alternatively, using results reported in the literature (14) and data from the specific project, a conservative value of undrained shear strength can be selected which lies halfway between the anisotropic extremes. This strength can then be used in an isotropic analysis (see Fig. 1) to establish the factor of safety against basal heave. Obviously, the latter approach is more applicable to situations in which stability is not critical.

SIMPLIFIED METHOD FOR PREDICTING MOVEMENTS OF BRACED CUTS

The data presented in Figs. 5-13 form the basis of a method for estimating wall movements and ground surface settlements for a braced excavation in soil deposit composed primarily of soft to medium clays. The prediction procedure involves the following steps:

1. Compute the factor of safety against basal heave using the technique outlined in Fig. 1 for isotropic soils or for anisotropic soils as per Clough and Hansen (7), at each construction stage where movements are desired. The factor of safety at each stage is to be used in the prediction procedures, except in a case where the factor of safety increases at later excavation stages due to the presence of an underlying strong layer. In this instance, the key factor of safety is the minimum one which develops during excavation.
2. Estimate the maximum lateral wall movements δH_{\max} using the relationship in Fig. 5 between the factor of safety and wall movements. The maximum ground settlement δV_{\max} can also be estimated directly assuming that it is in the range of 0.6-1.0 times the maximum wall movements.
3. Based on the wall stiffness, $EI/h^4\gamma$, the strut stiffness, $S/h\gamma$, the depth to firm layer D , and the excavation width B , determine the influence coefficients α_w , α_s , α_D , and α_B , using Figs. 7, 8, 9, and 10, respectively.
4. Determine the influence coefficient for the desired strut preloads using Fig. 11.
5. Select a value or the modulus multiplier M based on available test data or on information found in the literature (see Refs. 1, 4, 6, 10, 11, and 14). For the clays considered herein, an average value of $M = 300$ seems to yield good agreement between predicted and observed movements. Then determine the modulus multiplier influence coefficient, α_M , from Fig. 12.

TABLE 3.—Values of Parameters and Influence Coefficients for Predicting Wall Movement of Oslo Excavation

Parameter (1)	Parameter value (2)	Influence coefficient (3)	Coefficient value (4)
Factor of safety, FS	1	$\delta H_{\max}/H$	2.6%
Modulus multiplier, M	300	α_M	1.0
Average total unit weight of soil, γ	1.95 t/m ³	—	—
Max. Vertical distance between strut, h	2 m	—	—
Wall stiffness, $EI/[h^4\gamma]$	6,200/[2 ⁴ (1.95)] = 199	α_w	0.66
Average strut stiffness, $S/(h\gamma)$	1,100/[(2)(1.95)] = 282	α_s	1.0
Strut preloads	0	α_p	1.0
Excavation depth, H	11 m	—	—
Depth to firm layer, D	16 m = 1.5H	α_D	0.9
Excavation width, B	11 m = 1H	α_B	1.0

Note: Predicted maximum lateral movement = $(0.026)(1,100)(0.66)(0.9) \approx 17$ cm.

6. Using the value of δH_{\max} obtained in step 2 and the influence coefficients determined in steps 3, 4, and 5, a revised value for the maximum lateral wall movement is estimated as

$$\delta \dot{H}_{\max} = \delta H_{\max} \alpha_M \alpha_w \alpha_S \alpha_P \alpha_D \alpha_B \dots \quad (1)$$

in which δH_{\max} = the wall movement estimated from Fig. 5, and $\delta \dot{H}_{\max}$ is the revised estimate of the wall movement.

7. A revised estimate for the maximum surface settlement is obtained assuming it equals 0.6–1.0 times $\delta \dot{H}_{\max}$.

8. The ground settlement profile is established using the value of the maximum settlement from step 7 and Fig. 13.

9. The wall deflection profile is estimated by means of information given in Refs. 13 and 16.

To illustrate the use of the proposed method for movement prediction, the maximum wall movement of a well-documented braced excavation in Oslo, Norway (Ref. 17) is estimated. Details of the calculations to obtain the influence coefficients are given in Table 3. It should be noted that the shear strength used to calculate the factor of safety against basal heave was obtained from results of detailed vane shear and triaxial tests (1,17). Effects of shear strength anisotropy on the factor of safety were considered by both the rigorous and approximate techniques mentioned previously. By either approach, the basal heave factor of safety was approx 1. Substituting the values in Table 3 into Eq. 1, the predicted maximum wall movement is 17 cm. This is in good agreement with the observed maximum wall movements which ranged between 16 cm and 24 cm.

COMMENT ON USE OF METHOD FOR TIED-BACK WALLS

The methodology presented herein is primarily designed for crosslot braced walls. However, it can be used in its present form for tied-back walls providing that the anchors are embedded in an unmoving soil or rock mass. Such conditions are relatively common especially where the upper soils are soft or medium clays since the anchorage is usually established in lower firmer strata. Should the anchorage be subject to movement, the method is no longer applicable since this introduces displacements not considered in its development.

PROBLEMS INTRODUCED BY CONSTRUCTION TECHNIQUE

It is well known that poor construction procedures can easily lead to substantially increased movements of support walls and the retained soil. Numerous examples exist of problems created by improper connections, opening of caissons next to walls, dewatering, overexcavation below strut levels, placement of surcharge next to the wall, and excessive delays in strut installation (3,4,5,9,22). When predicting braced cut movements, these factors should be considered in deciding the degree of conservatism to use. Their effects can be minimized by proper specifications and good construction practice.

SUMMARY AND CONCLUSIONS

The purpose of this paper is to derive a procedure for prediction of wall and soil movements for excavations in clay deposits supported by crosslot braced walls. A methodology is developed by combining the results of field performance and finite element analyses. The combination of the results from the two sources is important, since the field data provide a hard, general data base to judge performance, but little information on effects of change in design details. The finite element technique provides the controlled environment within which effects of variations in design details can be judged.

The field data and the finite element results showed that strong correlations could be established between system movement and the factor of safety against basal heave. The rate and magnitude of movement increases rapidly as the factor of safety approaches one.

Based on the established behavior trends of field cases and the results of finite element analyses, a simple method for predicting movements associated with crosslot braced excavations in soft to medium clays is developed. Nondimensionalized charts are provided for estimating the magnitudes and distributions of wall movements and surface settlements as a function of: (1) The factor of safety against basal heave evaluated at the desired construction stage; (2) soil stiffness; (3) support stiffness; (4) strut preloads; and (5) excavation geometry. The method is easy to use and gives a reliable estimate of wall movements when tested against observed data. It is expected to be especially valuable to a design engineer in making quick assessments of the influence of changes in design parameters.

ACKNOWLEDGMENTS

The writers would like to express their appreciation to their colleagues Lawrence A. Hansen, Philippe H. Mayu, R. R. Davidson, and G. M. Denby who helped assemble data and took part in useful analyses concerning the design method developed herein. Messers. H. Taylor and F. Rollo of Harding Lawson Associates of San Francisco, and Dr. Ralph B. Peck generously provided data for several unpublished case histories. The cooperation of Mr. Edmund McCarthy of Peter Kiewit Sons Contractors is also appreciated in helping obtain data on one of the projects. Financial support for the work was obtained from the University of Petroleum and Minerals, Dhahran, Saudi Arabia and NSF Grant No. ENG-05999.

APPENDIX I.—REFERENCES

1. Berre, T., and Bjerrum, L., "Shear Strength of Normally Consolidated Clays," *Proceedings of the 8th International Conference on Soil Mechanics and Foundation Engineering*, Vol. 1.1, 1973, pp. 39-49.
2. Bjerrum, L., and Eide, O., "Stability of Strutted Excavations in Clay," *Geotechnique*, London, England, Vol. 6, No. 1, 1956, pp. 32-47.
3. Broms, B., and Stille, H., "Failure of Anchored Sheet Pile Walls," *Journal of the Geotechnical Engineering Division*, ASCE, Vol. 102, No. GT3, Proc. Paper 12000, Mar., 1976, pp. 235-254.
4. Clough, G. W., and Mana, A. I., "Lessons Learned in Finite Element Analyses

- of Temporary Excavation," *Numerical Methods in Geomechanics*, ASCE, C. S. Desia, ed., Vol. I, June, 1976, pp. 243-265.
5. Clough, G. W., and Davidson, R. R., "Effects of Construction on Geotechnical Performance," *Proceedings, Specialty Session III, Ninth International Conference on Soil Mechanics and Foundation Engineering*, 1977, pp. 15-33.
 6. Clough, G. W., and Denby, G. M., "Stabilizing Berm Design for Temporary Walls in Clay," *Journal of the Geotechnical Engineering Division*, ASCE, Vol. 103, No. GT2, Proc. Paper 12745, Feb., 1977, pp. 75-90.
 7. Clough, G. W., and Hansen, L. A., "Effects of Clay Anisotropy on Braced Wall Behavior," accepted by the ASCE Geotechnical Division Journal for Publication, 1981.
 8. Clough, G. W., Hansen, L. A., and Mana, A. I., "Prediction of Behavior of Supported Excavations Under Marginal Stability Conditions," *Proceedings, 3rd International Conference on Numerical Methods in Geomechanics*, Vol. IV, 1979, pp. 1485-1502.
 9. D'Appolonia, D. J., "Effects of Foundation Construction on Nearby Structures," *Proceedings of the Fourth Pan American Conference on Soil Mechanics and Foundation Engineering*, Vol. I, June, 1971.
 10. D'Appolonia, D. J., Poulos, H. G., and Ladd, C. C., "Initial Settlement of Structures on Clay," *Journal of the Soil Mechanics and Foundations Division*, ASCE, Vol. 97, No. SM10, Proc. Paper 8438, Oct., 1971, pp. 1359-1377.
 11. Duncan, J. M., and Buchignani, A. L., "An Engineering Manual for Settlement Studies," *Geotechnical Engineering Report*, Department of Civil Engineering, University of California, Berkeley, Calif., June, 1976.
 12. Goldberg, D. T., Jaworski, W. E., and Gordon, M. D., "Lateral Support Systems and Underpinning," *Reports FHWA-RD-75-128 to 131*, Vols. 1, 2, 3, 4, Federal Highway Administration, Washington, D.C., Apr., 1976.
 13. Hansen, L. H., "Prediction of Behavior of Braced Excavations in Anisotropic Clay," thesis presented to Stanford University, at Stanford, Calif., in 1980, in partial fulfillment of the requirements for the degree of Doctor of Philosophy.
 14. Ladd, C. C., Foott, R., Ishihara, K., Schlosser, F., and Poulos, H. G., "Stress-Deformation and Strength Characteristics," *Proceedings, Ninth International Conference on Soil Mechanics and Foundation Engineering*, Vol. II, 1977, pp. 421-494.
 15. Lambe, T. W., "Braced Excavations," *Lateral Stresses in the Ground and Design of Earth-Retaining Structures*, ASCE, June, 1970, pp. 149-218.
 16. Mana, A. I., "Finite Element Analyses of Deep Excavation Behavior in Soft Clay," thesis presented to Stanford University, at Stanford, Calif., in 1980, in partial fulfillment of the requirements for the degree of Doctor of Philosophy.
 17. "Measurements at a Strutted Excavation, Oslo Subway, Vaterland 1, km. 1373," *Technical Report 6*, Norwegian Geotechnical Institute, Oslo, Norway, 1962.
 18. "Measurements at a Strutted Excavation, Oslo Subway, Vaterland 2, km. 1408," *Technical Report 7*, Norwegian Geotechnical Institute, Oslo, Norway, 1962.
 19. "Measurements at a Strutted Excavation, Oslo Subway, Vaterland 3, km. 1450," *Technical Report 8*, Norwegian Geotechnical Institute, Oslo, Norway, 1962.
 20. Mitchell, J. K., *Fundamentals of Soil Behavior*, John Wiley & Sons, Inc., New York, N.Y., 1976, 415 pp.
 21. Murphy, D. J., Clough, G. W., and Woolworth, R. S., "Temporary Excavations in Varved Clay," *Journal of the Geotechnical Division*, ASCE, Vol. 101, Proc. Paper 11179, Mar., 1975, pp. 279-295.
 22. O'Rourke, T. D., Cording, E. J., and Boscardin, M., "The Ground Movements Related to Braced Excavations and Their Influence on Adjacent Buildings," *Report No. DOT-TST 76T-23*, United States Department of Transportation, Washington, D.C., Aug., 1976.
 23. Peck, R. B., "Deep Excavations and Tunneling in Soft Ground," *Proceedings of the 7th International Conference on Soil Mechanics and Foundation Engineering*, State-of-the-Art-Volume, 1969, pp. 225-290.
 24. Reed, M. W., "Observed Behavior of an Excavation in an Unusually Soft San Francisco Bay Mud Deposit," thesis presented to Stanford University, at Stanford, Calif., in 1980, in partial fulfillment of the Engineers Degree.
 25. Tait, R. G., and Taylor, H. T., "Design Construction and Performance of Rigid and Flexible Bracing Systems for Deep Excavations in San Francisco Bay Mud,"

presented at the January, 1974, ASCE National Meeting, held at Los Angeles, Calif. (Paper Preprint No. 2161).

26. Terzaghi, K., *Theoretical Soil Mechanics*, John Wiley & Sons, Inc., New York, N.Y., 1943.
27. Tsui, Y., "A Fundamental Study of Tied-Back Wall Behavior," thesis presented to Duke University, at Durham, N.C., in 1974, in partial fulfillment of the requirements for the degree of Doctor of Philosophy.

APPENDIX II.—NOTATION

The following symbols are used in this paper:

- A = cross-sectional area;
- B = excavation width;
- D = depth to rigid base;
- d = distance from excavation;
- E = Young's modulus;
- FS = factor of safety against basal heave;
- H = depth of excavation;
- H_w = depth of wall embedment;
- h = maximum vertical distance between support levels;
- I = moment of inertia;
- k_0 = coefficient of lateral earth pressure at-rest;
- L = length;
- M = modulus multiplier, $E = MS_u$;
- N_c = bearing capacity factor;
- S = effective strut stiffness per unit of length;
- S_t = sensitivity;
- S_u = undrained shear strength of clay;
- w_p = plasticity index;
- w = water content;
- α_B = excavation width influence coefficient;
- α_D = depth to firm layer influence coefficient;
- α_M = modulus multiplier influence coefficient;
- α_P = strut preload influence coefficient;
- α_S = strut stiffness influence coefficient;
- α_W = wall stiffness influence coefficient;
- δ_H = lateral wall displacement;
- δ_V = ground settlement;
- $\Delta\delta$ = increment of deflection;
- Δt = time increment;
- γ = total unit weight of soil;
- σ'_v = effective initial vertical stress in soil; and
- ν = Poisson's ratio.

SOIL-STEEL STRUCTURE RESPONSE TO LIVE LOADS

By Baidar Bakht¹

INTRODUCTION

In this paper the term soil-steel structures is being used for bridges and culverts which are composed of corrugated steel plate shells embedded in an envelope of engineered soil. Although the studies described herein were conducted on structures having shells of corrugated steel plates, the conclusions are general enough to be applicable to similar structures having flexible shells of other materials such as aluminum. The metallic shells of soil-steel structures are generally designed only for thrust resulting from dead and live loads (2,11). Moments are usually neglected.

Because of the ease of construction, soil-steel structures are regarded as relatively simple structures, and thus are generally expected to be designed by simple methods. Notwithstanding the ease of construction, the interaction between the metallic shell and the soil envelope is very complex, depending upon such factors that cannot be easily included even in fairly elaborate design procedures. The need for simplistic design procedures led to the development of various approximate methods of calculating load effects in the metallic shell. In the past, soil-steel structures usually had fairly large depths of cover, being in excess of about 8 ft (2.5 m). Consequently, live load effects were quite small in comparison with the dead load effects. In such cases, quite justifiably, little effort was expended to realistically determine live load effects. Several simplified methods with overly simplified and sometimes questionable assumptions were developed to assess live load effects. Any attempt to experimentally verify predictions of live load effect does not seem to have been reported in the literature.

The legacy of treating live load effects with oversimplifying assumptions has been extended to even recent times when the depths of cover are no longer always large. Tests on actual structures, described later in the paper, confirm that the current methods of determining live load effects in soil-steel structures are over conservative.

The objectives of this paper are to: (1) Review the current methods of

¹Sr. Research Officer, Research and Development Branch, Ontario Ministry of Transportation and Communications, Downsview, Ontario, Canada.

Note.—Discussion open until November 1, 1981. To extend the closing date one month, a written request must be filed with the Manager of Technical and Professional Publications, ASCE. Manuscript was submitted for review for possible publication on June 30, 1980. This paper is part of the Journal of the Geotechnical Engineering Division, Proceedings of the American Society of Civil Engineers, ©ASCE, Vol. 107, No. GT6, June, 1981. ISSN 0093-6405/81/0006-0779/\$01.00.

determining live load responses; (2) describe live load tests on three in-service soil-steel structures and present significant results; (3) present an improved simplified method for determining live load responses; and (4) present a justification for including the impact factor in the consideration of live load effects even when the depth of cover is larger than about 3 ft (0.91 m).

EXISTING METHODS

Some of the currently used common methods for determining live load responses in soil-steel structures are given as follows.

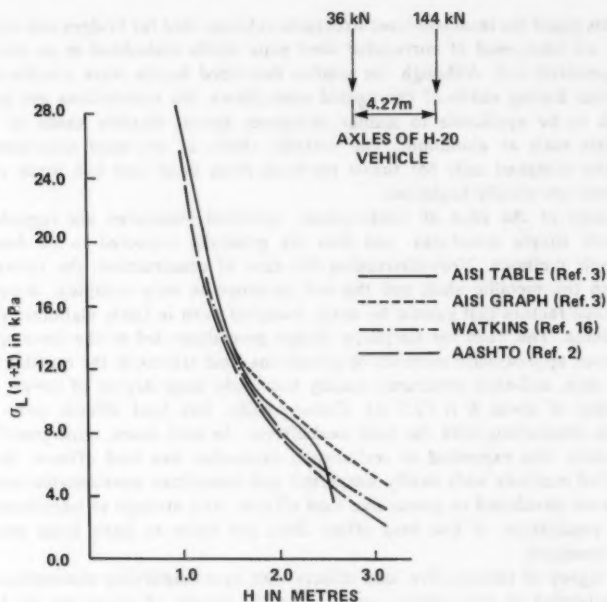


FIG. 1.—Equivalent Distributed Load at Crown

Watkins' Method.—According to this method (Ref. 16) the conduit wall thrust, T_L , due to live loads above is given by:

$$T_L = 0.5C_p\sigma_L(1+I)D_h \dots \dots \dots (1)$$

in which C_p = a "pressure transfer" coefficient; I = the impact factor; σ_L = the equivalent distributed pressure at crown level; and D_h = the conduit span. Parameter C_p , which strictly speaking accounts for the arching action of only dead loads, depends upon the degree of soil compaction, corrugation profile, and the pipe diameter. Its values are given in graphical form. For soil-steel structures made of 6 in. \times 2 in. (152 mm \times 51 mm) corrugated plates and

having a maximum span of 24 ft (7.3 m), these values, which are said to have been obtained experimentally for circular pipes, range between 0.65 and 1.3. For highway loading I is assumed to be 0.3 for H equal to zero, and 0.0 for $H > 3$ ft (0.91 m).

The equivalent pressure, σ_L at crown level is obtained by using the Boussinesq theory for force effects in an elastic half space (15). According to this theory, σ_L is given by:

$$\sigma_L = P \frac{C_b}{H^2} \quad \dots \dots \dots (2)$$

in which P = the concentrated load at the surface; H = the depth of cover

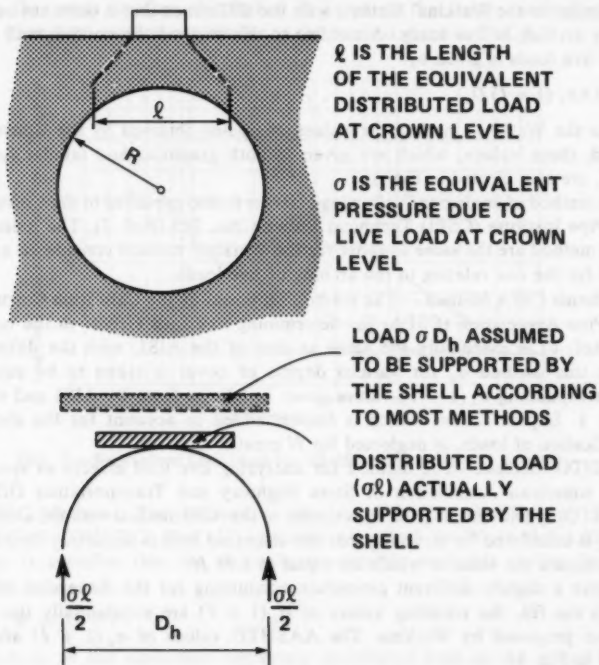


FIG. 2.—Thrust in Shell When Length of Equivalent Distributed Load is Smaller than Conduit Span

above crown; and C_b = the Boussinesq coefficient which depends upon the location of the reference point with respect to the load. The values of $\sigma_L(1 + I)$ corresponding to American Association of State Highway and Transportation Officials (AASHTO) H-20 truck (2) are reproduced in Fig. 1. Several assumptions inherent in this method are open to question: (1) It seems unlikely that the

Boussinesq equation, which is strictly applicable to an elastic half space, could be applicable in the vicinity of a large void in the half space; (2) the application of the pressure transfer coefficient in Eq. 2 suggests that both live and dead loads undergo similar arching actions above the conduit. Tests described later in the paper demonstrate that the live load effects in a structure with an horizontally elliptical conduit are larger than those in a similar structure with a round conduit. This is contrary to the behavior of soil-steel structures under dead loads; and (3) Eq. 1 is based on the premise that the live load pressure at crown extends to the full conduit span. In case of shallow covers, the length of the distributed load might be smaller than the span in which case D_h in Eq. 1 should be replaced by the length of the distributed load. This point is shown in Fig. 2.

AISI Method.—The American Iron and Steel Institute (AISI) method (Ref. 3) is similar to the Watkins' Method with the difference that it does not account for any arching of live loads. According to this method the conduit wall thrust due to live loads is given by:

$$T_L = 0.5 \sigma_L (1 + I) D_h \quad (3)$$

As in the Watkins' method the values of σ_L are obtained by the Boussinesq method; these values, which are given in both graphical and tabular form in Ref. 3, are also plotted in Fig. 1.

This method of analyzing for live load effects is also specified in the Corrugated Steel Pipe Institute (CSPI) Technical Bulletin No. 205 (Ref. 7). The limitations of this method are the same as those for the Watkins' method considered earlier, except for the one relating to the arching of live loads.

California CSPA Method.—The method proposed by the California Corrugated Steel Pipe Association (CSPA) for determining live load effects in the conduit wall (Ref. 6) is essentially the same as that of the AISI, with the difference that in this method σ_L for various depths of cover is taken to be equal to the corresponding $\sigma_L (1 + I)$ values given in tabular form by AISI and shown in Fig. 1. Impact factor, which is further added to account for the dynamic magnification of loads, is neglected for H greater than 3 ft.

AASHTO Method.—The method for analyzing live load effects as specified in the American Association of State Highway and Transportation Officials (AASHTO) specifications (Ref. 2) is similar to the AISI method with the exception that σ_L is calculated by assuming that the dispersed load is uniformly distributed over a square the sides of which are equal to $1.75 H$.

Despite a slightly different procedure accounting for the dispersion of load through the fill, the resulting values of $\sigma_L (1 + I)$ are substantially the same as those proposed by Watkins. The AASHTO values of $\sigma_L (1 + I)$ are also plotted in Fig. 1.

Kaiser Aluminum Method.—The Kaiser Aluminum method for flexible metal culverts and long-span super-metal culverts is reported by Selig et al. (Ref. 13). The thrust due to live load is calculated as follows:

$$T_L = K_{p3} LL \quad (4)$$

in which $K_{p3} = 1.25 - H/D_h$ for $0.25 < H/D_h < 0.75$; $K_{p3} = 1.00$ for $H/D_h < 0.25$; $K_{p3} = 0.5$ for $H/D_h > 0.75$; and LL is obtained from a table which for the AASHTO HS-20 loading is reproduced in graphical form in Fig. 3.

The values of LL were obtained by analyzing an elastic half space by the

Boussinesq theory (13) for surface loadings due to two side by side AASHTO vehicles, and a line load. The line load which produced the same maximum vertical stress at a level H below the surface, as the corresponding maximum stress due to the HS-20 vehicles, was regarded as the equivalent line load. Values of K_{p3} were derived, by an upper-bound curve-fitting process from results of a large number of finite element analyses of plane-strain models of soil-steel structures of different shapes and sizes. Live load bending moment, M_L , in the metal shell is also calculated by similar empirical equations.

The version of Kaiser Aluminum method given in Ref. 14 suggests that live load effects remain virtually constant for depths of cover between 0.3 m and about 5.0 m. This implication contradicts the long held belief that live load effects decrease rapidly with the increase in depths of cover. Tests described later in the paper confirm this belief. It is noted that later versions of the Kaiser Aluminum method are similar to the method given in Ref. 9.

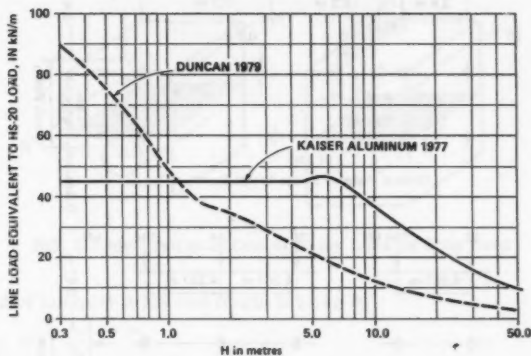


FIG. 3.—Equivalent Live Load for HS-20 Loading (Refs. 9 and 14)

OHBD Method.—The preliminary version of the Ontario Highway Bridge Design Code (OHBD) (Ref. 11) specifies a method similar to the AASHTO method. It specifies that the thrust in the conduit wall due to live loads is given by:

$$T_L = \sigma_L R_i m_f (1 + I) \dots \dots \dots (5)$$

in which σ_L = the equivalent uniformly distributed load at the crown level; R_i = the radius of curvature at crown; m_f = the modification factor for multilane loading; and I = the dynamic load allowance expressed as a fraction of the live load. Parameter σ_L is obtained by dispersing the wheel loads of the OHBD truck (shown in Fig. 4) from their contact areas at the profile grade down to the crown at a slope of two vertically to one horizontally. Parameter m_f is specified to be equal to 1.0 when there is only one vehicle on the embankment, and equal to 0.95 in the case of two vehicles. For one vehicle I is specified to be 0.4 for H equal to zero and not less than 0.1 for depths of cover of 6.6 ft (2 m) and more. Linear interpolation of I is allowed between $H = 0.0$

ft and 6.6 ft (2 m). In the case of two vehicles the dynamic load allowance is obtained by multiplying the value of I for one vehicle with 0.7.

The commentary to the OHBD Code (Ref. 12) provides the governing values of $\sigma_L(1 + I)m_f$ corresponding to various depths of cover in a graphical form. It is admitted in the commentary that the live load criteria specified in the Code is definitely conservative.

Like most other simplified methods, the OHBDC method is also based on the assumption that the distributed load at crown level extends to the full span of the conduit. This assumption would prove quite conservative when the depth of cover is small with respect to the span (see Fig. 2). In addition, the inclusion of R_t , rather than $0.5D_h$, in Eq. 5 is another source of possible errors. In

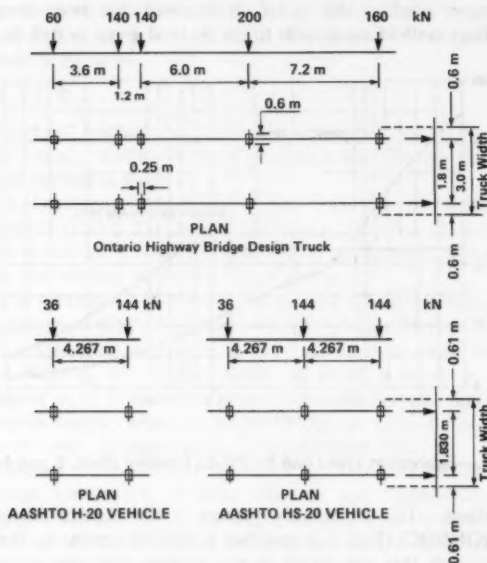


FIG. 4.—Design Vehicles

the case of horizontally elliptical pipes $2R_t$ is larger than D_h , in which case the value of T_L given by Eq. 5 is larger than if the corresponding value of $0.5D_h$ was used instead of R_t . This error would be on the safe side in the case of horizontally elliptical pipes, but in the case of vertically elliptical pipes, in which D_h is larger than $2R_t$, this error would be on the unsafe side.

Strip Methods.—Computer based analyses of soil-steel structures have so far been mostly limited to two-dimensional plane strain analyses of a unit width slice of the structure. The inherent assumption in these analyses is that there are no variations of force effects in the longitudinal direction of the pipe. This assumption, while being quite realistic under dead loads, may not be so under

live loads which disperse through the fill both longitudinally and transversely. The two commonly used methods of idealizing live loads for plane strain analyses are presented as follows.

Katona et al. (Ref. 10) use the Boussinesq theory to idealize the concentrated loads as equivalent line loads running parallel to the conduit axis. According to this theory, the maximum vertical pressure, σ_{\max} , along a horizontal line due to concentrated load P is given by

$$\sigma_{\max} = \frac{3}{2} \frac{P}{\pi} \frac{H^3}{h^5} \quad \dots \dots \dots (6)$$

in which h and H are as defined in Fig. 5. The corresponding σ_{\max} due to

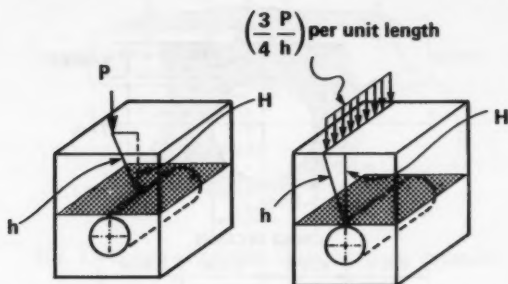


FIG. 5.—Idealization of Concentrated Load by Strip Load

a line load of intensity p per unit length is given by

$$\sigma_{\max} = \frac{2p}{\pi} \frac{H^3}{h^4} \quad \dots \dots \dots (7)$$

Equating Eq. 6 and Eq. 7

$$p = \frac{3}{4} \frac{P}{h} \quad \dots \dots \dots (8)$$

A line load, the intensity of which is given by Eq. 8, is assumed to be the idealized load that is employed in the plane-strain analysis. Duncan (9) utilizes the same technique as utilized by Katona et al. (10). However, instead of determining an equivalent strip load for a single load, he calculates the equivalent line load which, according to the Boussinesq theory, produces the same peak vertical stress as do the two HS-20 vehicles shown in Fig. 4. Thus calculated values of live loads are plotted in Fig. 3, which also shows similar equivalent live loads used in that version of the Kaiser Aluminum method which is given in Ref. 14.

As mentioned earlier, the applicability of the Boussinesq theory for elastic half space in the vicinity of the conduit which constitutes a rather large disturbance in the half space, is open to question. According to this theory loads disperse

equally in all directions, but test results described later show that above a conduit the dispersion of a concentrated load in different directions does not conform to any single pattern. This suggests that the idealization of concentrated load by Eq. 8 could only be regarded as a crude approximation, in which case any rigorous analysis, being subject to the same approximations as the load idealization, cannot be relied upon to predict very realistic results.

TEST DETAILS

In order to measure thrusts and moments in the metal shell due to live loads, three structures were tested. The first tested structure was the Deux Rivières

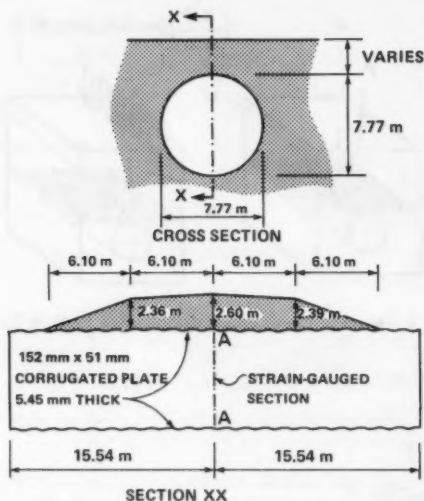


FIG. 6.—Details of Deux Rivières Soil-Steel Structure

structure on Highway 17 in Northern Ontario. The details of this structure are given in Fig. 6. This structure was constructed about 10 years ago. The second and third tested structure were the Adelaide Creek and White Ash Creek structures respectively. Both of these structures, which are located in South-western Ontario, were constructed about 6 years ago. Their details are shown in Figs. 7 and 8.

Little information is available about the backfill details except that it is composed of well compacted high quality granular material. Live load thrusts and moments in the metallic shell were monitored by means of temperature-compensated uniaxial strain gages, installed on the inside of the pipes. At every station three gages were applied—one at the top of the crest, one at the bottom of the valley, and the third at the geometric neutral axis of the corrugated plate. As

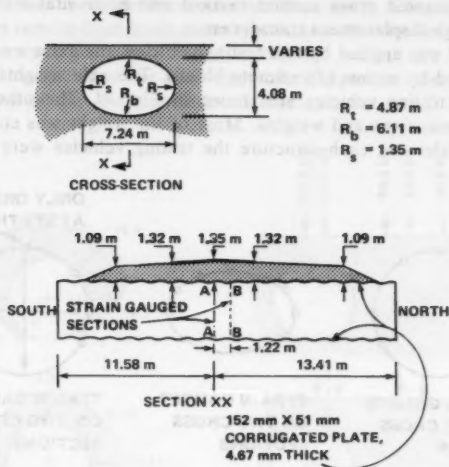


FIG. 7.—Details of Adelaide Creek Soil-Steel Structure

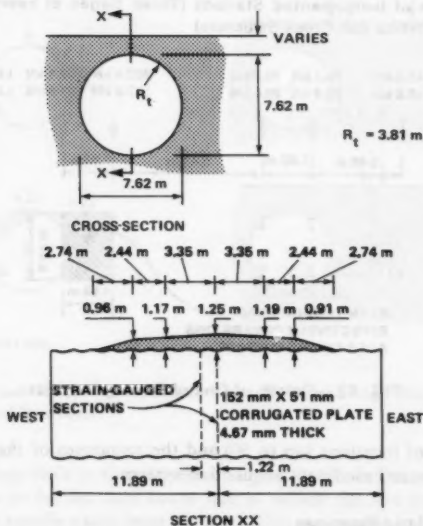


FIG. 8.—Details of White Ash Creek Soil-Steel Structure

shown in Fig. 9 seven–nine stations were instrumented at a given cross section. At each instrumented cross section vertical and horizontal movements were recorded through displacement transducers.

The live load was applied by two testing vehicles, the axles weights of which can be regulated by means of concrete blocks. The axle weights and spacings of one of the testing vehicles are shown in Fig. 10. The other vehicle has very similar dimensions and weights. Most of the weight was concentrated on the rear two axles. At each structure the testing vehicles were positioned at

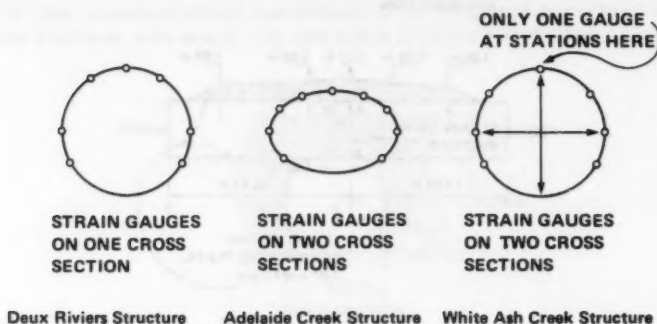


FIG. 9.—Location of Instrumented Stations (Three Gages at Every Station Except Two Stations in White Ash Creek Structure)

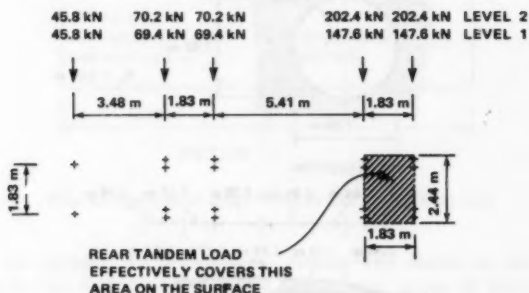


FIG. 10.—Details of One of Testing Vehicles

a large number of locations (up to 50) and the responses of the gages recorded through a computer based data acquisition system.

MEASURED STATIC LOAD RESPONSES

Thrusts.—A few values of thrusts computed from measured strains, all which were found to be elastic, are given in Figs. 11, 12, 13, and 14. All measured

strains showed remarkably similar patterns. Contrary to the usual assumption the live load thrust is not uniform around the conduit. Those portions of the shell which are remote from loads are subjected to very little thrust. The possible causes for the nonuniformity of thrust around the conduit are moments in the shell and friction between the shell and soil. Because of the relatively small flexural rigidity of the shell the induced moments are small, as shown later,

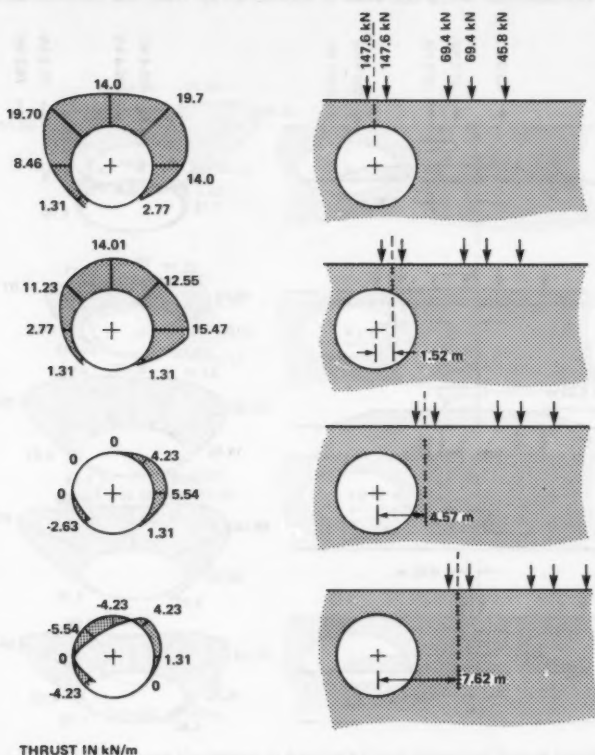


FIG. 11.—Live Load Thrust Variations in Deux Rivieres Bridge Due to Longitudinal Variations of Load Positions

and thus contribute little to the nonuniformity of thrust. In this case the interface friction appears to be the only cause due to which the live load thrust in the shell diminishes rapidly away from the load. This conclusion has been confirmed by analytical studies done by Abdel-Sayed et al. (1).

It was observed that the maximum thrust is induced when the two axes are symmetrically placed above the cross section center line. A scrutiny of

Figs. 11 through 14 will reveal that the distance of the load from the section under consideration has different influence in different directions. For the Adelaide Creek structure the thrust at one of the haunches is plotted in Fig. 15 with respect to the load position in different directions. It can be seen that when the load is moved away from a section along the conduit axis, its influence decreases very rapidly, being almost nil when it is at half a span distance away from the section. When the load is moved away from the conduit axis along

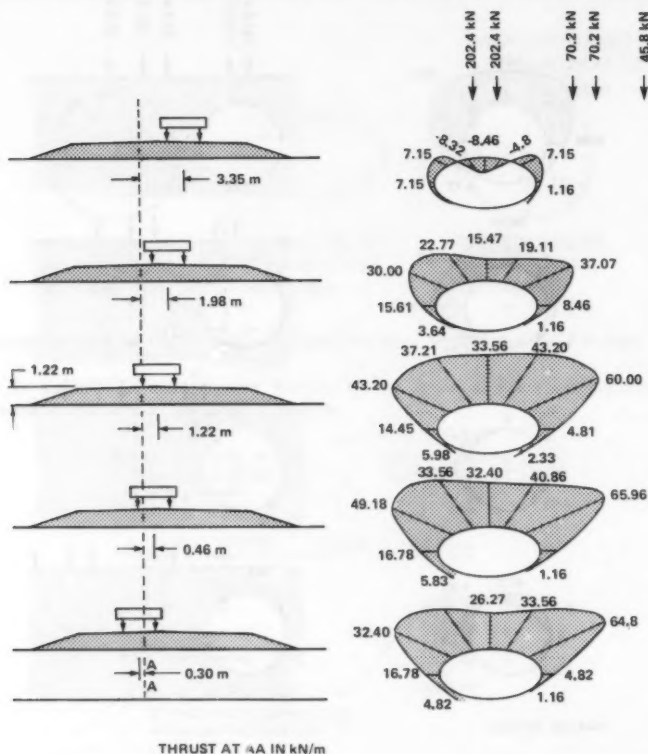


FIG. 12.—Live Load Thrust in Adelaide Creek Structure

the roadway, the influence of the load on the section under consideration decreases much less rapidly, with the shape of thrust-distance curve being concave while that of the former one is convex.

In light of the previous observation it is obvious that the assumption of load being dispersed uniformly in all directions is not valid. It is clear that a concentrated load disperses much more rapidly in the longitudinal direction of the conduit than it does in the transverse direction.

Moments.—Moments in the conduit wall, as computed from the measured strains were found to be negligible in the Deux Rivieres and the White Ash Creek structures, both of which have round conduits. In the White Ash Creek structure the maximum observed moment, which occurred at the haunches, corresponded to a top fiber stress of 0.25 ksi (1.72 MPa) under a tandem load of 91 kips (405 kN). It is recalled that in North America the legally permitted tandem load rarely exceeds 45 kips (200 kN). The observed maximum live load

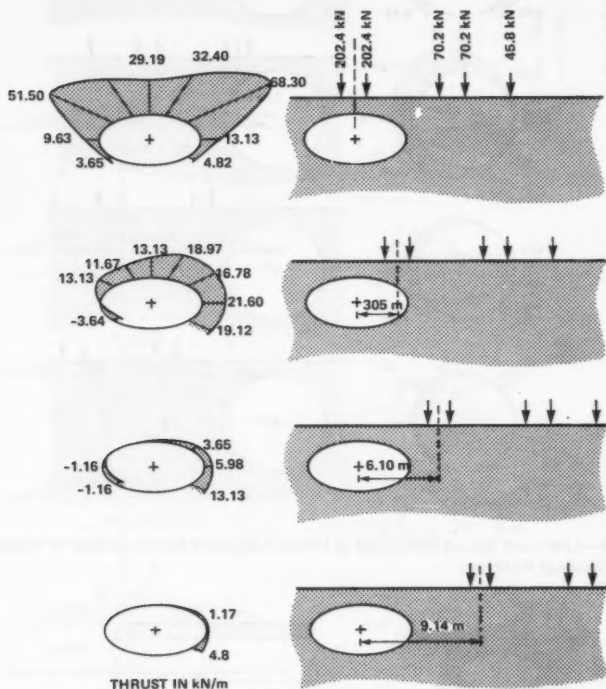


FIG. 13.—Live Load Thrust Variations in Adelaide Creek Structure Due to Longitudinal Variations of Load Positions

moment in the Deux Rivieres structure, which has a larger depth of cover than the White Ash Creek structure, was even smaller.

Somewhat larger moments were observed in the low profile Adelaide Creek structure. For this structure, moments computed from observed strains are plotted in Fig. 16 for various positions. It can be seen that even these moments are not large. The maximum observed moment, which again occurs at one of the haunches, corresponds to a top fiber stress of 0.93 ksi (6.41 MPa). Reference 4 contains further information on measured moments.

MEASURED DYNAMIC LOAD RESPONSES

Selected strain gages and deflection transducers were continually recorded during controlled vehicle passes over the Adelaide Creek and White Ash Creek structures. Vehicle passes were made at different speeds, and for some passes the vehicle was made to travel over an artificial irregularity in the riding surface

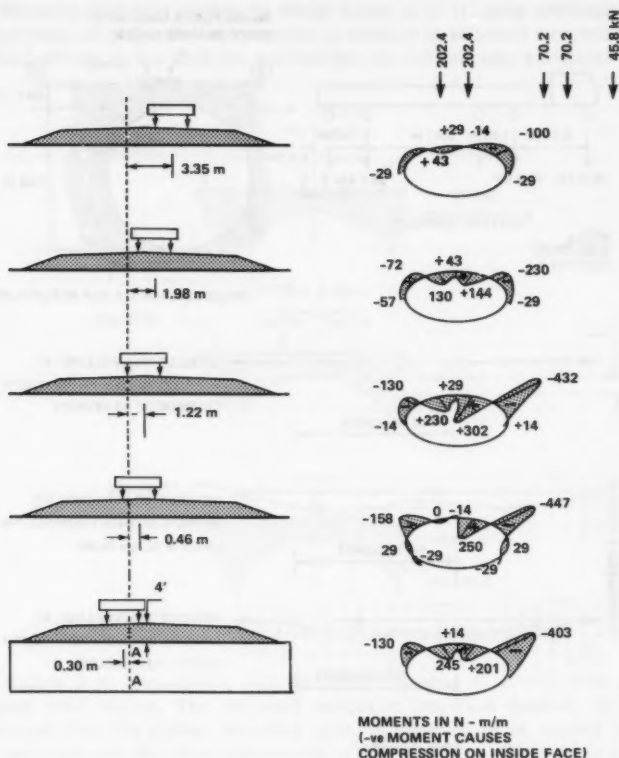


FIG. 16.—Live Load Moments in Adelaide Creek Structure

created by placing a 0.5 in. (13 mm) thick wooden plank directly above the crown. For each structure five strain gages and the crown deflection were monitored. The measured strains and deflections were plotted onto a strip chart recorder. Representative strip chart output for one gage on the White Ash Creek structure dynamic test is shown in Fig. 17.

In a bridge, the dynamic magnification of loads is mainly caused by the interaction of the dynamic systems of the vehicle and the structure (8). This

interaction, which is present even if the riding surface of the bridge is smooth, results in a strain-time curve that is not smooth. The observed curve corresponding to a smooth riding surface on the soil-steel structure was almost free of irregularities, as shown in Fig. 17, suggesting that because of the considerable damping characteristics of the structure there was little interaction between the dynamic systems of the vehicle and structure. An irregularity in the riding

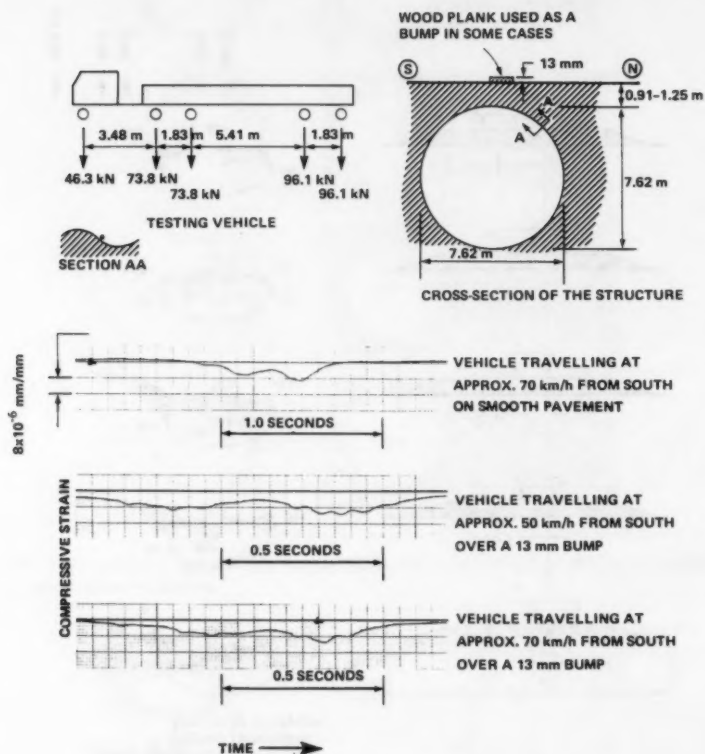


FIG. 17.—Dynamic Axial Strains in White Ash Creek Structure

surface causes the vehicle to bounce up and down thus inducing irregularities in the strain-time curve. These irregularities can be transformed into representative values of the dynamic load allowance (impact factor), which was found to be 0.18 and 0.17 for the Adelaide Creek and White Ash Creek structures respectively.

Having observed that irregularities in the riding surface can cause some dynamic magnification of load effects in a soil-steel structure, it seems prudent to assume that the riding surface of a soil-steel structure is not always smooth, and therefore

include a finite value of the dynamic load allowance (DLA) in the design. This approach has been adopted in the OHBD Code (11) according to which the DLA for the Adelaide Creek and White Ash Creek structures, for one vehicle loading works out to 0.19 and 0.24 respectively.

PROPOSED SIMPLIFIED METHOD

Preliminary analytical studies by Abdel-Sayed et al. (1) have confirmed that for the range of properties encountered in practice in soil-steel structures, the live load effects in the shell are not sensitive to soil property variations. This

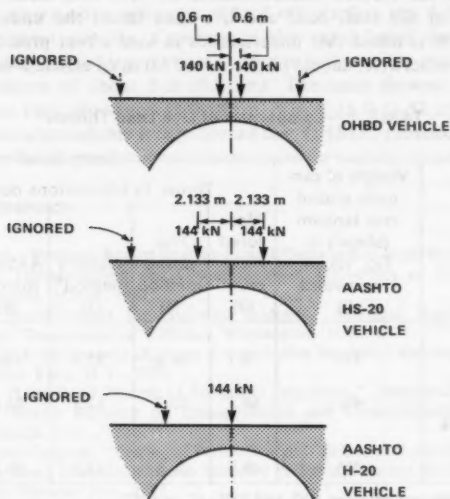


FIG. 18.—Positions of Vehicles for Maximum Live Load Thrust

observation is in concurrence with findings of Katona et al. (10) with regard to dead load effects. The proposed simplified empirical method, which is developed from the earlier described tests, is expected to be applied to real life structures and thus kept independent of soil properties. Flexible pavements are not believed to significantly affect the distribution of loads, therefore their properties are not considered in the analysis.

The proposed method is a modification of the AASHTO method (2). From the test results it is concluded that positions of the various design loads for the maximum live load thrust are as shown in Fig. 18. It is assumed that the live load disperses at a slope of 1:1 in the direction of the conduit span and at an angle of two vertical to one horizontal along the length of the conduit. The adoption of different angles of dispersion emerges from the observed behavior shown in Fig. 15, and from analytical studies conducted by Abdel-Sayed et al. (1). The dispersed load is assumed to be uniformly distributed at the crown

level over a rectangular area subtended by the extremities of individual dispersed loads. Thus obtained value of the intensity of the distributed load, σ_L , after it is modified to account for impact and multiple presence of vehicles, is multiplied by the smaller of half the conduit span and half the length of the distributed load along the span, to give the per unit length thrust in the shell.

Values of the thrust predicted by the proposed method are compared in Table 1 with some of the measured maximum values and those obtained by adopting a few of the earlier mentioned methods to the testing vehicle. It can be seen that the values predicted by the proposed method are most consistently close to the measured maximum values. In the case of the very low profile Adelaide Creek structure the method underestimates the live load thrust by 22%, but in the context of the total dead and live load thrust the underestimation is less than 10%. It is noted that uncertainties in load effect prediction, be they conservative or otherwise, should be accounted for in an efficient design process.

TABLE 1.—Comparison of Live Load Thrusts

Structure (1)	Weight of centrally placed rear tandem (shown in Fig. 10), in kilonewtons (2)	Thrust, in kilonewtons per meter				
		Measured maximum (3)	Proposed method (4)	Watkins method ^a (5)	AASHTO method (6)	Kaiser aluminum method ^b (7)
Deux Rivieres (Fig. 6)	295	19.7	34.8	35.4	29.8	66.4
Adelaide Creek (Fig. 7)	405	68.3 ^c	53.3	92.3	84.8	150.3
White Ash Creek structure (Fig. 8)	405	48.9	66.6	114.3	99.9	159.2

^a Assumed compaction between 90% and 95%; $C_p = 0.82$.

^b Equivalent uniformly distributed load calculated according to Eq. 8.

^c Limited to less than 15% of the circumference. Rest about 33%.

For such a design process a method producing both conservative and unconservative results within a given range of accuracy, such as the proposed method, is considered acceptable. However, when the design method requires only conservative estimates of load effects the AASHTO method appears to be the most suitable means of determining live load effects in a soil-steel structure.

It should be noted that the proposed method is developed from results of only a limited number of tests. It is proposed only as an interim measure until further information about the behavior of soil-steel structures under live loads is available.

CONCLUSIONS

A number of simplified methods for predicting soil-steel structure responses under live loads are considered. Most of the methods appear to reduce the

live loads to equivalent distributed loads which are then treated like the dead loads. Because of the usually large ratio of dead to live load effects, little attention appears to have been paid in the past to verify the live load effect prediction.

Results of tests on three soil-steel structures with relatively shallow covers show the need of more accuracy in the prediction of live load effects. Previous methods of determining live load effect were found to be over conservative (see Table 1). A modification to existing simplified methods for predicting thrust due to live loads is proposed. The method, retaining the simplicity of the previous methods, is able to predict the maximum live load thrust fairly accurately. The predicted values, however, are not always conservative. If the design process requires only conservative estimates of load effects than the AASHTO method appears to be most suitable. Contrary to the usual belief the dynamic load allowance (impact factor) is not equal to zero in soil-steel structures with depths of cover in excess of about 3 ft (0.91 m). The tests showed as high values of the dynamic load allowance as 0.18 for $H = 4.33$ ft (1.32 m). Until further research results are available it is proposed that OHBDC provisions for dynamic load allowance be adopted.

APPENDIX I.—REFERENCES

1. Abdel-Sayed, "Progress Report on Live-Load Effects in Soil-Steel Structures," Ontario Ministry of Transportation and Communication, University of Windsor, Windsor, Ontario, Canada, March, 1981.
2. "Standard Specifications for Highway Bridges," American Association of State Highway and Transportation Officials, Washington, D.C., 1977.
3. *Handbook of Drainage and Highway Construction Products*, American Iron and Steel Institute, New York, N.Y., 1971.
4. Bakht, B., "Live Load Testing of Soil-Steel Structures," *Structural Research Report 80-SRR-4*, Ontario Ministry of Transportation and Communications, Downsview, Ontario, Canada, Nov., 1980.
5. Bakht, B., and Csagoly, "Testing of Perley Bridge," *Research Report No. 207*, Research and Development Division, Ontario Ministry of Transportation and Communications, Downsview, Ontario, Jan., 1977.
6. "Structural Design of Corrugated Steel Pipe," California Corrugated Steel Pipe Association, Oct., 1977.
7. "Composite Design for Soil-Steel Structures," *Technical Bulletin No. 205*, Corrugated Steel Pipe Institute, Port Credit, Ontario, Dec., 1968.
8. Csagoly, P. F., Campbell, T. I., and Agarwal, A. C., "Bridge Vibration Study," *Research Report 181*, Ontario Ministry of Transportation and Communications, Downsview, Ont., Sept., 1972.
9. Duncan, J. M., "Behavior and Design of Long-Span Metal Culverts," *Journal of the Geotechnical Engineering Division*, ASCE, Vol. 105, No. GT3, Proc. Paper 14429, Mar., 1979, pp. 399-418.
10. Katona, M. G., Smith, J. M., Odells, R. S., and Allgood, J. R., "Cande—A Modern Approach for the Structural Design and Analysis of Buried Culverts," *Federal Highway Administration Report No. FHWA-RD-77-5*, Washington, D.C., Oct., 1976.
11. "Ontario Highway Bridge Design Code," Ontario Ministry of Transportation and Communications, Downsview, Ontario, Canada, Jan., 1979.
12. "Ontario Highway Bridge Design Code Commentary," Ontario Ministry of Transportation and Communications, Downsview, Ontario, Canada, 1979.
13. Poulos, H. G., and Davis, E. H., "Elastic Solutions for Soil and Rock Mechanics," John Wiley and Sons, Inc., New York, N.Y., 1974.
14. Selig, E. T., Abel, J. F., Kulhawy, F. H., and Falby, W. E., "Review of the Design and Construction of Long-Span, Corrugated-Metal, Buried Conduits," *Federal Highway*

Administration Report FHWA-RD-77-131, Washington, D.C., Aug., 1977.

15. Taylor, D. W., *Fundamentals of Soil Mechanics*, John Wiley and Sons, Inc., New York, N.Y., 1948.
16. Watkins, R. K., "Buried Structures," *Foundation Engineering*, Van Nostrand Reinhold Co., Inc., New York, N.Y., 1975.

APPENDIX II.—NOTATION

The following symbols are used in this paper:

- C_b = Boussinesq coefficient;
- C_p = pressure transfer coefficient;
- D_h = conduit span;
- H = depth of cover;
- h = distance of load from reference location as defined in Fig. 5;
- I = dynamic load allowance (impact factor);
- K_{p3} = coefficient defined by Eq. 4;
- LL = equivalent line load;
- M_L = live load moment per unit length;
- m_f = modification factor accounting for multi presence of vehicles;
- P = intensity of concentrated load;
- p = intensity of line load;
- R_t = radius of curvature of conduit at crown;
- T_L = conduit wall thrust per unit length;
- σ_{max} = maximum intensity of pressure; and
- σ_L = equivalent distributed load at crown level.

CEMENTED SANDS UNDER STATIC LOADING

By G. Wayne Clough,¹ M. ASCE, Nicholas Sitar,² Robert C. Bachus,³
Associate Members, ASCE, and Nader Shafii Rad⁴

INTRODUCTION

Cemented sands are found in many areas of the world and one of their distinguishing characteristics is their ability to stand in steep natural slopes. The cementation in the sand is provided by small amounts of agents, such as silica, hydrous silicates, hydrous iron oxides, and carbonates deposited at the points of contact between sand particles (6). Cementation or cementation-like effects can also be produced by a dense packing of sand grains (3) or by a matrix of silt and clay particles. Large deposits of cemented sands are found along the California coast. The slopes in them are typically 60° or steeper from the horizontal and reach heights of 100 m (300 ft) even though individual pieces of the sand can be crushed by light finger pressure. Fig. 1 depicts such a slope which is located just south of San Francisco; also shown is the intense urban development taking place near the crest of the slope. The question of stability in this type situation is obviously an important one in view of the fact that a slope failure can easily lead to loss of life and property. Field observations and reviews of historical documents reveal that slope failures in these areas are not uncommon, and occur under gravity and earthquake-type loadings (9,10). The failures are typically shallow and occur rapidly.

In order to provide parameters which can be used in analyses of the slopes and information to help understand the reasons for the material behavior, a series of laboratory tests were performed to classify the soils and define their response under static compression and tension loadings. A total of 137 laboratory tests were performed on four naturally-cemented sands found in the San Francisco Bay Area, and on artificially-cemented sands fabricated to simulate the natural soil behavior. The artificially-cemented samples were used to define effects of amounts of cementing agent and sand density on soil response. The naturally-cemented soils were chosen to vary from very strong to very weak so as to

¹Prof. of Civ. Engrg., Stanford Univ., Stanford, Calif. 94303.

²Asst. Prof. of Civ. Engrg., Univ. of California, Berkeley, Calif. 94720.

³Asst. Prof. of Civ. Engrg., Georgia Inst. of Tech., Atlanta, Ga. 30332.

⁴Grad. Research Asst., Dept. of Civ. Engrg., Stanford Univ., Stanford, Calif. 94303.

Note.—Discussion open until November 1, 1981. To extend the closing date one month, a written request must be filed with the Manager of Technical and Professional Publications, ASCE. Manuscript was submitted for review for possible publication on September 11, 1980. This paper is part of the Journal of the Geotechnical Engineering Division, Proceedings of the American Society of Civil Engineers, ©ASCE, Vol. 107, No. GT6, June, 1981. ISSN 0093-6405/81/0006-0799/\$01.00.

cover a range of behavior. All samples of the natural soils were obtained by hand cutting large blocks of the material in order to minimize disturbance effects. Moisture contents of the soils, which ranged from 5%–15%, were maintained at the in-situ values during testing. Cementing agents were identified by thin section analysis.

The results of the tests show the behavior of a cemented sand to be strongly influenced by the amount of cementing agent, sand density, confining pressure, and grain size distribution. Also, failure modes are found to vary with confining pressure, level of cementation, and sand density. Importantly, it appears that many of the natural materials in some very steep and high bluffs contain only a relatively small amount of cementation. This suggests that cementation plays a significant and, perhaps often overlooked role in slope performance. The

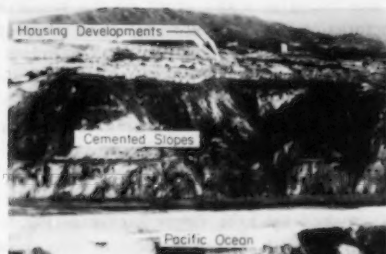


FIG. 1.—Photographs of Steep Slope in Weakly-Cemented Sand, Daly City, Calif. (Note Urban Development at Crest)

material presented herein should help clarify the effects of cementation on sand behavior under static loadings.

SAMPLE PREPARATION AND TEST PROGRAM

The naturally-cemented soil samples were obtained from two sites, both located on the San Francisco Peninsula (see Fig. 2). The first is situated at the Stanford Linear Accelerator Center (SLAC), just west of the main campus of Stanford University. Two types of cemented sands were recently exposed by excavations for an addition to the linear accelerator. The soils were in a moist condition, with the water table located below the bottom of the slope. One of the sands is characterized in this paper as strongly cemented (SLAC-1), while the second is termed weakly cemented (SLAC-2). The strongly-cemented sand had to be cut using a power saw during sampling and could not be crushed by hand pressure. The weakly-cemented sand could be cut easily by hand trowel, and tended to break apart under light finger pressure. In a recent geotechnical investigation for the linear accelerator, blow counts from Standard Penetration Tests for both materials were observed to be above 75 blows/ft (2).

Approximately 0.015-m^3 (0.50-cu ft) block samples of both soils were cut from freshly-opened excavations, wrapped carefully in plastic bags, and transported to the laboratory for storage in the humid room. Extreme care was

required in handling the weakly-cemented sand since a small shock would break the sample into pieces. On the average, two specimens would have to be trimmed in order to obtain one intact sample for testing. Trimming, itself, was a challenge. First, the samples were hand-sawed down to a size about 30% above the final dimensions, and capped by a layer of parafin on top and bottom. The specimen was then placed in a conventional trimming device held in place by caps which had protrusions embedded into the parafin. Next, the specimen was rotated, and slowly shaved by a variety of successively finer steel blades until the proper diameter was reached. Finally, the sample was removed from the trimmer, and the excess soil and parafin caps at the top and the bottom carefully cut off, thus providing clean, square ends for testing.

The second site is located on the bluffs along the Pacifica Coast at the northern end of the city of Pacifica, Calif., approx 15 mile south of San Francisco, and one mile south of the San Andreas Fault Line. Seventy degree slopes



FIG. 2.—Location Map for Sampling Sites (1 mile = 1 km)

stand up to 45 m (150 ft) high above the beaches at the sampling site. The bluffs are made up primarily of a weakly-cemented sand of a shallow marine origin which is typically cross-bedded. Samples of this sand, called PAC-1 in this paper, were obtained, as well as samples of a less prominent, somewhat stronger unit called PAC-2. The PAC-2 sand is found as a layer in the lower portions of the PAC-1 sand, and is horizontally bedded. It contains considerably more fines content than the PAC-1 sand. There is no water table, per se, in the slopes, and the soils are not saturated. Small amounts of perched water are observed above the PAC-2 sand layers with modest seeps occurring at the upper part of the layers in some areas.

Handling of samples of both the PAC-1 and PAC-2 sands required care in order to avoid disturbance. Sampling and trimming procedures were the same as those used at the SLAC site. Based on visual classifications, the PAC-1

sand was termed weakly cemented and the PAC-2 sand was termed moderately cemented.

Artificially-Cemented Samples.—Artificially-cemented sands were used in the testing program in order to have a material which simulated the natural sands, but which could be readily prepared to a preassigned density and degree of cementation. The samples were intentionally manufactured so as to be relatively weak, and were tested in triaxial compression to large strain levels. Creation of the artificially-cemented samples was a much easier process than the block sampling operation used with the naturally-cemented sand, and allowed greater control over important variables. Details of the sample preparation process are given in the second writer's thesis (11), and only a brief summary is presented here. The artificially-cemented samples were prepared by mixing Type II Portland cement and a uniform sand together at 8% moisture content. A grain size curve for the soil is shown in Fig. 3; its D_{50} (medium grain size) is 0.75 mm. Two percent or four percent cement by weight of the samples was used. The mix was compacted into a 70-mm (2.76-in.) diam, and 138-mm (5.43-in.) long cylindrical

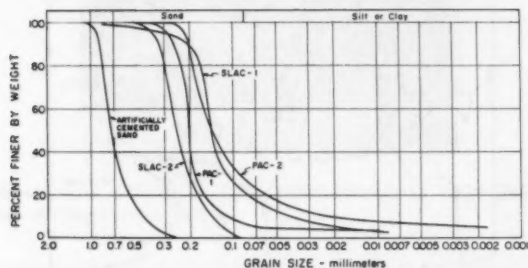


FIG. 3.—Grain Size Curves for Naturally-Cemented Soils from Stanford Linear Accelerator and Pacifica Sites, and Sand used in Artificially-Cemented Samples

lucite mold with a narrow, 1-mm, (0.04-in.) slit cut along one side. The mold was held together by taut hose clamps so as to keep the slit closed during sample preparation. The soil-cement mix was compacted into the mold into layers with uniform density; subsequently the molds were wrapped in moisture-proof bags and stored in a humid room to cure for 14 days before testing. After curing, the hose clamps were loosened, and the spring in the lucite molds opened the slit, thus releasing the soil samples and allowing them to easily slide out. Repeated testing of duplicate samples showed that uniform results could be obtained by the sample preparation procedure.

Test Program.—Classification testing involved performing sieve and hydrometer tests on the sands, and Atterberg limit tests on soil fraction passing the No. 200 sieve where appropriate. Unconfined and drained triaxial loading tests were conducted to determine the soil response under compressive stresses. Volume changes were measured in all of the triaxial tests except those on the strongly-cemented sand. Brazilian tension tests were performed for most of the soils to define tensile strengths. This involves loading a specimen by

compressing it along the longitudinal axis; a pure tensile stress is generated across the diameter of the sample leading to splitting along the longitudinal axis (11). The tensile testing was done because of the strong theoretical and field evidence that failures in the steep cemented sand slopes are initiated by tensile splitting in the upper half of the slopes (5,9,10,13). A total of 85 laboratory tests were performed on the artificially-cemented samples, and 52 on the naturally-cemented sands.

BASIC PROPERTIES OF NATURALLY-CEMENTED SANDS

In Table 1, the average physical properties of each of the naturally-cemented sands are given. One of the more interesting aspects revealed by the data is the similarity of the properties for the SLAC-2 and PAC-1 sands and those for the SLAC-1 and PAC-2 sands. As mentioned earlier, the SLAC-2 and PAC-1 sands are both weakly cemented and required extra care in handling to avoid damaging them. They have a lower density and fines content than the SLAC-1

TABLE 1.—Average Physical Properties of Naturally-Cemented Sands, SLAC and Pacifica Sites

Sand identification (1)	Dry unit weight, in kilonewtons per cubic meter (2)	Moisture content, as a percentage (3)	Void ratio (4)	Degree of saturation, as a percentage (5)	D_{50} , in millimeters (6)	Pass 200 sieve, as a percentage (7)
SLAC-1	17.6	10	0.48	56	0.14	18
SLAC-2	16.5	14	0.57	61	0.24	0
PAC-1	16.7	5	0.54	22	0.23	5
PAC-2	17.1	15	0.47	81	0.12	24

Note: $1 \text{ kN/m}^3 = 6.36 \text{ lb/cu ft}$.

and PAC-2 sands, which are more strongly cemented. The grain size curves in Fig. 3 show that the coarse fraction of all of the soils is quite similar, but that the more well-cemented soils have a significant fraction of fines. For both the well-cemented soils, the fine fraction is nonorganic and only slightly plastic, with a plasticity index of around 10. The moisture contents for the soils are less than 15% in all cases, with degrees of saturation varying from 22%–81%.

RESPONSE OF NATURALLY-CEMENTED SOILS TO LOAD

Typical stress-strain curves for three of the sands, SLAC-1, PAC-2 (moderately cemented), and PAC-1 (weakly cemented) are given in Figs. 4–6. The data were obtained in drained triaxial compression tests performed at confining pressures up to 414 kN/m^2 (60 psi). Volume changes were measured only for the PAC-1 and PAC-2 sands, and these are plotted below, the stress-strain curves in Figs. 5 and 6. The common characteristic of all of the results is

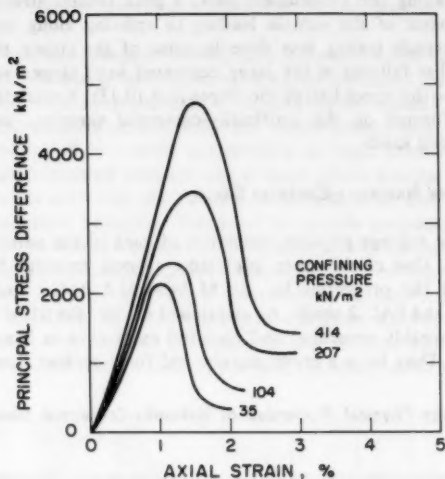


FIG. 4.—Typical Stress-Strain Curves, SLAC-1 Sand, Strongly Cemented ($1 \text{ kN/m}^2 = 20.9 \text{ lb/sq ft}$) (after Alf, 1978)

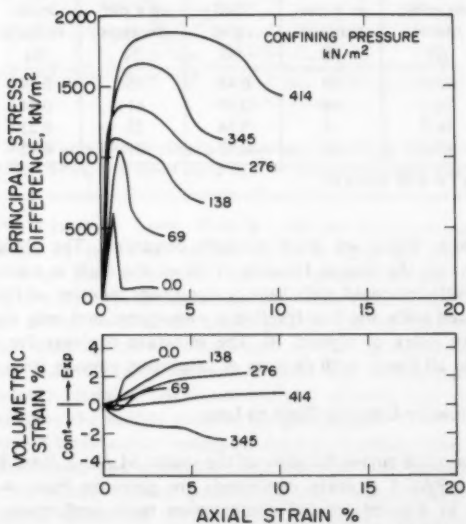


FIG. 5.—Typical Stress-Strain Curves, PAC-2 Sand, Moderately Cemented ($1 \text{ kN/m}^2 = 20.9 \text{ lb/sq ft}$)

that the stiffness and peak strength increases with increasing confining pressure. Volume change data for the PAC-1 and PAC-2 soils show that strong volumetric expansion is occurring during shear at the lower confining pressure levels. This phenomenon diminishes as confining pressure increases and at $\sigma_3 = 414 \text{ kN/m}^2$ (60 psi), volume change is essentially zero throughout shear.

An important characteristic shown by the stress-strain data in Figs. 4-6 is that the post-peak response is highly dependent on degree of cementation and confining pressure. The strongest soil, SLAC-1, shows a brittle failure behavior at all confining pressure levels, whereas the moderately- and weakly-cemented soils demonstrate a transitional response from brittle to ductile failure as confining

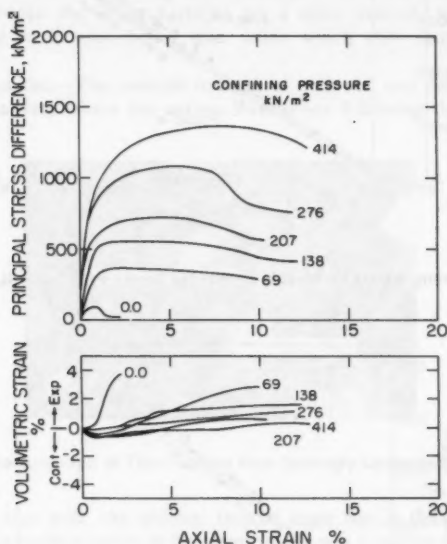


FIG. 6.—Typical Stress-Strain Curves, PAC-1 Sand, Weakly Cemented ($1 \text{ kN/m}^2 = 20.9 \text{ lb/sq ft}$)

pressures increase. For the moderately-cemented soils demonstrate a transitional response from brittle to ductile failure as confining pressures increase. For the moderately-cemented soil, PAC-2, brittle failure occurs up to about 276 kN/m^2 (40 psi), after which ductile behavior is observed. The weakly-cemented soil, PAC-1, shows a brittle failure only in unconfined compression; the application of only 69 kN/m^2 (10 psi) is enough to generate ductile behavior. Similar trends were observed for the SLAC-2 sand. The reason for the transition in brittle to ductile failure modes appears to be related to the relative contributions to the sand response by the cementation and frictional components of the deformation resistance mechanisms. This will be better demonstrated by the results of the artificially-cemented sand tests, shown later in this paper.

Peak Strength Envelopes in Compression.—The peak strength values for the weakly-cemented sands, PAC-1 and SLAC-2, are presented in Fig. 7, plotted in the form of a q - p diagram with coordinates of $(\sigma_1 - \sigma_3)/2$ versus $(\sigma_1 + \sigma_3)/2$. This type of presentation is used in lieu of a Mohr diagram so that the failure condition can be represented by points rather than by Mohr circles. The data for the two soils may be fitted by straight lines which have the same

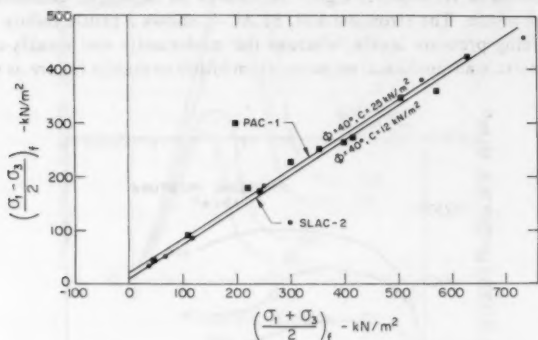


FIG. 7.—Peak Strength Data for Weakly-Cemented Sands, PAC-1 and SLAC-2 ($1 \text{ kN/m}^2 = 20.9 \text{ lb/sq ft}$)

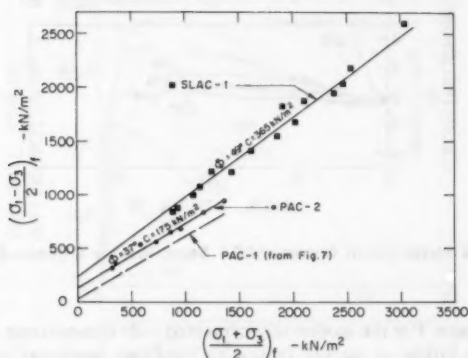


FIG. 8.—Peak Strength Data for Moderately- and Strongly-Cemented Sands, PAC-2 and SLAC-1 ($1 \text{ kN/m}^2 = 20.9 \text{ lb/sq ft}$)

slope but slightly different intercepts. The lines suggest that both soils have a friction angle of 40° , but that PAC-1 has a cohesion intercept of 25 kN/m^2 (3.6 psi) while that of SLAC-2 is 12 kN/m^2 (1.7 psi). The relatively small cohesion intercept of the PAC-1 soil is particularly interesting in view of the fact that it makes up a large portion of areas of the very high and steep slopes

along the Pacific Coast of the San Francisco peninsula.

Peak strength values for the SLAC-1 and PAC-2 soils are plotted in Fig. 8 on a q - p diagram. Data for both soils closely follow straight lines, although the SLAC-1 soil is much stronger than the PAC-2 soil. Both the SLAC-1 and PAC-2 sands have strengths well above those of the PAC-1 and SLAC-2 sands. As with the weakly-cemented sands, there is a significant frictional component of strength; $\phi = 49^\circ$ and 37° for the SLAC-1 and PAC-2 soils, respectively.

The high friction angle of the SLAC-1 soil is apparently produced by its relatively high density and the significant degree of interlocking of its angular particles. A thin section made of this soil (see Fig. 9) shows a fabric of closely-fitting and interpenetrating sand particles. The white fringes along the boundaries between the larger particles are a silica cement, while the large dark areas are concentrations of iron oxide which also contribute to the cementation.

Residual Strengths.—The residual strength of each soil was determined from the stress-strain data where the curves leveled out following the peak in the

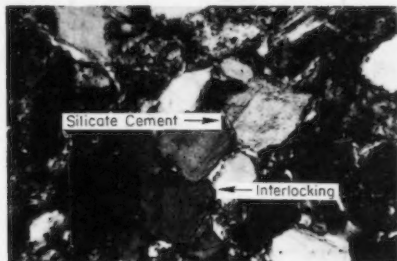


FIG. 9.—Photomicrograph of Thin Section from Strongly-Cemented Sand, SLAC-1

curve. For all four soils, the residual friction angle was in the range 35° – 36° . There was also a residual cohesion intercept, which was small for weakly-cemented sands, 6 kN/m^2 and 5 kN/m^2 (2.2 psi and 0.7 psi) for SLAC-2 and PAC-7, respectively, but significant for the other two soils, 75 kN/m^2 and 60 kN/m^2 (10.9 psi and 8.7 psi) for SLAC-1 and PAC-2, respectively. The high residual cohesion intercept for the latter two soils is undoubtedly due to the presence of silt and clay particles which could contribute a natural cohesion or capillary tension effects.

Tensile Strengths.—Brazilian tension tests were performed on only the SLAC-2 and PAC-1 soils. The tension test results are not plotted with the compression data in Fig. 7 because the strengths are so small that they do not show clearly in the diagram. The tensile strength of the SLAC-2 soil averaged 10 kN/m^2 , or 12% of its unconfined compression strength, while that of PAC-1 soil averaged 9 kN/m^2 , 9% of its unconfined compression strength.

Deformation Modulus Values.—Because of the different shapes of the stress-strain curves (see Figs. 4–6), there is no single modulus value which can be used to compare all the soils. For this analysis, initial tangent modulus values

are used for PAC-1, PAC-2, and SLAC-2, while the modulus of the linear portion of the stress-strain curve of soil SLAC-1 is used. In Fig. 10, these values are normalized by atmospheric pressure, p_a , and plotted on log-log scales against confining pressure, σ_3 , divided by p_a . The data for each of the soils reasonably fit straight lines, a behavior commonly observed for uncemented sands as well (12). The equation of the straight lines on the log-log plot takes the form:

$$E_t = K p_a \left(\frac{\sigma_3}{p_a} \right)^n \quad \dots \dots \dots (1)$$

in which E_t = the initial tangent modulus; K = the intercept at $\sigma_3/p_a = 1$; and n = the slope of the line. The values K and n are given in Fig. 10. The K and n parameters for the PAC-1 and SLAC-2 sands are close to those

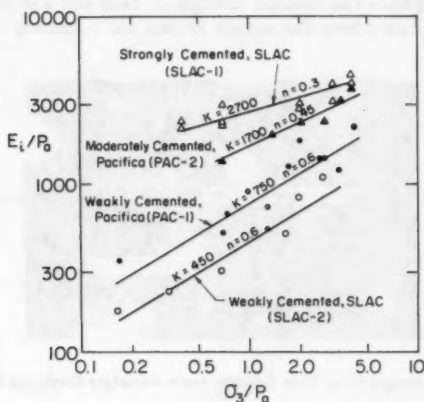


FIG. 10.—Variation of Initial Tangent Modulus Values, E_t , with Confining Pressure, σ_3

reported for uncemented dense sands (12), while those for SLAC-1 and PAC-2 yield modulus values well above those for uncemented sands. In general, the K values increase while the n values decrease with the level of cementation of the sand.

THIN SECTION ANALYSIS OF NATURALLY-CEMENTED SOILS

As shown in Fig. 9, the nature of the particle arrangements, principal cementing agents, and the grain shapes for the cemented sands can be ascertained from thin sections of the soils. Thin sections were made of representative samples of each of the naturally-cemented sands described herein. They showed that all of the sands contained similar basic cementing agents, mainly silicates and iron oxides, with minor amounts of carbonates. Of course, clay and silt-sized soil fractions in the stronger soils also likely contributed to their cementation.

The weaker sands exhibited less cementation bonds and their particles were more rounded and less densely packed than the stronger sands. Typically, for the PAC-1 sand, many of the particles showed red straining around the edges, indicating a thin weathered zone. These factors obviously contributed to the lower strength and stiffness of the weakly-cemented sands relative to the moderately- and strongly-cemented sands.

RESPONSE OF ARTIFICIALLY-CEMENTED SAND TO LOAD

Stress-strain and volume change curves are shown in Figs. 11 and 12 for artificially-cemented sands prepared to 74% relative density, D_r , using 4% and

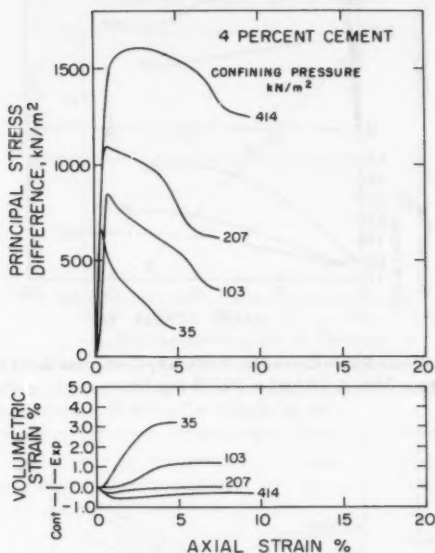


FIG. 11.—Typical Stress-Strain Curves for Artificially-Cemented Sand with 4% Cement at Relative Density = 74% ($1 \text{ kN/m}^2 = 20.9 \text{ lb/sq ft}$)

2% cement by weight, respectively. The basic trends observed for the stress-strain and volume change data of the naturally-cemented sands in Figs. 5 and 6 are also exhibited by the artificially-cemented sands. There is a frictional response in that the stiffness and strengths increase with confining pressure. In addition, there is a distinct transition from brittle to ductile failure as the confining pressures increase, and the transition occurs earlier for the less well-cemented sand. Finally, the sands generally show a volumetric increase during shear, and this decreases as confining pressure increases.

Peak Strength Envelopes.—Peak strength envelopes defined from the compression and tension tests for the 4% and 2% cement content sands at $D_r = 74\%$

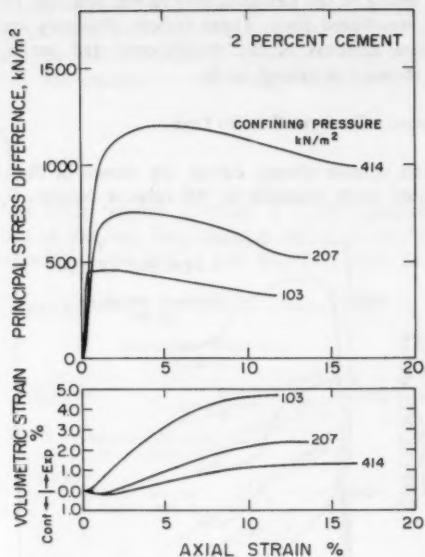


FIG. 12.—Typical Stress-Strain Curves for Artificially-Cemented Sand with 2% Cement at Relative Density = 74% ($1 \text{ kN/m}^2 = 20.9 \text{ lb/sq ft}$)

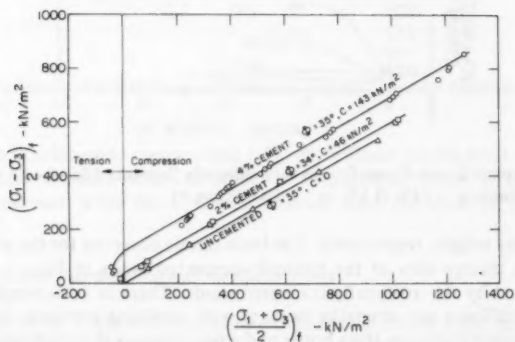


FIG. 13.—Peak Strength Values for Artificially-Cemented Sand and Uncemented Sand at Relative Density = 74% ($1 \text{ kN/m}^2 = 20.9 \text{ lb/sq ft}$)

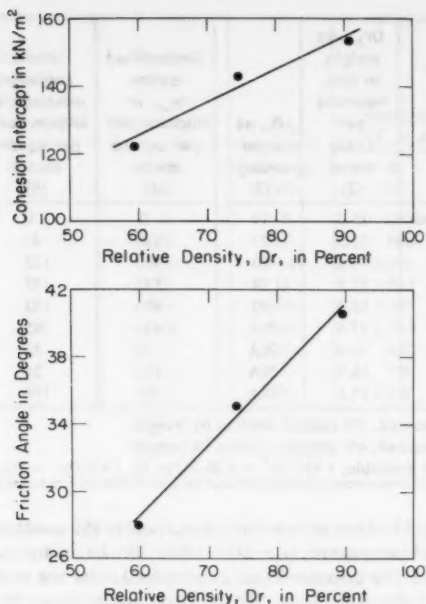


FIG. 14.—Variation of Friction Angle and Cohesion Intercept with Relative Density for 4% Cement Specimens ($1 \text{ kN/m}^2 = 20.9 \text{ lb/sq ft}$)

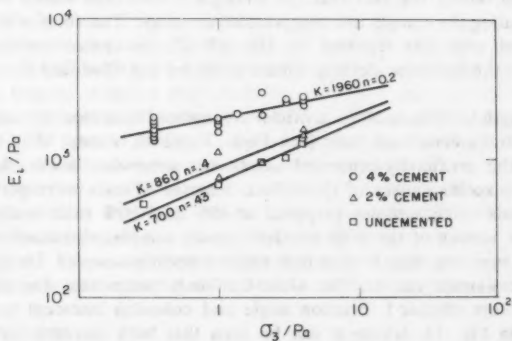


FIG. 15.—Variation of Initial Tangent Modulus with Confining Pressure for Artificially-Cemented Samples with Relative Density = 74%

TABLE 2.—Strength and Deformation Parameters

Soil type (1)	Dry unit weight, in kilonewtons per cubic meter (2)	D_r , as a percentage (3)	Unconfined stress σ_{uc} , in kilonewtons per square meter (4)	Peak cohesion intercept, in kilonewtons per square meter (5)	Peak ϕ , in degrees (6)
Uncemented sand	15.3	74	0	0	35
AC—C2% ^a	15.5	74	180	46	34
AC—C4% ^b	14.6	60	405	123	29
AC—C4% ^b	15.8	74	545	143	35
AC—C4% ^b	16.9	90	670	152	41
SLAC-1	17.6	NA	1,930	365	49
SLAC-2	16.5	NA	50	12	40
PAC-1	16.7	NA	110	25	40
PAC-2	17.1	NA	700	175	37

^aArtificially-cemented, 2% cement content by weight.

^bArtificially-cemented, 4% cement content by weight.

Note: NA = not available; 1 kN/m³ = 6.36 lb/cu ft; 1 kN/m² = 20.9 lb/sq ft.

are given in Fig. 13. Also shown for comparison is the envelope for the basic uncemented sand compacted to a $D_r = 74\%$. In the compression range, the envelopes of both the cemented and uncemented soils are essentially straight lines with nearly the same slope. The friction angles range from 34° – 35° . Of course, as the amount of cement increases, the cohesion intercept increases. The tensile strengths of the cemented sands range from 11%–13% of the unconfined compressive strength, and the failure envelope in the tensile region is curved to reflect the fact that the strength is less than would be indicated by extrapolating the straight line compression envelope. This form of the envelope is consistent with that reported by Mitchell (7) for cement-stabilized sands, and follows the behavior defined theoretically by the Modified Griffith theory (11).

The strength envelopes of the artificially-cemented soils closely resemble those of the naturally-cemented soils (see Figs. 7 and 8), except that the friction angles of the artificially-cemented sands are somewhat lower. In order to investigate possible causes of this effect, a series of tests were performed for the 4% sands using samples prepared at 60% and 90% relative density. The stress-strain curves of the 90% relative density samples demonstrated a more brittle type response than for the 60% relative density samples. Using the peaks of the stress-strain curves, the Mohr-Coulomb parameters for the strength envelopes were obtained. Friction angle and cohesion intercept were plotted versus D_r in Fig. 14, where it can be seen that both increase with D_r . The friction angle varies from 29° – 41° , while the cohesion intercept increases from 120 kN/m²–150 kN/m² (17.4 psi and 21.7 psi). Clearly, density, or packing, or both, has a significant influence on cemented soil strength, in addition to the nature of the cementing material.

for Naturally- and Artificially-Cemented Sands

Residual ϕ , in degrees (7)	Residual cohesion intercept, in kilonewtons per square meter (8)	Tensile stress σ_T , in kilonewtons per square meter (9)	σ_T/σ_{uc} , as a per- centage (10)	Modulus Parameters [$E_t = K p_a (\sigma_3/p_a)^n$]	
				K (11)	n (12)
32	0	0	0	700	0.43
33	5	20	11	860	0.4
34	10	NA	NA	1,050	0.3
35	20	70	13	1,960	0.2
35	25	NA	NA	1,900	0.2
36	75	NA	NA	2,700	0.3
36	6	6	12	450	0.6
35	5	10	9	750	0.6
35	60	NA	NA	1,700	0.45

Residual Strengths.—The Mohr-Coulomb parameters for the portion of the stress-strain curves which leveled out following the peaks of the stress-strain curves of the artificially-cemented soils were very consistent. For the uncemented sand there was no residual cohesion and the residual friction angle was 32° . The cemented samples yielded a small residual cohesion which ranged from 5 kN/m^2 (0.7 psi) for the 2% cement specimens to 25 kN/m^2 (3.6 psi) for the 4% cement specimens, with $D_r = 90\%$. Residual friction angles varied from 33° for the 2% cement specimens to 35° for the 4% cement specimens.

Deformation Modulus Values.—Initial tangent modulus values for the uncemented sand and cemented samples with 2% and 4% cement prepared at $D_r = 74\%$ are plotted in Fig. 15 versus confining pressure using log-log scales. Both initial tangent modulus and confining pressure values are normalized by dividing by atmospheric pressure. As with the naturally-cemented sands, the normalized initial tangent modulus for the artificially-cemented sands increases approximately linearly with normalized confining pressure, and can be defined by Eq. 1. The data in Fig. 15 show the K value, or intercept at $\sigma_3/p_a = 1.0$, to increase with degree of cementation, while the slope of the lines, n , decreases. The results are consistent with information previously reported by Mitchell (7) and Dupas and Pecker (3) on cement stabilized sands as well as the general trends shown in Fig. 10 for the naturally-cemented soils.

ANALYSIS OF RESULTS

In Table 2 key parameters from the load tests on the naturally- and artificially-cemented sands are listed. One of the more interesting aspects of these data is the relative similarity of the residual friction angles of all of the soils. This

is in sharp contrast to the diversity of the peak friction angles. It also appears that all of the cemented sands exhibit a small, but consistent, residual cohesion intercept. This may be due to capillary tension effects or the presence of small amounts of cementing agents whose strength is of a ductile nature and does not drop to zero at large strains.

Contributions of Resistance Components.—In light of the relative similarity of the residual strengths, it is of interest to consider how the resistance to load is developed prior to and following failure. The differences in resistance mobilization at a confining pressure of 103 kN/m^2 (15 psi) are shown in Fig. 16 by comparing stress-strain curves for the uncemented and 2% and 4% artificially-cemented sand samples. Also shown are the volume change curves, normalized by the volume change at failure. Three phenomena may be noted: (1) The peak strength increases with degree of cementation; (2) the strain at

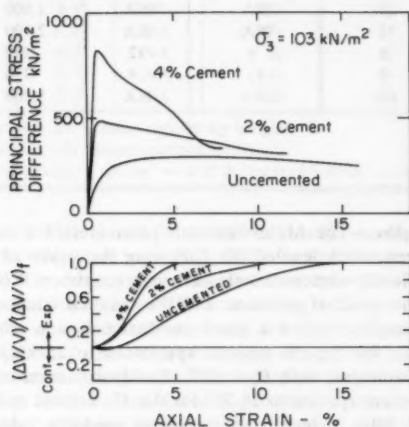


FIG. 16.—Comparison of Stress-Strain and Volume Change Response of Cemented and Uncemented Sands ($1 \text{ kN/m}^2 = 20.9 \text{ lb/sq ft}$)

peak strength mobilization decreases with degree of cementation; and (3) the volume increase during shear is concentrated over a smaller strain range and occurs at a lower strain as degree of cementation increases. This type of behavior is consistent throughout all of the data obtained for naturally- and artificially-cemented sands.

Perhaps the most interesting of the phenomena noted in Fig. 16 is the difference in rate of volumetric expansion and the strain at which it occurs. These data suggest that there are differences in strength mobilization between cemented and uncemented sands due not only to basic cementation effects, but also due to volumetric work components. An insight to this is provided by Fig. 17 where the stress-strain curves of the uncemented soil has been subtracted out of those of the 2% and 4% cement specimens for three confining pressures. The residual curves shown in Fig. 17 represent the difference between the cemented and

uncemented behavior. At an axial strain of 1% or less, the residual curves peak, with the stress peak being essentially the same for a given level of cementation for all confining pressures. Following the peak, the residual stresses decline gradually, and approach a small stable value at 8%-10% axial strain. It appears that the peak in the difference curves corresponds to the full mobilization of cementation bonds. This is consistent with the work of Mitchell (7) and Sacena and Lastrico (8) who have shown that cementation bonds in sands are broken at small strain levels. After the peak, the residual curves drop only gradually because of the volumetric work component contributions which are mobilized at different strain levels in the cemented and uncemented

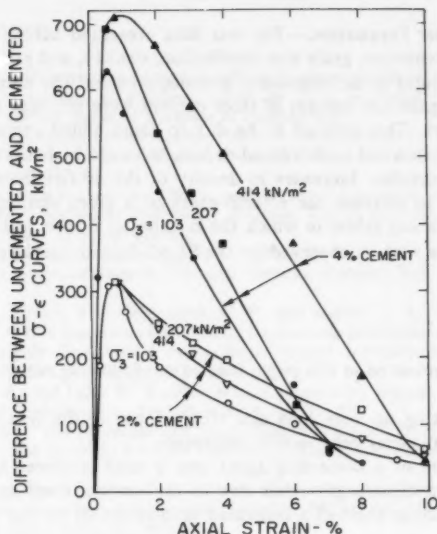


FIG. 17.—Difference between Cemented and Uncemented Sand Stress-Strain Response for Samples at Relative Density = 74% ($1 \text{ kN/m}^2 = 20.9 \text{ lb/sq ft}$)

sands. If cementation was the only difference between the cemented and uncemented sands, a much more pronounced decline should be observed. The residual curves do not return to zero even at large strains because of the residual cohesion present in the cemented sands but not the uncemented sands.

Failure Modes.—It has been noted for both the naturally- and artificially-cemented samples that the failure mode for a weakly-cemented sand is brittle at lower confining pressures and ductile at higher confining pressures. The reason for this behavior may be traced from the relative contributions of resistance components. At low confining pressures, the cementation component is far more significant than the frictional component. Because of the brittle failure of the cementation bonds, the sand itself exhibits brittle failure in this pressure range.

On the other hand, at high confining pressures, the frictional component of strength becomes dominant for weakly-cemented sands, and a more ductile response results. In the case of a strongly-cemented sand, the cementation is the most significant component of resistance even at higher confining pressures, and thus, a brittle failure mode is observed at low and high confining pressures (see Fig. 4).

Effect of Cement on Strength and Deformation Parameters.—The data in Table 2 show that cementation in sands has the basic effect of adding a cohesion intercept and a tensile strength to the sand, increasing its stiffness, but not changing its friction angle significantly. The stiffness, tensile strength, and cohesion intercept are all sensitive to the amount and the nature of the cementing agent.

Effect of Other Parameters.—The test data presented herein suggest that in addition to cementation, grain size distribution, density, and grain arrangements play important roles in the behavior of a cemented sand. The naturally-cemented sands with a significant percent of fines content were stronger than those with little to no fines. This appears to be due to some added cementing effect in the fines themselves and an increased density achieved by better packing modes with the fine particles. Increases in density of the artificially-cemented sands were observed to increase the effectiveness of a given amount of cementing agent. Finally, a soil fabric in which the boundaries of the particles fit closely or interpenetrate such as observed for the SLAC-1 sand, yield very high friction angles.

CONCLUSIONS

The results presented in this paper lead to the following conclusions.

1. Sands making up very high and steep slopes in the San Francisco Bay Area are in many cases very weakly cemented.
2. Introduction of a cementing agent into a sand produces a material with two components of strength—that due to the cement itself and that due to friction. The friction angle of a cemented sand is similar to that of uncemented sands.
3. A weakly-cemented sand shows a brittle failure mode at low confining pressures with a transition to ductile failure at higher confining pressures.
4. For brittle-type cementing agents, the cementation bonds are broken at very low strains while the friction component is mobilized at larger strains.
5. Volumetric increases during shear occur at a faster rate and at a smaller strain for cemented sands than uncemented sands.
6. Density, grain size distribution, grain shapes, and grain arrangements all have a significant effect on the behavior of a cemented sand.
7. The principal cementing agent, for the sands tested herein were silicates and iron oxides.
8. The residual strength of a cemented sand is close to that of an uncemented sand, although some degree of residual cohesion was observed for all the cemented sands investigated.
9. The tensile strength of a cemented sand is about 10% of the unconfined compressive strength.

ACKNOWLEDGMENTS

The writers would like to thank Jo Crosby of Jo Crosby Associates and T. Leslie Youd of the United States Geological Survey for their advice and encouragement during the study. Thanks is also due J. K. Mitchell of the University of California, Berkeley who provided assistance in preparation methods for the artificially-cemented sand specimens. Abdulaziz Alfi, a former graduate student at Stanford University performed the tests on one of the sands. The research was primarily sponsored by the United States Geological Survey, Contract No. USGS 14-08-0001-16836. N. Sitar also received support from the National Science and Engineering Council at Canada.

APPENDIX.—REFERENCES

1. Alfi, A. A. S., "Experimental Study of a Strongly Cemented Sand," thesis presented to Stanford University, at Stanford, Calif., in 1978, in partial fulfillment of the requirements for the degree of Bachelor of Engineering.
2. "Geotechnical Investigation—Proposed Positron-Electron Project," *Report No. 0651-130*, Stanford Linear Accelerator Center, Stanford, Calif., Dames and Moore Consulting Engineers, June, 1977, 37 pp.
3. Dupas, J. M., and Pecker, A., "Static and Dynamic Properties of Sand-Cement," *Journal of the Geotechnical Engineering Division*, ASCE, Vol. 105, No. GT3, Proc. Paper 14425, Mar., 1979, pp. 419-436.
4. Dusseault, M. B., and Morgenstern, N. R., "Shear Strength of Athabasca Oil Sands," *Canadian Geotechnical Journal*, Toronto, Ontario, Canada, Vol. 15, No. 2, 1978, pp. 216-238.
5. Harp, E. L., Wilson, R. C. Wiczorek, G. F., and Keefer, D. K., "Landslides from the February 4, 1976 Guatemala Earthquake: Implications for Seismic Hazard Reduction in the Guatemala City Area," *Proceedings*, Second International Conference on Microzonation, Vol. I, 1978, pp. 353-366.
6. Kryniene, D. P., and Judd, W. R., *Principles of Engineering Geology and Geotechnics*, McGraw-Hill Publishing Co., Inc., New York, N.Y., 1957.
7. Mitchell, J. K., "The Properties of Cement Stabilized Soils," *Proceedings*, Workshop on Materials and Methods for Low Cost Road, Rail and Reclamation Work, Sept., 1976.
8. Saxena, S. K., and Lastrico, R. M., "Static Properties of Lightly Cemented Sand," *Journal of the Geotechnical Engineering Division*, ASCE, Vol. 104, No. GT12, Proc. Paper 14259, Dec., 1978, pp. 1449-1464.
9. Sitar, N., Clough, G. W., and Bachus, R. C., "Behavior of Weakly Cemented Soil Slopes Under Static and Seismic Loading Conditions," *Report No. 44*, The John A. Blume Earthquake Engineering Center, Stanford University, Stanford, Calif., 1980.
10. Sitar, N., and Clough, G. W., "Behavior of Slopes in Weakly Cemented Soils Under Seismic Loading," *Proceedings*, Second United States National Conference on Earthquake Engineering, 1979, pp. 1006-1015.
11. Sitar, N., "Behavior of Slopes in Weakly Cemented Soils Under Static and Dynamic Loading," thesis presented to Stanford University, at Stanford, Calif., in 1979, in partial fulfillment of the requirements for the degree of Doctor of Philosophy.
12. Wong, K. S., and Duncan, J. M., "Hyperbolic Stress-Strain Parameters for Nonlinear Finite Element Analysis of Stresses and Movements in Soil Masses," *Geotechnical Engineering Report*, Department of Civil Engineering, University of California, Berkeley, July, 1974, 90 pp.
13. Yamanouchi, T., Gotoh, K., and Murata, H., "Stability of Cut Slopes in Shirasu," *Proceedings*, Fifth Asian Regional Conference on Soil Mechanics and Foundation Engineering, Vol. I, Dec., 1975, pp. 45-49.

STABILITY OF LOADED FOOTINGS ON REINFORCED SOIL

By Joe O. Akinmusuru,¹ A. M. ASCE and Jones A. Akinbolade²

INTRODUCTION

Although the systematic study of reinforced earth did not start until very recently, to the villager in tropical Africa and Southern Asia, the practice of building houses and roads on fiber-reinforced earth and constructing earth walls with different types of reinforcing intrusions is an age-old art. Rope fibers and bamboo sheets are used to strengthen rural road bases and the soil below low-cost low-rise buildings. Vertically arranged rectangular grids of bamboo sheets and stalks of palm branches are also used as the central core around which mud walls are built. Such composite walls have higher strengths and are more resistant to cracks and crack propagation than plain unreinforced mud walls. The main advantage of this method of construction is the low cost. Since Vidal (15,16) pioneered the study of reinforced earth, much work has been done by several authors (1-4, 6-14) on the analysis, design, model and field testing, and construction of reinforced soil structures, the bulk of this work due to Lee and others at UCLA.

Much of the work reported herein relates to earth retaining structures. However, the work of Binquet and Lee (2,3) show that reinforced soil technology is also applicable to bearing capacity problems. Because the reinforcing action under a footing requires good frictional bond between the horizontal ties and the soil, the use of free draining granular soil fills is advantageous.

There is a growing need in developing countries for research to be undertaken aimed at channelling local technology to the design and construction of low-cost highway and housing projects. This is pertinent with the abundance of cheap locally obtainable raw materials coupled with the high cost of imported materials of construction. Thus, while in most of the previous research available in the literature steel reinforcing strips have been used, in the work reported in this paper, a locally obtainable rope fiber material was used. This paper presents the results of laboratory model tests with square footings on a deep homogeneous

¹Lect. in Geotechnical Engrg., Faculty of Tech., Univ. of Ife, Ile-Ife, Nigeria.

²Engr., N.A.P. Consultants, Ibadan, Nigeria; formerly Research Student, Faculty of Tech., Univ. of Ife, Ile-Ife, Nigeria.

Note.—Discussion open until November 1, 1981. To extend the closing date one month, a written request must be filed with the Manager of Technical and Professional Publications, ASCE. Manuscript was submitted for review for possible publication on January 31, 1980. This paper is part of the Journal of the Geotechnical Engineering Division, Proceedings of the American Society of Civil Engineers, ©ASCE, Vol. 107, No. GT6, June, 1981. ISSN 0093-6405/81/0006-0819/\$01.00.

sand bed reinforced with flat strips of the rope fiber material, the type commonly used for the purpose in the rural areas of Southern Nigeria. Parameters studied were the effects on the bearing capacity of a footing of horizontal spacings of the fiber strips, vertical spacings between horizontal layers of reinforcement, number of layers, and depths below the footing of the first layer.

LABORATORY EXPERIMENTS

The model tests were performed in a well-stiffened square-based wooden box 39.4 in. (1.0 m) wide with a depth of 28 in. (0.7 m). The soil used was uniformly graded dry sand passing through British Standard (B.S.) No. 14 sieve and retained on B.S. No. 200 sieve; $D_{50} = 0.43$ mm and $D_{10} = 0.14$ mm; specific gravity = 2.70. The tests were conducted at a density of 109 pcf (1,700 kg/m³) and a friction angle of 38°.

The reinforcing material is locally known as "iko." Apart from being used in earth reinforcement, it is also locally used for making sleeping mats and

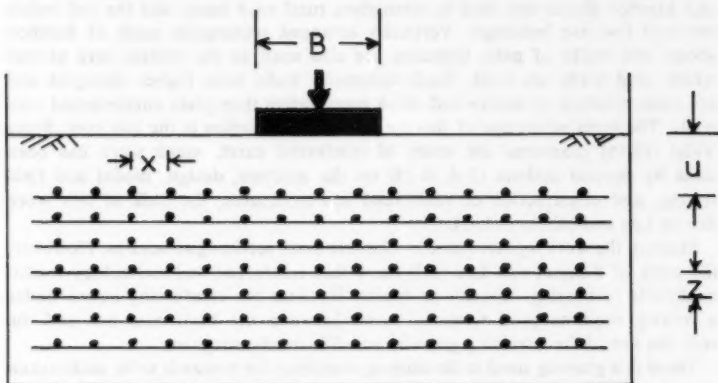


FIG. 1.—Geometry of Earth Reinforcement Problem

for spreads for drying crop seeds. The fiber strips used were 0.4 in. (10 mm) wide and 0.001 in. (0.03 mm) thick. The breaking strength was 11.6×10^3 psi (80 N/mm²). Pullout tests conducted to measure the soil-tie frictional resistance under confining conditions similar to the actual conditions in the model resulted in an average soil-tie frictional angle of 12°.

The footing used was a 4 in. (100 mm) square-sided rigid steel plate 0.5 in. (13 mm) thick. A recess was made into the center of the plate to accommodate a ball bearing through which vertical loads were applied to the footing. Vertical loads were applied with the aid of a lever arrangement of high mechanical advantage, and footing movements were measured with a dial gage. The loads were applied in small increments and the resulting movements noted so that the entire load-displacement curve to failure for each experiment was obtained.

The load-displacement curves generally showed the same trend in all tests:

the graphs did not show constant ultimate bearing capacities with increased displacements. After yield, the load-displacement behavior exhibited strain-hardening with load increasing linearly with displacement. The ultimate bearing capacity in any test was defined as that load corresponding to the beginning of the strain-hardening portion of the curve.

The earth bed was prepared by placing the sand in 1 in. (25 mm) lifts and compacting each lift to the same state of compaction by tamping with the same compactive effort. As the vertical spacings between layers of reinforcement were multiples of the depth of a lift of soil, the reinforcing strips were laid

TABLE 1.—Test Series

Parameter (1)	Variable (2)
Depth of top layer below footing, u/B	0.25, 0.50, 0.75, 1.00, 1.50
Horizontal spacings between adjacent strips, x/B	0, 0.50, 0.75, 1.00, 1.50
Vertical spacings between adjacent layers, z/B	0, 0.50, 0.75, 1.00, 1.50
Numbers of layers, N	0, 1, 2, 3, 4, 5

Note: Footing width $B = 4$ in. (100 mm). Reinforcement width = 0.4 in. (10 mm).

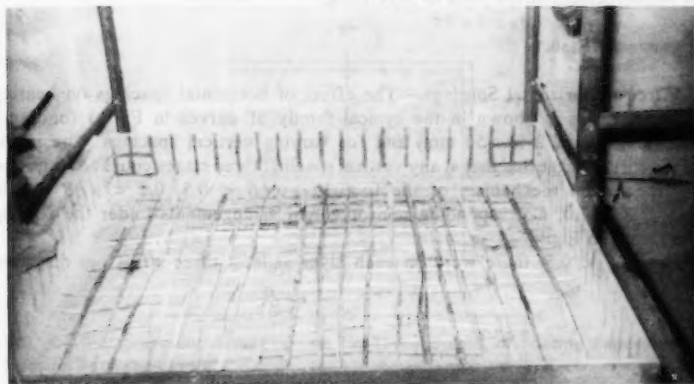


FIG. 2.—Typical Reinforcement Arrangement

on top of compacted lifts before the addition of more soil. The reinforcing strips were almost as long as the 39.4 in. (1.0 m) sides of the smooth bed of compacted sand in horizontal square grids in directions parallel to the sides of the footing and the box. In each experiment, all the strips in one direction were first laid and those in the other direction were then laid on top. The middle strip in each direction of each layer always passed directly under the center of the footing. The geometry of the problem is shown in Fig. 1 and the parameters studied are listed in Table 1.

The ultimate bearing pressure q_o for the unreinforced earth was found as the average of three values to be 13 psi (91 kN/m²). This was used as comparator for all subsequent tests. A bearing capacity ratio (BCR) was defined for the purpose such that

$$\text{BCR} = \frac{q}{q_o} \dots \dots \dots (1)$$

in which q was the average ultimate bearing pressure for the reinforced soil. Note that unlike in the definition of Binquet and Lee (2,3), the bearing capacity ratio was restricted to ultimate failure conditions since the beneficial effect of earth reinforcement is independent of how the BCR is defined (2). For the situations where the horizontal spacings x equal zero, all the strips in each direction were laid in such a way that adjacent strips were in contact. This was equivalent to a linear density ratio (LDR) (2) of 200%. For the hypothetical cases in which the vertical spacings between layers z equal zero, all the strips required for all the layers were arranged directly on each other. This type of condition was of course not practically beneficial as only the topmost and lowest strip faces were available for the mobilization of friction with the soil. In Table 1, the condition whereby the number of layers N equals zero corresponds to the case of the unreinforced soil. Figure 2 shows a typical arrangement of reinforcement strips prior to backfilling.

EXPERIMENTAL RESULTS

Effect of Horizontal Spacings.—The effect of horizontal spacings on bearing capacity ratios is shown in the typical family of curves in Fig. 3 for depth of first layer of 2 in. (50 mm) and for varying vertical spacings. The shape of the curves suggested that at any vertical spacing, three stages could be identified for the failure mechanism of the footing: $-x/B < 0.5$, $0.5 < x/B < 1.0$, and $x/B > 1.0$. Corresponding reinforcement arrangements under the footing are shown in Fig. 4.

For $x/B < 0.5$, there were on each layer at least three strips per direction

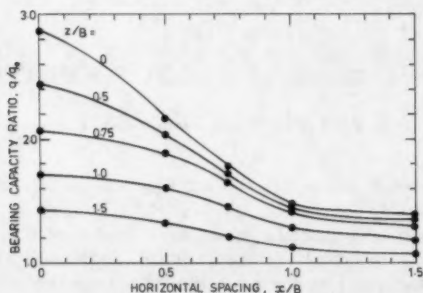


FIG. 3.—Variation of Bearing Capacity Ratios with Horizontal Spacings between Strips at Different Vertical Spacings between Layers ($u/B = 0.5$, $N = 5$)

under the footing. This congestion delayed the mobilization of shear resistance along potential rupture planes under the footing. This mode of failure was thus tantamount to block action in the horizontal direction. In Fig. 3, the rate of decrease of BCR in this range with increasing horizontal spacing was low. However, the rate of decrease for $0.5 < x/B < 1.0$ was steeper. On each layer, there was only one strip per direction under the footing and therefore less congestion. The rate of decrease of BCR with increasing spacing in this range was approximately linear. Beyond $x = B$, the rate of decrease of BCR was very low effectively showing that there was little change in bearing capacity with increasing horizontal spacings. Also, there was little difference between the bearing capacities at each horizontal spacing for all vertical spacings between

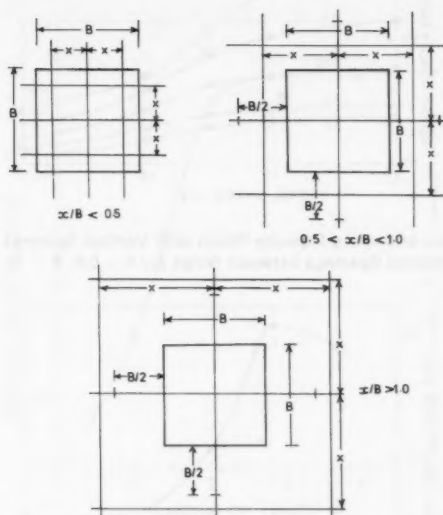


FIG. 4.—Reinforcement Arrangements for Three Stages of Footing Failure at any Spacing between Layers

reinforcement layers. In all cases, the bearing capacities tended to that of the unreinforced earth as the horizontal spacings between adjacent strips are indefinitely increased.

Effect of Vertical Spacings.—The influence of vertical spacings between layers of reinforcement on bearing capacities is shown in the typical curves in Fig. 5 which are similar in shape to those in Fig. 3. Binquet and Lee (3) identified three modes of footing failure: $u/B > 0.67$ corresponding to shear above reinforcements, $u/B < 0.67$ and $N < 3$ or short ties giving rise to tie pullout, $u/B < 0.67$ and $N > 3$ for long ties for which the upper ties break. For the curves in Fig. 5, the modes for which $u/B < 0.67$ applied and the shear zones penetrated the layers of reinforcement. The bearing capacity of the footing

thus depended on the strength of the reinforcement ties. Three stages of failure are suggested by the curves in Fig. 5. For $z/B < 0.5$, block action of the reinforcement in the vertical direction took place and there was little decrease in bearing capacity with increasing spacing. The rate of decrease of bearing capacity for $0.5 < z/B < 1.0$ was steeper and approximately linear. With increasing vertical spacing, it was observed that tie break was restricted to the topmost layer or two. For $z/B > 1.0$, although $N > 3$, the situations obtained resulted

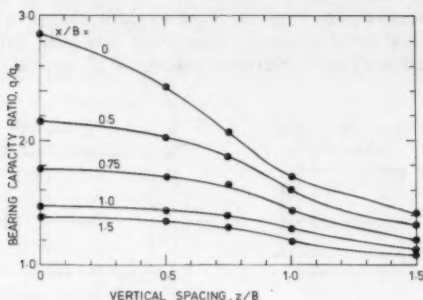


FIG. 5.—Variation of Bearing Capacity Ratios with Vertical Spacings between Layers at Different Horizontal Spacings between Strips ($u/B = 0.5$, $N = 5$)

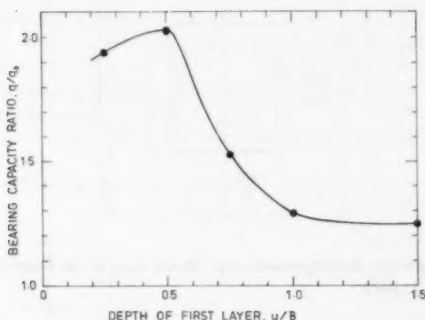


FIG. 6.—Influence of Depths of First Layer of Reinforcement on Bearing Capacity Ratios ($x/B = 0.5$, $z/B = 0.5$, $N = 5$)

in tie pullout rather than tie break because of the size of the spacings. Beyond $z = B$, the rate of decrease of BCR was low indicating little change in bearing capacity with increasing vertical spacings. Also, this range was tantamount to the footing being effectively supported on the topmost layer of reinforcement because of the size of the spacing; there was little interaction of the lower layers with the failure zones of the footing.

Effect of Depth of Top Layer below Footing.—A typical graph plotted from

the experimental data obtained to examine the effect on the bearing capacity of a footing of the depth of the topmost layer of reinforcement is shown for $x/B = 0.5$, $z/B = 0.5$, and $N = 5$ in Fig. 6. The peak of the curve was obtained at $u/B = 0.5$. For u/B values up to 0.5, there was a slight increase in bearing capacity due to the fact that the topmost layer was positioned too close to the footing base and its effect would be greatly decreased, making the next layer more effective. Thus, because for $u/B < 0.5$ the soil mass above the first layer was too small to generate enough frictional resistance for the footing, there was a probable failure due to the tie being depressed by the wedge of soil below the footing thus reducing conditions to one whereby the depth of top layer $= u + z$. For $u/B > 0.5$, the bearing capacity decreased

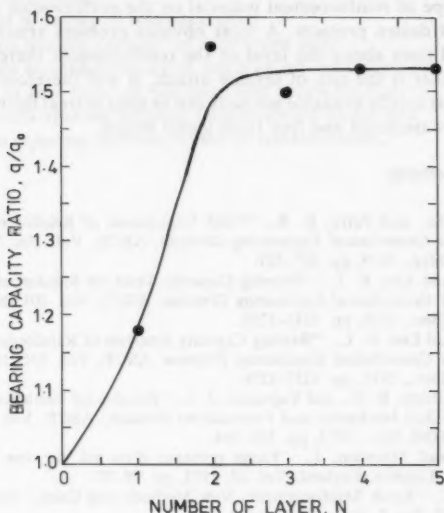


FIG. 7.—Influence of Number of Layers of Reinforcement on Bearing Capacity Ratios ($x/B = 0.5$, $z/B = 0.5$, $u/B = 0.75$)

as the Binquet-Lee (3) first failure mode was brought about and the reinforcement layers acted as a strong rigid boundary underlying a footing on a shallow soil bed (5). If u was increased indefinitely, the BCR- u/B curve approaches $q/q_0 = 1$.

Effect of Number of Layers.—To investigate the effect of the number N of layers on the BCR, a typical curve has been drawn in Fig. 7 for $x/B = 0.5$, $z/B = 0.5$, and $u/B = 0.75$. It was observed that for number of layers increasing up to three, there was sharp increase in bearing capacity. However, for $N > 3$, little change occurred in the capacity indicating, as Binquet and Lee (2) observed, that the addition of more layers of reinforcement after the third or fourth does not contribute much to bearing capacity improvement.

SUMMARY AND CONCLUSIONS

This paper has described laboratory-scale bearing capacity model tests on square footing on a homogeneous sand bed reinforced with strips of a local rope material. Results obtained have shown that the bearing capacity of a footing depends on horizontal spacings between strips, vertical spacings between layers, depth below the footing of the first layer, and number of layers of reinforcement. It was shown that depending on the strip arrangement, ultimate bearing capacity values can be improved by a factor of up to three times that of the unreinforced soil. However, practical considerations could limit suitable arrangements to bearing capacity improvement factors of about two.

As a consequence of this study, it is necessary to look into the long-term effect of this type of reinforcement material on the performance of actual rural housing or road design projects. A most obvious problem arises as the water table in the soil rises above the level of the reinforcement thereby weakening the strips. Another is the risk of termite attack. It will therefore be necessary to determine what locally available methods can be used to treat the reinforcements to render them waterproof and free from insect attack.

APPENDIX I.—REFERENCES

1. Al-Hussaini, M., and Perry, E. B., "Field Experiment of Reinforced Earth Wall," *Journal of the Geotechnical Engineering Division*, ASCE, Vol. 104, No. GT3, Proc. Paper 13596, Mar., 1978, pp. 307-321.
2. Binquet, J., and Lee, K. L., "Bearing Capacity Tests on Reinforced Earth Slabs," *Journal of the Geotechnical Engineering Division*, ASCE, Vol. 101, No. GT12, Proc. Paper 11792, Dec., 1975, pp. 1241-1255.
3. Binquet, J., and Lee, K. L., "Bearing Capacity Analysis of Reinforced Earth Slabs," *Journal of the Geotechnical Engineering Division*, ASCE, Vol. 101, No. GT12, Proc. Paper 11793, Dec., 1975, pp. 1257-1276.
4. Lee, K. L., Adams, B. D., and Vagneron, J. J., "Reinforced Earth Retaining Walls," *Journal of the Soil Mechanics and Foundations Division*, ASCE, Vol. 99, No. SM10, Proc. Paper 10068, Oct., 1973, pp. 745-764.
5. Mandel, J., and Salencon, J., "Force portante d'un sol sur une assise rigide," *Geotechnique*, London, England, Vol. 22, 1972, pp. 79-93.
6. Michael, B. J., "Earth Reinforcement, New Methods and Uses," *Civil Engineering*, ASCE, Vol. 49, No. 1, Jan., 1979, pp. 51-57.
7. Price, D. I., "Reinforced Earth," *Ground Engineering*, Brentwood, England, Vol. 8, No. 2, Mar., 1975, pp. 19-24.
8. Richardson, G. N., and Lee, K. L., "Seismic Design of Reinforced Earth Walls," *Journal of the Geotechnical Engineering Division*, ASCE, Vol. 101, No. GT2, Proc. Paper 11143, Feb., 1975, pp. 167-188.
9. Richardson, G. N., and Lee, K. L., "Seismic Testing of Reinforced Earth Walls," *Journal of the Soil Mechanics and Foundations Division*, ASCE, Vol. 103, No. GT1, Proc. Paper 12696, Jan., 1977, pp. 1-17.
10. Schlosser, F., and Long, N. T., "Comportement de la Terre Armee dans la Ouvrages de Soutenement," *Proceedings*, 5th European Conference on Soil Mechanics and Foundation Engineering, Vol. 1, 1972.
11. Schlosser, F., and Long, N. T., "Etude de Comportement de Materian Terre Armee," *Annales de l'Institut Technique du Batiment et des Travaux Publics*, No. 304, Apr., 1973.
12. Schlosser, F., and Long, N. T., "Recent Results in French Research on Reinforced Earth," *Journal of the Construction Division*, ASCE, Vol. 100, No. CO3, Proc. Paper 10800, Sept., 1974, pp. 223-237.
13. Steiner, R. S., "Reinforced Earth Bridges Highway Sinkhole," *Civil Engineering*,

- ASCE, Vol. 45, No. 7, July, 1975, pp. 54-56.
14. Tinubu, A. O., "Reinforced Earth—A Literature Review and Laboratory Study," thesis presented to Clemson University, in 1976, in partial fulfillment of the requirements for the degree of Master of Science.
 15. Vidal, H., "La Terre Armee," *Annales de l'Institut Technique de Batiment et des Travaux Publics*, July-Aug., 1966, pp. 888-936.
 16. Vidal, H., "The Principle of Reinforced Earth," *Highway Research Record*, No. 282, 1969, pp. 1-16.

APPENDIX II.—NOTATION

The following symbols are used in this paper:

- B = width of footing;
- N = number of layers of reinforcement;
- q = ultimate bearing capacity of reinforced soil;
- q_o = ultimate bearing capacity of soil with no reinforcement;
- u = depth of first layer of reinforcement below footing;
- x = horizontal spacing between reinforcement strips; and
- z = vertical spacing between layers of reinforcement.

DISCUSSION

DISCUSSION

Note.—This paper is part of the Journal of the Geotechnical Engineering Division, Proceedings of the American Society of Civil Engineers, ©ASCE, Vol. 107, No. GT6, June, 1981. ISSN 0093-6405/81/0006-0831/\$01.00.

DISCUSSIONS

Discussions may be submitted on any Proceedings paper or technical note published in any *Journal* or on any paper presented at any Specialty Conference or other meeting, the *Proceedings* of which have been published by ASCE. Discussion of a paper/technical note is open to anyone who has significant comments or questions regarding the content of the paper/technical note. Discussions are accepted for a period of 4 months following the date of publication of a paper/technical note and they should be sent to the Manager of Technical and Professional Publications, ASCE, 345 East 47th Street, New York, N.Y. 10017. The discussion period may be extended by a written request from a discussor.

The original and three copies of the Discussion should be submitted on 8-1/2-in. (220-mm) by 11-in. (280-mm) white bond paper, typed double-spaced with wide margins. The length of a Discussion is restricted to two *Journal* pages (about four typewritten double-spaced pages of manuscript including figures and tables); the editors will delete matter extraneous to the subject under discussion. If a Discussion is over two pages long it will be returned for shortening. All Discussions will be reviewed by the editors and the Division's or Council's Publications Committees. In some cases, Discussions will be returned to discussors for rewriting, or they may be encouraged to submit a paper or technical note rather than a Discussion.

Standards for Discussions are the same as those for Proceedings Papers. A Discussion is subject to rejection if it contains matter readily found elsewhere, advocates special interests, is carelessly prepared, controverts established fact, is purely speculative, introduces personalities, or is foreign to the purposes of the Society. All Discussions should be written in the third person, and the discussor should use the term "the writer" when referring to himself. The author of the original paper/technical note is referred to as "the author."

Discussions have a specific format. The title of the original paper/technical note appears at the top of the first page with a superscript that corresponds to a footnote indicating the month, year, author(s), and number of the original paper/technical note. The discussor's full name should be indicated below the title (see Discussions herein as an example) together with his ASCE membership grade (if applicable).

The discussor's title, company affiliation, and business address should appear on the first page of the manuscript, along with the *Proceedings* paper number of the original paper/technical note, the date and name of the *Journal* in which it appeared, and the original author's name.

Note that the discussor's identification footnote should follow consecutively from the original paper/technical note. If the paper/technical note under discussion contained footnote numbers 1 and 2, the first Discussion would begin with footnote 3, and subsequent Discussions would continue in sequence.

Figures supplied by the discussor should be designated by letters, starting with A. This also applies separately to tables and references. In referring to a figure, table, or reference that appeared in the original paper/technical note use the same number used in the original.

It is suggested that potential discussors request a copy of the *ASCE Authors' Guide to the Publications of ASCE* for more detailed information on preparation and submission of manuscripts.

IN SITU TEST BY FLAT DILATOMETER^a

Discussion by John H. Schmertmann,² F. ASCE

This paper makes the rare contribution of telling the profession about an original and useful insitu testing device together with well documented examples of its use. The dilatometer test seems to offer a great deal of important soil property information using relatively simple and practical equipment and methods. On first reading this seems almost too good to be true. However, this writer has had some personal experience using this equipment in Florida and can add a note of optimism regarding its practicality and potential usefulness.

After about 6 months of experience our company has found this equipment very practical to use in conjunction with the Dutch static cone penetration test (CPT). The same 10-ton thrust hydraulic equipment and rods used to insert the static cone easily adapt to the dilatometer. Instead of using inner rods the operator has to prethread the push rods with the plastic tubing from the dilatometer that contains the gas pressure and electrical signal lines from the dilatometer. Typically, we have found that we can make a dilatometer sounding at a rate of about 10 min/m, when taking the A and B dilatometer reading at 0.2-m. (8-in.) depth intervals. We have also found that with the 10-ton CPT equipment we can push the dilatometer from the surface through soils with standard penetration (SPT) resistance blowcount of about $N = 30$ or less to reach a layer of interest. Stronger surface soils would probably require preboring to permit dilatometer access.

The dilatometer test also offers the unique potential of permitting a rapid determination of a soil's consolidation behavior, essentially within minutes rather than the days or weeks required for undisturbed sampling and laboratory consolidation testing. Furthermore, the engineer can just as easily perform the test in soils such as silts and clayey silts as in clays—soils that often defy effective undisturbed sampling and when so sampled often produce laboratory data indicating too high compressibility. The writer has had a few opportunities to check dilatometer compressibility predictions, based on the formulas presented by the author in his paper, against laboratory measured values. Woodward-Clyde Consultants from Overland Park, Kans., Universal Engineering Testing Co. from Orlando, Fla., and the University of Florida provided the oedometer test results. Fig. 14 herein shows the comparisons. The data "points" include any uncertainty involved with either the comparative dilatometer data (primarily because of abrupt changes in test results between adjacent tests near the elevation of parallel oedometer test samples) or the laboratory data (primarily because of uncertainty as to whether to consider the soil normally consolidated or over consolidated). The reader can see that the dilatometer produced reasonable values of compres-

^aMarch, 1980, by Silvano Marchetti (Proc. Paper 15290).

²Principal, Schmertmann & Crapps, Inc., Consulting Geotechnical Engrs., 4509 N.W. 23rd Ave., Suite 19, Gainesville, Fla. 32601.

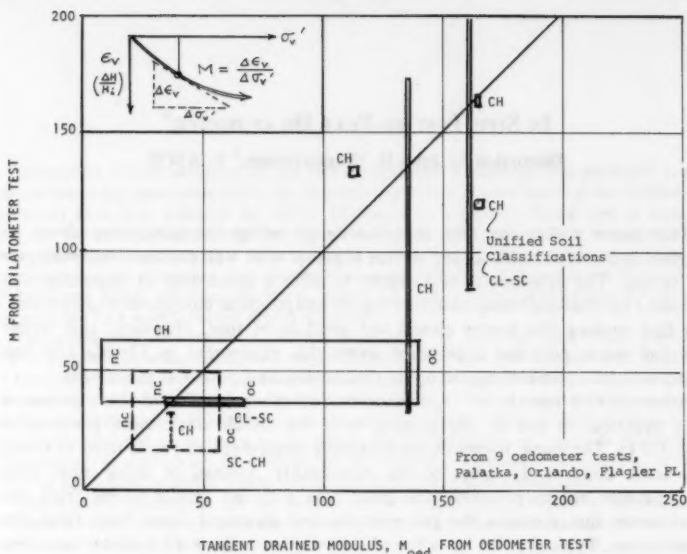


FIG. 14.—Comparisons between One-Dimensional Compressibility Predictions by Dilatometer and by Oedometer Methods

sibility that match laboratory predictions within a factor of about 2 and that on the average tend to fall on the conservative (dilatometer prediction high) side.

Based on this writer's experience to data, it appears that the author's dilatometer test may, at least in some circumstances, provide a rapid and relatively inexpensive substitute for undisturbed sampling and laboratory oedometer testing. It can test potentially compressible soils otherwise very difficult to sample properly, and provides approximately continuous data along any single dilatometer sounding.

Closure by Silvano Marchetti³

The writer thanks Schmertmann for the additional information he presented concerning the convenience and limitations of using the Dutch static cone penetration test (CPT) equipment for performing a dilatometer test (DMT) sounding. The writer supports Schmertmann's statements concerning the practicality of using static cone insertion equipment for dilatometer testing. Schmert-

³Visiting Assoc. Prof., Civ. Engrg. Dept., 346 Well Hall, Univ. of Florida, Gainesville, Fla. 32611; also Assoc. Prof. at Soil Mech., Faculty of Engrg., L'Aquila Univ., Italy.

mann suggested an SPT blowcount penetration limit of about 30 for 10-ton CPT equipment. However, the SPT drill rig and hammer itself can drive the dilatometer into and through even higher blowcount soils. The writer has successfully tested and driven through soils with SPT N values as high as 50–70. Also, in very weak soils that will not easily support the CPT and SPT equipment, the writer has successfully used handpushed or lightweight ram-driven equipment to advance the dilatometer to depths of 6 m (20 ft). On the other extreme, the maximum test depth reached so far has been 140 m (460 ft) using the system shown in Fig. 1(d).

Schmertmann added to the correlation information between the dilatometer predictions of the drained oedometer modulus, M , compared to oedometer test results. He noted, for some Florida soils, conservative agreement within a factor of about 2. This factor also represents the approximate data band width in Fig. 13(a) in the paper. [However, the maximum deviation from a prediction line through the data points of Fig. 13(a) is only about $\pm 35\%$.] It is encouraging to see this agreement between Italian and Florida soils and the writer expects that the data base for all the correlations discussed in the paper will expand with the expanding use of the dilatometer test.

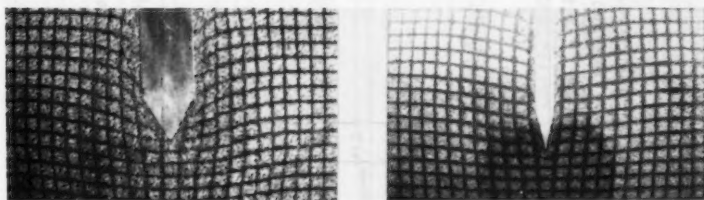


FIG. 15.—Model Test Results in Sand Showing Distorsions Induced by 36-mm Diam Conical Tip and by 14-mm Thick Blade of Dilatometer (from Ref. 28)

The writer agrees with Schmertmann that the rapid prediction of the magnitude of expected consolidation settlements within a factor of 2, compared to the more expensive and much longer times involved in obtaining oedometer test results, should in many practical cases provide an adequate substitute for at least some consolidation testing that would otherwise be required. It should prove particularly useful for preliminary settlement estimates and also offers the advantage of providing many more data points than an engineer can normally obtain by oedometer testing.

The writer would also like to respond here to several questions of general interest concerning the paper brought to the writer's attention either verbally or by mail:

1. The DMT as a penetration test.—The dilatometer test belongs conceptually and practically to the class of penetration tests and not to the class of pressuremeter tests. Penetration tests distort the insitu soil by displacement. The enforced distortion depends to a considerable extent on the geometry (and only marginally on the operator). The dilatometer, with its flat-plate shape, and with its sharp

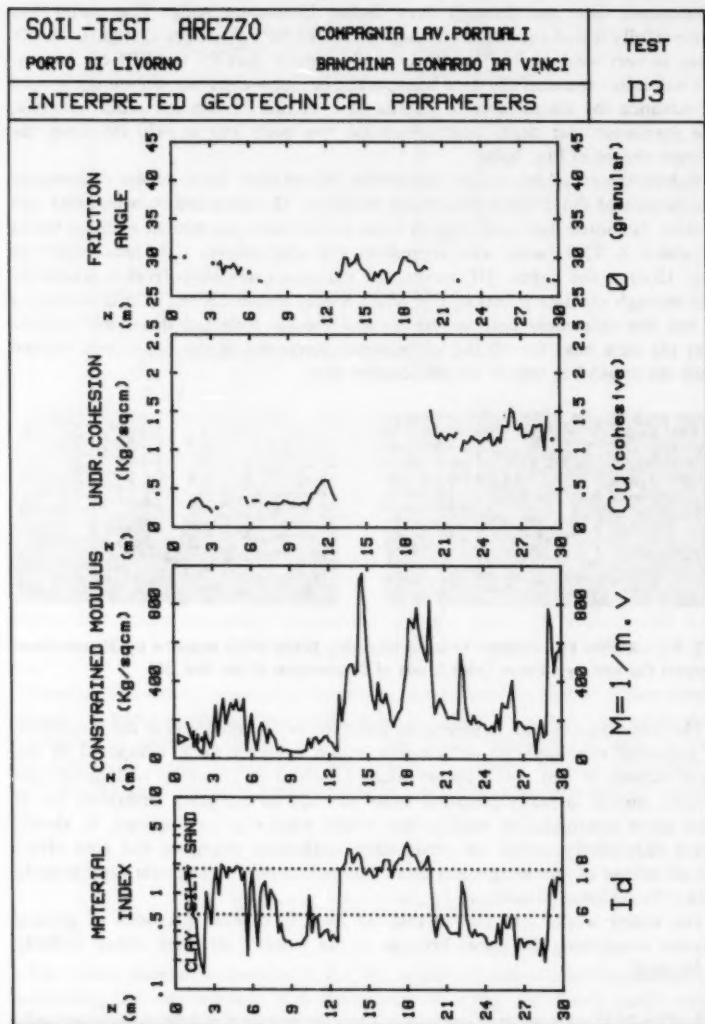


FIG. 16(a).—Example of DMT Results: Profiles Plotted by Computer

cutting edge, should, as Fig. 3 in the paper and the added Fig. 15 of model tests in sand demonstrate, modify the original stress-strain state of the in situ soil to a lesser degree than penetration tests such as the CPT and SPT. This

SOIL-TEST AREZZO				DILATOMETER TEST M.D3				TEST PERFORMED 4 Ottobre 1979							
COMPAGNIA LAR PORTUALI BANCHINA LEONARDO DA VINCI				PORTO DI LIVORNO CANALE INDUSTRIALE				Test depth: m 1 to m 30 Water table m 1.5							
				INTERPRETED GEOTECHNICAL PARAMETERS											
Po = Corrected A reading Pi = Corrected B reading Ganna = Bulk unit weight Sigma' = Effective overb. stress U = Pore pressure Id = Material index Kd = Horizontal stress index Ed = Dilatometer modulus				Ka/sqcm Kg/sqcm 1/cu m Kg/sqcm Kg/sqcm (-) (-) Kg/sqcm				Ks Ocr q M Cu Fi In situ earth press. coeff. (-) Overconsolidation ratio (-) Erased overburden above g.s. Kg/sqcm Constrained modulus (Sigma')/Kg/sqcm Undrained cohesion (cohesive)/Kg/sqcm Friction angle (cohesionless) (-)							
m	Po	Pi	Ganna	Sigma'	U	Id	Kd	Ed	Ke	Ocr	q	M	Cu	Fi	DESCRIPTION
1.0	1.2	3.5	1.88	18.0	0.0	1.89	7.0	85	1.5	16.6	2.7	185			30 SILTY SAND, LOW RIGIDITY
1.2	1.6	4.4	1.78	21.0	0.0	1.89	7.8	66	1.6	8.4	1.6	149			SILT, LOW DENSITY
1.4	1.6	3.2	1.70	25.0	0.0	1.56	8.5	43	1.7	9.5	2.1	180			SILTY CLAY, LOW CONSIST
1.6	1.6	3.2	1.70	27.0	0.0	1.56	8.5	43	1.6	9.5	2.1	180			SILTY CLAY, LOW CONSIST
1.8	2.4	4.4	1.68	28.0	0.0	1.70	27.0	23.0	1.6	2.4	2.4	54			CLAY, SOFT
2.0	2.4	4.4	1.68	30.0	1.1	1.18	8.0	16	1.6	8.7	2.3	35			CLAY, SOFT
2.2	2.4	2.5	1.58	31.1	1.1	1.15	7.8	12	1.5	7.8	1.9	25			MUD
2.4	1.9	3.0	1.78	32.1	1.1	1.82	5.8	70	1.3	5.3	1.4	137			SILT, LOW DENSITY
2.6	2.8	2.8	1.78	33.1	1.1	1.48	2.6	47	1.2	5.3	1.3	89			CLAYEY SILT, LOW DENSITY
2.8	2.8	3.4	1.78	35.1	1.1	1.48	2.6	47	1.2	4.3	1.1	56			CLAYEY SILT, LOW DENSITY
3.0	1.6	3.4	1.78	36.1	2.2	1.19	4.2	66	1.8	3.2	0.8	188			SILT, LOW DENSITY
3.2	2.2	3.8	1.88	37.2	2.2	1.82	5.6	140	1.3	18.1	3.4	273			29 SILTY SAND, LOW RIGIDITY
3.4	2.8	3.8	1.78	39.2	2.2	1.96	4.8	66	1.1	3.9	1.1	116			SILT, LOW DENSITY
3.6	2.8	4.4	1.88	40.4	2.2	1.97	4.4	128	1.1	7.6	2.6	221			29 SILTY SAND, LOW RIGIDITY
3.8	2.8	6.6	1.78	42.4	2.2	1.85	5.5	159	1.2	18.5	3.9	389			29 SILTY SAND, MED RIGIDITY
4.0	2.8	6.6	1.78	44.4	2.2	1.85	5.5	105	1.1	16.8	2.6	188			29 SANDY SILT, LOW DENSITY
4.2	2.8	5.9	1.88	45.3	3.3	1.88	4.1	136	1.1	6.8	2.3	295			29 SILTY SAND, LOW RIGIDITY
4.4	2.8	6.8	1.88	47.3	3.3	1.67	5.3	152	1.2	7.6	3.1	286			29 SANDY SILT, MED DENSITY
4.6	2.8	6.8	1.88	48.3	3.3	1.74	4.6	144	1.1	6.6	2.7	255			29 SANDY SILT, MED DENSITY
4.8	2.8	7.2	1.98	50.3	3.3	1.88	4.8	167	1.1	8.3	3.6	383			29 SILTY SAND, MED RIGIDITY
5.0	2.5	5.5	1.88	51.3	3.3	1.82	4.3	148	1.0	6.2	2.6	258			29 SILTY SAND, LOW RIGIDITY
5.2	2.5	6.7	1.88	53.3	4.4	1.37	5.1	136	1.2	5.1	2.2	258			28 SANDY SILT, MED DENSITY
5.4	2.5	6.8	1.88	54.3	4.4	1.37	5.8	167	1.2	4.9	2.2	387			29 SANDY SILT, MED DENSITY
5.6	2.5	3.8	1.78	56.4	4.4	2.3	5.8	23	1.2	4.1	1.8	42			37 CLAY, LOW CONSISTENCY
5.8	2.8	5.4	1.78	58.4	4.4	1.11	4.1	97	1.0	3.1	1.2	158			31 SILT, LOW DENSITY
6.0	2.8	6.6	1.78	59.4	4.4	1.19	3.9	144	1.0	4.6	2.1	230			28 SANDY SILT, MED DENSITY
6.2	3.1	4.6	1.78	61.4	4.4	0.63	4.3	58	1.0	3.3	1.4	95			34 CLAYEY SILT, LOW DENSITY
6.4	3.1	3.8	1.78	62.4	4.4	0.28	4.2	23	1.0	3.2	1.4	44			35 CLAY, LOW CONSISTENCY
6.6	3.1	3.8	1.78	63.4	4.4	0.28	4.2	23	1.0	3.2	1.4	44			35 CLAY, LOW CONSISTENCY
6.8	3.1	6.2	1.78	65.4	5.5	1.24	3.9	117	1.0	3.8	1.3	157			34 SILTY SAND, LOW DENSITY
7.0	3.1	5.5	1.78	66.4	6.6	1.31	3.4	189	9	2.5	1.0	185			27 SANDY SILT, LOW DENSITY
7.2	3.1	4.4	1.78	68.4	6.6	0.69	3.4	58	9	2.3	0.9	81			29 CLAYEY SILT, LOW DENSITY
7.4	3.1	5.8	1.78	69.4	6.6	1.89	3.6	181	9	2.5	1.1	151			32 SILTY, LOW DENSITY
7.6	3.1	5.5	1.78	71.4	6.6	0.96	3.4	85	9	2.5	0.9	122			30 SILTY, LOW DENSITY
7.8	3.1	7.0	1.78	72.4	6.6	0.74	3.4	74	9	2.5	0.9	183			30 SILTY, LOW DENSITY
8.0	3.1	4.0	1.78	73.4	6.6	0.39	3.3	35	9	2.2	0.7	98			31 SILTY CLAY, LOW CONSIST
8.2	3.1	4.2	1.78	75.4	7.7	0.42	3.2	43	8	2.1	0.8	57			30 SILTY CLAY, LOW CONSIST
8.4	3.2	4.0	1.78	76.4	7.7	0.34	3.3	31	8	2.2	0.9	42			31 SILTY CLAY, LOW CONSIST
8.6	3.4	4.2	1.78	77.4	7.7	0.31	3.5	31	9	2.4	1.1	44			34 CLAY, LOW CONSISTENCY
8.8	3.4	4.2	1.78	79.4	7.7	0.34	3.4	31	9	2.3	1.0	43			33 CLAY, LOW CONSISTENCY
9.0	3.2	4.8	1.78	82.4	8.8	0.29	3.2	27	8	2.1	0.8	36			31 CLAY, LOW CONSISTENCY
9.2	3.2	4.8	1.78	82.4	8.8	0.29	3.1	27	8	2.1	0.8	36			31 CLAY, LOW CONSISTENCY
9.4	3.4	4.8	1.78	83.8	8.8	0.27	2.8	27	8	1.9	0.7	35			31 CLAY, LOW CONSISTENCY
9.6	3.4	4.8	1.78	84.8	8.8	0.30	2.9	27	8	1.8	0.7	34			30 CLAY, LOW CONSISTENCY
9.8	3.1	4.8	1.78	86.8	8.8	0.38	2.9	27	8	1.8	0.7	33			30 CLAY, LOW CONSISTENCY
10.0	3.4	4.2	1.78	87.9	9	0.33	2.9	31	8	1.8	0.7	38			31 SILTY CLAY, LOW CONSIST
10.2	3.4	4.4	1.78	89.9	9	0.36	2.9	35	8	1.8	0.7	44			32 SILTY CLAY, LOW CONSIST
10.4	3.6	5.0	1.78	91.9	9	0.39	2.8	43	8	2.0	1.0	58			33 SILTY CLAY, LOW CONSIST
10.6	3.9	5.8	1.78	91.9	9	0.35	2.8	43	8	2.0	1.0	58			33 SILTY CLAY, LOW CONSIST
10.8	4.3	6.2	1.78	93.9	9	0.39	2.8	43	8	2.0	1.0	58			33 SILTY CLAY, LOW CONSIST
11.0	4.4	6.4	1.88	94.1	1.0	0.57	3.7	74	9	2.6	1.5	189			45 SILTY CLAY, MED CONSIST
11.2	4.9	6.2	1.78	96.1	1.0	0.35	4.1	51	1.0	3.0	1.9	88			51 SILTY CLAY, LOW CONSIST
11.4	5.2	6.2	1.88	97.1	1.0	0.30	4.3	58	1.0	3.3	2.2	95			55 SILTY CLAY, MED CONSIST
11.6	5.2	6.2	1.88	99.1	1.0	0.30	4.3	66	1.1	3.2	2.2	111			60 SILTY CLAY, MED CONSIST
11.8	5.5	7.4	1.88	1.00	1.0	0.42	4.5	85	1.1	3.5	2.5	118			64 SILTY CLAY, MED CONSIST
12.0	5.6	7.8	1.88	1.02	1.1	0.33	4.4	54	1.1	3.5	2.5	91			61 CLAY, MEDIUM CONSISTENCY
12.2	5.1	6.5	1.78	1.04	1.1	0.37	3.9	54	1.0	2.8	1.8	83			52 SILTY CLAY, LOW CONSIST
12.4	4.5	5.6	1.78	1.05	1.1	0.34	3.2	43	8	2.1	1.2	57			42 SILTY CLAY, LOW CONSIST
12.6	4.1	5.8	1.78	1.06	1.1	0.32	2.8	35	7	1.7	1.2	42			36 CLAY, LOW CONSISTENCY
12.8	4.6	10.8	1.88	1.08	1.1	0.73	3.3	229	8	3.6	2.8	329			28 SANDY SILT, MED DENSITY
m	Po	Pi	Ganna	Sigma'	U	Id	Kd	Ed	Ke	Ocr	q	M	Cu	Fi	DESCRIPTION

FIG. 16(b).—Example of DMT Results: Numerical Output

reduces the amount of extrapolation required to estimate the undisturbed in situ behavior and thereby should improve the quality of the correlations with engineering design parameters.

2. Form of displaying results—Figs. 4-10 of the original paper express the DMT results in terms of the "intermediate parameters" I_D , K_D , E_D , because the scope in the paper was to study the correlations between these three parameters and conventional geotechnical parameters. Presently (January, 1981) the usual form in which DMT results are displayed is the one in Fig. 16. This figure shows an example of DMT results analyzed and displayed using a computer program having built in the correlations described in the paper. The reader may notice that Fig. 16 includes friction angle predictions for the cohesionless layers. However the correlations used for such predictions result from only a limited number of cohesionless deposits, not adequate at present (January, 1981) to make any general recommendations.

3. Reproducibility of results—An example of results documenting the reproducibility of the DMT results, rated as "high" in the paper, is given in Fig. 17. The DMT readings were taken in the course of two soundings, a few meters

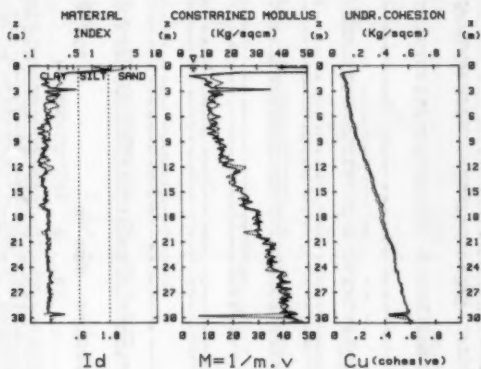


FIG. 17.—Results of Two DMT Soundings Carried out in NC Norwegian Marine Clay (Onsøy site)

apart, by 4 different operators (F. Cestari, S. Lacasse, T. Lunne and the writer) alternating with each other. The agreement appears very satisfactory.

4. In aged clays DMT overpredicts K_o and OCR—Various questions received by the writer seem to indicate that the paper did not emphasize enough that the DMT overpredicts both K_o and OCR in clays exhibiting marked aging or cementation effects. Possible reasons were discussed on pp. 314 and 315 of the paper. For instance in markedly aged NC clays OCR values predicted by the DMT are well above 1 (but, interestingly, approximately constant with depth). Conversely, DMT evaluations of OCR appreciably above 1 in a NC clay deposit may indicate possibly important aging/cementation effects.

5. Use of c_u determined by DMT—As noted in the paper, the c_u values predicted by DMT are generally lower than field vane values, with their ratio usually in the range of 0.7-1.0. The c_u values determined by DMT are comparable with the field vane c_u after reduction using the Bjerrum correction. Based on

this it has been the writer's practice when selecting the strength profile for design purposes in nonsensitive clays to use the c_u predicted by the DMT without any modification. Similar conclusions were reached by D'Antonio (27) in a recent presentation of a case history comparing profiles of c_u determined in situ using the field vane test, the CPT and DMT, and laboratory triaxial UU tests. The design profile of c_u for evaluating the stability of a 3-km long quaywall, in 13.5 m of water, was finally selected by D'Antonio as the "conservative average" of the unmodified c_u determined by the DMT.

APPENDIX.—REFERENCES

27. D'Antonio, V., "Soil Investigations and Stability Analysis of Gravity Quaywalls," (in Italian), to be published in *Giornale del Genio Civile*, Consiglio Superiore dei Lavori Pubblici, Roma, 1981.
28. Marchetti, S., and Panone, C., "Distorsions Induced in Sands by Probes of Different Shapes," (in Italian), to be published in *Rivista Italiana di Geotecnica*, Vol. 15, 1981.

Errata.—The following correction should be made to the original paper:

Page 314, Table 3: Should be replaced by the following table

TABLE 3.—Proposed Soil Classification Based on I_D Value

Peat or sensitive clays	CLAY		SILT			SAND	
		Silty	Clayey		Sandy	Silty	
I_D values	0.10	0.35	0.6	0.9	1.2	1.8	3.3

IN-SITU VOLUME-CHANGE PROPERTIES BY ELECTRO-OSMOSIS—EVALUATION^a

Discussion by Ian W. Johnston³

While reading with great interest the paper and its companion paper (2), the writer became concerned with one critical aspect of both the theory and its evaluation. This concern surrounds the application of the boundary condition

$$\frac{\partial u}{\partial r} = \alpha \frac{\partial \phi}{\partial r} \quad \text{at } r = a \quad \text{for all } z \text{ and } t \quad \dots \dots \dots (1)$$

and the assumption that the soil is uniform and therefore of constant specific

^aApril, 1980, by James K. Mitchell and Sunirmal Banerjee (Proc. Paper 15371).

³Lect., Dept. of Civ. Engrg., Monash Univ., Melbourne, Victoria, Australia 3168.

resistivity. It arises from the writer's experiences during an investigation into excess porewater pressures developed by electro-osmosis (9,10). Part of that investigation involved an examination of a one-dimensional electro-osmotic field with equipment specifically designed to eliminate a number of complicating factors including electrolysis, gas evolution, variable applied voltages and a variety of electro-chemical effects as indicated previously by the writer (5). Each test consisted of one drained and one undrained electrode between which a constant selected voltage was applied, and the porewater pressures and voltage variations carefully monitored along the length of the test specimens.

Initially, as is the assumption of the authors, the writer assumed that the soil and its electrical properties were homogeneous and isotropic and that the one-dimensional diffusion equation, solved for the boundary conditions given in the theory paper (2), would predict the variations in porewater pressure throughout the test specimens. Indeed, when the average degree of consolidation derived from both experimental and theoretical results were compared, a quite acceptable correlation was obtained. However, extreme care must be taken in the interpretation of this result as curve fitting methods were used to determine the coefficient of consolidation, c_v , and the time constant, T , thereby ensuring a reasonable fit. Also, at this stage of the comparison, the theoretical analysis made on the basis of a constant voltage gradient between the electrodes, appeared further substantiated by the fact that c_v values obtained from the electro-osmotic tests were in quite acceptable agreement with c_v values obtained from immediately preceding isotropic consolidation tests, even though the porewater pressures at the undrained electrodes appeared to increase somewhat quicker than the theory predicted. A more severe test for this "electrically homogeneous" solution of the diffusion equation involved a direct comparison between the theoretical and experimental porewater pressure isochrones along the whole length of the specimen and not merely the average values nor those of any one specific section only. It soon became obvious that the two sets of isochrones bore little resemblance in both magnitude and shape.

A close examination was made of the voltage variations between the electrodes. It was found that although the voltage applied between the electrodes was constant throughout each test, the voltage gradient at specific sections of the specimens was not necessarily constant with location nor time. While random local variations in voltage gradient were to be expected for the undisturbed natural soil specimens used, it was observed that in all tests, the voltage gradients immediately adjacent to the undrained electrodes were high initially but after a short time changed to give a relatively uniform gradient across the whole of each specimen.

It follows from the boundary condition previously given, for a high initial voltage gradient at the undrained electrode, a high porewater pressure gradient must develop initially with the result that the final steady-state porewater pressure at the undrained electrode is obtained very rapidly. The time taken to reach this final state was determined experimentally to be a few minutes.

On the basis of these observations, a second closed form "immediate response" solution to the diffusion equation was obtained in which the boundary condition given above was replaced by

$$u_t = u_{\infty} \quad \text{for all } t \text{ at the undrained electrode} \quad (2)$$

A comparison of the "immediate response" solution with the experimental

results (9,10) showed that not only did the average degree of consolidation curves correspond with a much more acceptable correlation between c_v values obtained from both electro-osmotic and preceding isotropic consolidation tests, but also and more importantly the "immediate response" solution predicted the observed porewater pressures throughout each specimen with a remarkable degree of precision.

It appears then, that on the basis of the foregoing experiences, because of unavoidable nonhomogeneities in a natural soil mass when electro-osmosis is applied, the voltage and therefore the porewater pressure gradients immediately adjacent to the undrained electrodes are high. This leads to a very rapid increase of porewater pressures to their final steady-state values at the undrained electrode. Practically, this increase may be considered instantaneous. Further evidence of this phenomenon is discussed in Butterfield and the writer (8).

The problem confronting the writer therefore concerns the interpretation of the results obtained by the authors for the development of excess porewater pressures at the undrained electrode. As noted previously, although the "electrically homogeneous" solution did produce quite acceptable agreement with the experimental average degree of consolidation by virtue of the curve fitting processes and further with values of c_v obtained from the isotropic and electro-osmotic stages of testing, it did not predict with any degree of accuracy the porewater pressure isochrones for the whole of each specimen.

It was only with the "immediate response" solution could agreement be obtained between theoretical and experimental results, specifically with regard to the porewater pressure isochrones for the whole of each specimen. It should be noted that this overall agreement deviated only slightly at the undrained electrodes where, as is central to the authors' evaluation, there was a delay of a few minutes before final steady-state conditions were reached.

It follows that using the "electrically homogeneous" solution as employed by the authors, reasonable predictions of c_v may be made under certain conditions but this may be quite fortuitous.

APPENDIX.—REFERENCES

8. Butterfield, R., and Johnston, I. W., "The Influence of Electro-Osmosis on Metallic Piles in Clay," *Geotechnique*, Vol. 30, No. 1, Mar., 1980, pp. 17-38.
9. Johnston, I. W., "Electro-Osmosis and Porewater Pressures; Their Effect on the Stresses Acting on Driven Piles," thesis presented to the University of Southampton, at Southampton, England, in 1972, in fulfillment of the requirements for the degree of Doctor of Philosophy.
10. Johnston, I. W., and Butterfield, R., "A Laboratory Investigation of Soil Consolidation by Electro-Osmosis," *Australian Geomechanics Journal*, Vol. G7, 1977, pp. 21-32.

**Closure by James K. Mitchell,⁴ F. ASCE
and Sunirmal Banerjee,⁵ A. M. ASCE**

Johnston has correctly called attention to what appears to be a significant factor influencing the validity of previous solutions for one-dimensional consolidation by electro-osmosis; namely, that the variation in electrical potential between electrodes is not linear, as has been commonly assumed. By replacing an "electrically homogeneous" solution with an "immediate response" solution Johnston obtained predicted pore pressure isochrones in much better agreement with measured values (5,8,9,10). Accordingly, the validity of the writers' solution for potential distribution (2), which forms the boundary conditions controlling the rate of pore pressure generation in the soil surrounding the electro-osmosis probe, is thrown into question.

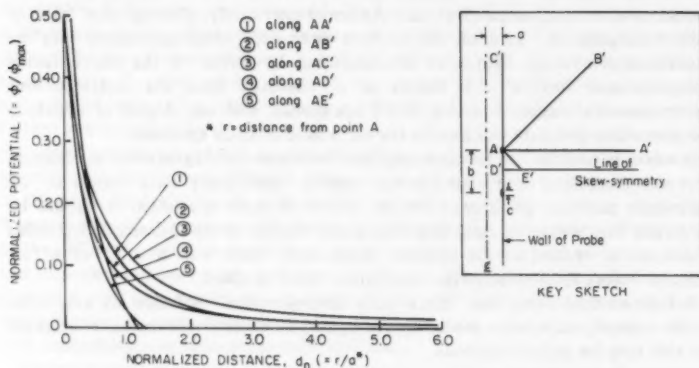


FIG. 18.—Variation of Potential around Electrodes ($b/a = 2.5$, $c/a = 0.25$)

In previous studies of electro-osmosis in one dimension, the potential distribution between electrodes has been determined assuming a uniform, homogeneous charge distribution that is unaffected by the presence of the electrodes. As a result, the problem of determination of electrical potential at any point was obtained by appropriate solution of the Laplace equation, which for the one-dimensional case leads to a linear distribution of electrical potential, or constant potential gradient, between the electrodes.

In reality, however, the presence of electrodes in the system introduces interfaces between two conducting media, the metal and the soil water-electrolyte solution. As a result a dielectric boundary layer will form in much the same way as the electrical double layer surrounding clay particles. The writers postulate that this phenomenon can be responsible for a high potential drop over a short

⁴Prof. of Chmn. of Civ. Engrg. Dept., 440 Davis Hall, Univ. of California at Berkeley, Berkeley, Calif. 94720.

⁵Asst. Prof. of Civ. Engrg., South Dakota School of Mines & Tech., Rapid City, S. Dak. 57701.

distance adjacent to an electrode giving a voltage distribution between electrodes more consistent with the discussor's "immediate response" solution than with the commonly assumed "electrically homogeneous" condition.

For the case studied by the writers (1,2) it is, in retrospect, fortuitous that a solution for the potential field problem to be solved for the special probe geometry was not available. As a result a more general method of solution was required. The solution developed in the writers' companion paper (2) takes into account the interface charges and their interaction with the potential field. The computed variation of potential with distance from the anode along five lines is shown for one set of b/a and c/a values in Fig. 18. Very high potential gradients adjacent to the electrode are indicated.

Thus the problem pointed out by the discussor should not exist for the solutions developed for interpretation of consolidation properties from the results of electro-osmosis measurements by the method presented in the paper. Admittedly, however, there may be other complicating factors such as thermal effects, gas evolution, and electrochemical effects, but these are separate problems.

It would be of interest in a subsequent study to rederive the one-dimensional solution in the same manner as the probe solution in Ref. 2 to see if potential distributions of the type presented by the discussor in Ref. 10 result.

the author's own research, and the book is a valuable contribution to the literature on the history of the book industry.

The book is divided into three parts. The first part, 'The Book Industry in the Nineteenth Century', deals with the early years of the industry, from the 1800s to the 1850s. The second part, 'The Book Industry in the Twentieth Century', deals with the years from the 1860s to the 1950s. The third part, 'The Book Industry in the Twenty-First Century', deals with the years from the 1960s to the present. The book is written in a clear and concise style, and it is a valuable resource for anyone interested in the history of the book industry.

The book is a valuable resource for anyone interested in the history of the book industry. It is written in a clear and concise style, and it is a valuable resource for anyone interested in the history of the book industry.



The book is a valuable resource for anyone interested in the history of the book industry.

The book is a valuable resource for anyone interested in the history of the book industry. It is written in a clear and concise style, and it is a valuable resource for anyone interested in the history of the book industry.

The book is a valuable resource for anyone interested in the history of the book industry. It is written in a clear and concise style, and it is a valuable resource for anyone interested in the history of the book industry.

The book is a valuable resource for anyone interested in the history of the book industry. It is written in a clear and concise style, and it is a valuable resource for anyone interested in the history of the book industry.



the 1990s, the number of people in the world who are undernourished has increased from 600 million to 800 million.

There is a growing awareness of the need to address the problem of food security. The United Nations World Food Programme (WFP) has been established to coordinate international efforts to combat hunger. The World Bank has also established a Global Food Security Programme (GFSP) to support countries in developing sustainable food systems.

One of the key challenges in addressing food security is the need to increase agricultural productivity. This can be achieved through a variety of measures, including improved irrigation, access to credit, and extension services. It is also important to ensure that small-scale farmers have access to markets and that their produce is sold at fair prices.

Another key challenge is the need to improve the nutritional quality of food. This can be achieved through a variety of measures, including promoting the consumption of a diverse range of foods, including fruits, vegetables, and animal products. It is also important to ensure that food is safe and free from contamination.

Finally, it is important to ensure that food systems are sustainable. This means that they should be able to meet the needs of the present without compromising the ability of future generations to meet their own needs. This can be achieved through a variety of measures, including promoting sustainable agricultural practices and reducing food waste.

Addressing the problem of food security is a complex task that requires the coordinated efforts of governments, the private sector, and civil society. It is essential that we all work together to ensure that everyone has access to enough food to live a healthy and productive life.

Journal of Agricultural Economics, 2008, 162, 153–160. © 2008 The Authors. Journal compilation © 2008 Blackwell Publishing Ltd

Keywords: food security, agricultural productivity, nutritional quality, sustainable food systems.

1. Introduction The problem of food security has become a global concern in the 21st century. It is estimated that over 800 million people in the world are undernourished, and this number is expected to increase in the coming years.

There are a number of factors that contribute to the problem of food security. These include population growth, climate change, and the increasing demand for food. In addition, there are a number of structural factors that contribute to the problem, such as the concentration of land in the hands of a few large landowners and the lack of access to credit and extension services for small-scale farmers.

One of the key challenges in addressing food security is the need to increase agricultural productivity. This can be achieved through a variety of measures, including improved irrigation, access to credit, and extension services. It is also important to ensure that small-scale farmers have access to markets and that their produce is sold at fair prices.

Another key challenge is the need to improve the nutritional quality of food. This can be achieved through a variety of measures, including promoting the consumption of a diverse range of foods, including fruits, vegetables, and animal products. It is also important to ensure that food is safe and free from contamination.

Finally, it is important to ensure that food systems are sustainable. This means that they should be able to meet the needs of the present without compromising the ability of future generations to meet their own needs. This can be achieved through a variety of measures, including promoting sustainable agricultural practices and reducing food waste.



the 1990s, the number of people in the world who are under 15 years of age is expected to increase from 1.1 billion to 1.5 billion (United Nations 1994). This increase in the number of children in the world is expected to be accompanied by a corresponding increase in the number of children in the United Kingdom.

There is a growing awareness of the need to ensure that the needs of children are met in the United Kingdom. The Department of Health (1994) has published a report on the health of children in the United Kingdom, which states that the health of children is a priority for the government. The report also states that the health of children is a priority for the public. The report also states that the health of children is a priority for the media.

The Department of Health (1994) has also published a report on the health of children in the United Kingdom, which states that the health of children is a priority for the government. The report also states that the health of children is a priority for the public. The report also states that the health of children is a priority for the media. The report also states that the health of children is a priority for the media.

The Department of Health (1994) has also published a report on the health of children in the United Kingdom, which states that the health of children is a priority for the government. The report also states that the health of children is a priority for the public. The report also states that the health of children is a priority for the media. The report also states that the health of children is a priority for the media.

The Department of Health (1994) has also published a report on the health of children in the United Kingdom, which states that the health of children is a priority for the government. The report also states that the health of children is a priority for the public. The report also states that the health of children is a priority for the media. The report also states that the health of children is a priority for the media.

The Department of Health (1994) has also published a report on the health of children in the United Kingdom, which states that the health of children is a priority for the government. The report also states that the health of children is a priority for the public. The report also states that the health of children is a priority for the media. The report also states that the health of children is a priority for the media.

The Department of Health (1994) has also published a report on the health of children in the United Kingdom, which states that the health of children is a priority for the government. The report also states that the health of children is a priority for the public. The report also states that the health of children is a priority for the media. The report also states that the health of children is a priority for the media.

The Department of Health (1994) has also published a report on the health of children in the United Kingdom, which states that the health of children is a priority for the government. The report also states that the health of children is a priority for the public. The report also states that the health of children is a priority for the media. The report also states that the health of children is a priority for the media.

TECHNICAL PAPERS

Original papers should be submitted in triplicate to the Manager of Technical and Professional Publications, ASCE, 345 East 47th Street, New York, N.Y. 10017. Authors must indicate the Technical Division or Council, Technical Committee, Subcommittee, and Task Committee (if any) to which the paper should be referred. Those who are planning to submit material will expedite the review and publication procedures by complying with the following basic requirements:

1. Titles must have a length not exceeding 50 characters and spaces.
2. The manuscript (an original ribbon copy and two duplicate copies) should be double-spaced on one side of 8-1/2-in. (220-mm) by 11-in. (280-mm) paper. Three copies of all figures and tables must be included.
3. Generally, the maximum length of a paper is 10,000 word-equivalents. As an *approximation*, each full manuscript page of text, tables or figures is the equivalent of 300 words. If a particular subject cannot be adequately presented within the 10,000-word limit, the paper should be accompanied by a rationale for the overlength. This will permit rapid review and approval by the Division or Council Publications and Executive Committees and the Society's Committee on Publications. Valuable contributions to the Society's publications are not intended to be discouraged by this procedure.
4. The author's full name, Society membership grade, and a footnote stating present employment must appear on the first page of the paper. Authors need not be Society members.
5. All mathematics must be typewritten and special symbols must be identified properly. The letter symbols used should be defined where they first appear, in figures, tables, or text, and arranged alphabetically in an appendix at the end of the paper titled Appendix.—Notation.
6. Standard definitions and symbols should be used. Reference should be made to the lists published by the American National Standards Institute and to the *Authors' Guide to the Publications of ASCE*.
7. Figures should be drawn in black ink, at a size that, with a 50% reduction, would have a published width in the *Journals* of from 3 in. (76 mm) to 4-1/2 in. (110 mm). The lettering must be legible at the reduced size. Photographs should be submitted as glossy prints. Explanations and descriptions must be placed in text rather than within the figure.
8. Tables should be typed (an original ribbon copy and two duplicates) on one side of 8-1/2-in. (220-mm) by 11-in. (280-mm) paper. An explanation of each table must appear in the text.
9. References cited in text should be arranged in alphabetical order in an appendix at the end of the paper, or preceding the Appendix.—Notation, as an Appendix.—References.
10. A list of key words and an information retrieval abstract of 175 words should be provided with each paper.
11. A summary of approximately 40 words must accompany the paper.
12. A set of conclusions must end the paper.
13. Dual units, i.e., U.S. Customary followed by SI (International System) units in parentheses, should be used throughout the paper.
14. A practical applications section should be included also, if appropriate.

the 1990s, the number of people in the world who are undernourished has increased from 600 million to 800 million.

There are a number of reasons why the world's population is still hungry. One of the main reasons is that the world's population is growing very fast. In 1990, there were about 5 billion people in the world. By 2000, there were about 6 billion people in the world. By 2010, there will be about 7 billion people in the world.

Another reason why the world's population is still hungry is that the world's food supply is not growing fast enough. The world's food supply is growing at about 1% per year. But the world's population is growing at about 1.2% per year. So the world's food supply is not growing fast enough to keep up with the world's population.

A third reason why the world's population is still hungry is that the world's food is not distributed evenly. In some parts of the world, there is a lot of food. But in other parts of the world, there is not enough food. This is because the world's food is not distributed evenly.

There are a number of things that we can do to help the world's population. We can grow more food. We can distribute food more evenly. We can help people in the world who are hungry. We can do many things to help the world's population.

One of the most important things that we can do is to help people in the world who are hungry. We can give them food. We can give them money. We can give them other things that they need. We can help them in many ways.

There are many organizations that help people in the world who are hungry. One of the most famous organizations is the Red Cross. The Red Cross helps people in many ways. It gives them food. It gives them money. It gives them other things that they need.

There are many other organizations that help people in the world who are hungry. One of the most important organizations is the United Nations. The United Nations helps people in many ways. It gives them food. It gives them money. It gives them other things that they need.

There are many things that we can do to help the world's population. We can grow more food. We can distribute food more evenly. We can help people in the world who are hungry. We can do many things to help the world's population.

One of the most important things that we can do is to help people in the world who are hungry. We can give them food. We can give them money. We can give them other things that they need. We can help them in many ways.

There are many organizations that help people in the world who are hungry. One of the most famous organizations is the Red Cross. The Red Cross helps people in many ways. It gives them food. It gives them money. It gives them other things that they need.

There are many other organizations that help people in the world who are hungry. One of the most important organizations is the United Nations. The United Nations helps people in many ways. It gives them food. It gives them money. It gives them other things that they need.

There are many things that we can do to help the world's population. We can grow more food. We can distribute food more evenly. We can help people in the world who are hungry. We can do many things to help the world's population.

One of the most important things that we can do is to help people in the world who are hungry. We can give them food. We can give them money. We can give them other things that they need. We can help them in many ways.

There are many organizations that help people in the world who are hungry. One of the most famous organizations is the Red Cross. The Red Cross helps people in many ways. It gives them food. It gives them money. It gives them other things that they need.

There are many other organizations that help people in the world who are hungry. One of the most important organizations is the United Nations. The United Nations helps people in many ways. It gives them food. It gives them money. It gives them other things that they need.



